Genesis of Cu-PGE-rich Footwall-Type Mineralization in the Morrison Deposit, Sudbury

by

Edward William Nelles

Thesis submitted in partial fulfillment
of the requirements for the degree of
Master of Science (MSc) in Geology

School of Graduate Studies
Laurentian University
Sudbury, Ontario

THESIS DEFENCE COMMITTEE/COMITÉ DE SOUTENANCE DE THÈSE

Laurentian Université/Université Laurentienne
School of Graduate Studies/École des études supérieures

Title of Thesis Titre de la thèse	GENESIS OF Cu-PGE-RICH FOOTWALL-TYPE MINERALIZATION IN THE MORRISON DEPOSIT, SUDBURY
Name of Candidate Nom du candidat	Nelles, Edward William
Degree Diplôme	Master of Science

Department/Program Département/Programme	Geology	Date of Defence Date de la soutenance	July 23, 2012

APPROVED/APPROUVÉ

Thesis Examiners/Examinateurs de thèse:

Dr. Michael Lesher
(Supervisor/Directeur de thèse)

Dr. Catharine Farrow
(Committee member/Membre du comité)

Dr. Bruno Lafrance
(Committee member/Membre du comité)

Dr. Pedro Jugo
(Committee member/Membre du comité)

Dr. Jacob Hanley
(External Examiner/Examinateur externe)

Approved for the School of Graduate Studies
Approuvé pour l'École des études supérieures
Dr. David Lesbarrères
M. David Lesbarrères
Director, School of Graduate Studies
Directeur, École des études supérieures

ACCESSIBILITY CLAUSE AND PERMISSION TO USE

Thesis Abstract

The Morrison deposit, located at the Levack mine in the City of Greater Sudbury, is a footwall-type Cu-Ni-platinum-group-element (PGE) deposit hosted within a zone of Sudbury Breccia in the Archean Levack Gneiss Complex beneath the North Range of the Sudbury Igneous Complex. It consists of sharp-walled, sulfide-rich veins that are enriched in Cu-Pt-Pd-Au relative to contact-type mineralization and can be subdivided based on vein geochemistry, mineralogy, texture, and morphology into a pyrrhotite-rich upper domain, a chalcopyrite-rich lower domain, and a pyrrhotite equal to chalcopyrite middle domain. All domains contain steeply to vertically dipping first-order sulfide veins, irregular and discontinuous second-order sulfide veins, and disseminated sulfides in country rocks. First- and second-order veins can be further subdivided into inclusion-free veins typically within Sudbury breccia matrix or along clast-matrix boundaries, and very irregular and inclusion-rich veins associated with leucosomes in mafic gneiss clasts and granophyric-textured dikes. First-order veins consist of pyrrhotite > chalcopyrite = pentlandite > magnetite in the upper domain, pyrrhotite = chalcopyrite > pentlandite > cubanite > magnetite in the middle domain, and chalcopyrite >> pentlandite > pyrrhotite = cubanite > magnetite in the lower domain. Second-order veins consist of pyrrhotite = chalcopyrite > pentlandite > magnetite and chalcopyrite = millerite = pentlandite in the middle domain, and chalcopyrite >> millerite, millerite > chalcopyrite, bornite >> chalcopyrite, and millerite > bornite > chalcopyrite in the lower domain. Second order veins are adjacent to and in contact with epidote, amphibole, chlorite, carbonate, quartz, and magnetite alteration minerals.

Sulfide mineralization in the Morrison deposit is similar to other footwall mineralization associated with the SIC. The veins appear to have been emplaced preferentially into zones of Sudbury Breccia that were within ~400m of the basal contact of the SIC, because that lithology is more permeable and because those zones are within the thermal aureole of the cooling SIC permitting penetration of sulfide melts. The mineralogical, textural, and geochemical zoning in the chalcopyrite-pentlandite-pyrrhotite-rich parts of the Morrison deposit are best explained by partial fractional and/or equilibrium crystallization of MSS and ISS. Bornite ± millerite-rich mineralization are interpreted to have formed by reaction of residual sulfide melts with wall rocks, consuming Fe and S to form actinolite-magnetite-epidote-chlorite-sulfide reaction zones and driving the sulfide melt across the thermal divide in that part of the Fe-Cu-Ni-S system to crystallize borniteSS ± milleriteSS. Gold-Pt-Pd appear to have been more mobile than other metals, forming localized zones of enrichment, although it is not clear yet whether they were mobile as Au-Pt-Pd-Bi-Te-Sb-rich melts or aqueous fluids.

Table of Contents

List of Figures

List of Tables

CHAPTER 1: Introduction to Thesis

Introduction

Although the nature and origin of the ores along the basal contact of the Sudbury Igneous Complex are fairly well understood, the origin of the ores in the underlying (footwall) rocks, in particular the transition between Cu-Pt-Pd-Au-poor contact ores and Cu-Pt-Pd-Au-rich footwall ores, and the origin of disseminated "low-S" Au-Pt-Pd-Bi-Te-rich ores, are not well understood. The Levack Mine on the North Range of the Sudbury Igneous Complex is one of only a few areas in Sudbury (e.g., McCreedy West, Nickel Rim South) where the contact-footwall systems are relatively continuous and therefore provide an opportunity to advance understanding of the transitions between mineralization types.

This study documents the form, textures, mineralogy, and geochemistry of mineralization within a large portion of the Morrison deposit that ranges from Cu-Pt-Pd-Au-poor pyrrhotite-(pentlandite)-(chalcopyrite) rich mineralization to Cu-Pt-Pd-Au-rich chalcopyrite-bornite-millerite-rich mineralization. It attempts to define the extent of footwall-type mineralizing systems and shows that the most likely mode of formation for the deposit is through the combination of fractional crystallization of high-temperature $(Fe,Ni)_{1-X}S$ and high-temperature $CuFe_2S_3$-$CuFeS_2$, interaction of that melt with wall rocks to form Fe-rich silicates, Cu_5FeS_4, and NiS, and exsolution of a final Au-Pt-Pd-Bi-Te-Sb-rich melt and/or aqueous fluid. The study has also created areas for further research and provided new insights for future exploration of footwall-type deposits.

Structure of Thesis

This thesis is presented in the form of a manuscript to be submitted for publication in a peer reviewed, internationally-circulated geoscience journal. Chapter 1 provides a brief non-technical introduction, an explanation of the structure of the thesis, a statement of responsibilities, and acknowledgements. Chapter 2 is the final draft of a manuscript formatted for submission to *Economic Geology*. Chapter 3 contains appendices that will be submitted as electronic appendices to *Economic Geology*.

Statement of Responsibilities

This thesis is presented as a journal paper with a co-author. The candidate did all of the research, collected and prepared all of the samples for analysis, performed all of the petrographic work, and geochemical models, and wrote the first draft of the thesis. Dr. C.M. Lesher helped design the project, provided supervision, guidance, and advice during the research, and edited the final version of the thesis. Drs. Pedro Jugo and Jacob Hanley provided very helpful comments during the final review and examination stage.

Acknowledgements

I am very grateful to C.M. Lesher for all of his guidance and assistance with this project. I also greatly appreciate the financial and logistical support of KGHM International Ltd. Specifically, I am grateful to all Levack mine employees who helped me with my field work. I would also like to thank Dr. Bruno Lafrance and Dr. Catharine Farrow for serving as members of my committee and for assistance in organizing the project. This project was supported by NSERC Discovery Grants to Dr. Lesher (203171-01 and 203171-07), and an NSERC Industry Postgraduate Scholarship and a SEG Foundation Fellowship to the candidate.

CHAPTER 2: Journal Paper

Genesis of Cu-PGE-rich Footwall-Type Mineralization in the Morrison Deposit, Sudbury

Nelles, E.W. and **Lesher, C.M.**

Mineral Exploration Research Center, Department of Earth Sciences, Laurentian University,
935 Ramsey Lake Road, Sudbury, Ontario, Canada P3E 2C6

ABSTRACT

The Morrison deposit, located at the Levack mine in the City of Greater Sudbury, is a footwall-type Cu-Ni-platinum-group-element (PGE) deposit hosted within a zone of Sudbury Breccia in the Archean Levack Gneiss Complex beneath the North Range of the Sudbury Igneous Complex. It consists of sharp-walled, sulfide-rich veins that are enriched in Cu-Pt-Pd-Au relative to contact-type mineralization and can be subdivided based on vein geochemistry, mineralogy, texture, and morphology into a pyrrhotite-rich upper domain, a chalcopyrite-rich lower domain, and a pyrrhotite equal to chalcopyrite middle domain. All domains contain steeply to vertically dipping first-order sulfide veins, irregular and discontinuous second-order sulfide veins, and disseminated sulfides in country rocks. First- and second-order veins can be further subdivided into inclusion-free veins typically within Sudbury breccia matrix or along clast-matrix boundaries, and very irregular and inclusion-rich veins associated with leucosomes in mafic gneiss clasts and granophyric-textured dikes. First-order veins consist of pyrrhotite > chalcopyrite = pentlandite > magnetite in the upper domain, pyrrhotite = chalcopyrite > pentlandite > cubanite > magnetite in the middle domain, and chalcopyrite >> pentlandite > pyrrhotite = cubanite > magnetite in the lower domain. Second-order veins consist of pyrrhotite = chalcopyrite > pentlandite > magnetite and chalcopyrite = millerite = pentlandite in the middle domain, and chalcopyrite >> millerite, millerite > chalcopyrite, bornite >> chalcopyrite, and millerite > bornite > chalcopyrite in the lower domain. Second-order veins are adjacent to and in contact with epidote, amphibole, chlorite, carbonate, and magnetite alteration minerals.

Sulfide mineralization in the Morrison deposit is similar to other footwall mineralization associated with the SIC. The veins appear to have been emplaced preferentially into zones of Sudbury Breccia that were within ~400m of the basal contact of the SIC, because that lithology is more permeable and because those zones are within the thermal aureole of the cooling SIC, permitting penetration of sulfide melts. The mineralogical, textural, and geochemical zoning in the chalcopyrite-pentlandite-pyrrhotite-rich parts of the Morrison deposit are best explained by partial fractional and/or equilibrium crystallization of MSS and ISS. Bornite ± millerite-rich mineralization are interpreted to have formed by reaction

of residual sulfide melts with wall rocks, consuming Fe and S to form actinolite-magnetite-epidote-chlorite-sulfide reaction zones and driving the sulfide melt across the thermal divide in that part of the Fe-Cu-Ni-S system to crystallize borniteSS ± milleriteSS. Gold-Pt-Pd appear to have been more mobile than other metals, forming localized zones of enrichment, although it is not clear yet whether they were mobile as Au-Pt-Pd-Bi-Te-Sb-rich melts or aqueous fluids.

INTRODUCTION

The processes that concentrated Cu, Ni, and platinum group elements (PGEs) within the footwall rocks of the Sudbury Igneous Complex have been debated since Hawley (1965) proposed fractional crystallization of monosulfide solid solution (MSS) from a sulfide melt to explain the zoning at the Frood-Stobie deposit. Since then, several processes have been proposed, including: 1) solid state diffusion down a thermal gradient induced by the overlying SIC (e.g., Naldrett and Kullerud, 1967; Keays and Crocket, 1970), 2) fractional crystallization of MSS ± intermediate solid solution (ISS) (e.g., Keays and Crocket, 1970; Chyi and Crocket, 1976; Naldrett et al., 1982; Li et al., 1992; Mungall, 2007), 3) remobilization of contact-type mineralization by circulation of hydrothermal fluids in the footwall (e.g., Farrow and Watkinson, 1992; Molnár et al., 1997), 4) early movement of PGEs and Au into the footwall as a fluid and the superposition of a fractionated sulfide melt (Farrow and Lightfoot, 2002; Hanley et al., 2005), and 5) dynamic remelting of contact-type mineralization followed by fractional crystallization of MSS±ISS and exsolution of an Au-Pt-Pd-Bi-Te-Sb-rich aqueous fluid or melt (Lesher et al., 2008, 2009).

The Morrison deposit contains a spatially continuous distribution of mineralization from pyrrhotite-rich pods and veins, through sharp-walled chalcopyrite-rich veins, to millerite- and bornite- and platinum, palladium and gold-rich veins (Farrow et al., 2009). It has not been as extensively studied as the McCreedy West 700 complex and PM deposit, the Coleman/McCreedy East 153 and 153 east deposits, or the Strathcona Copper and Deep Copper deposits, so the continuous nature of the mineralization and the lack of previous research at the Morrison deposit make it an excellent location to refine the mechanisms for the formation of footwall-type mineralization.

GEOLOGIC SETTING

Regional Geology

The Sudbury Structure is located in the southern Canadian Shield at the contact of the Southern Province (South Range) and the Superior Province (North Range) (Card et al., 1984), and includes the Sudbury Igneous Complex (SIC), underlying anatectic Footwall breccias and cataclastic and pseudotachylitic Sudbury Breccias (e.g., Rousell et al., 2003; Thompson and Spray, 1994), and overlying fallback and phreatic volcanic breccias of the Onaping Formation and basin-fill sediments of the Chelmsford and Onwatin Formations (Fig. 1).

The SIC comprises a Main Mass of mesocumulates and granopyric residue and associated inclusion- and sulfide-bearing radial and concentric quartz dioritic dikes, a discontinuous lower layer of inclusion-rich and sulfide-bearing noritic rock (Sublayer) and Footwall Breccias, and overlying suevitic and phreatic breccias of the Onaping Formation (see reviews by Farrow and Lightfoot, 2002; Ames and Farrow, 2007 and references therein).

The Main Mass of the SIC comprises an upper layer of fine-grained granite and micropegmatite with well-developed granophyric textures, a transitional zone of Fe-Ti-oxide bearing quartz gabbro, and a lower layer of felsic/mafic/quartz-rich norite, and is interpreted to represent a differentiated impact melt sheet. Within the footwall rocks of the SIC are irregular zones of cataclastic/pseudotachylitic breccia known as Sudbury Breccia.

The footwall rocks on the 'South Range' of the SIC are clastic metasedimentary and mafic-(felsic) metavolcanic rocks of the 2500-2100 Ma Huronian Supergroup, whereas the footwall rocks on the 'North Range" and 'East Range" of the SIC are granulite facies supracrustal and plutonic rocks of the 2647 +/- 2 Ma Levack Gneiss Complex (Fig. 1). Both have been intruded by 2450 Ma Matachewan dikes, 2490-2470 Ma East Bull Lake Suite mafic-ultramafic intrusions, and 2210-2217 Ma Nipissing Suite mafic-ultramafic intrusions (see review by Ames and Farrow, 2007).

The abundant impact and anatectic breccias, together with other features (e.g., subcircular geometry, shattercones, planar deformation features in quartz, distal impact ejecta: see

review by Grieve et al., 2010) suggest that the SIC was produced by a large meteorite impact (Dietz, 1964) at 1850 Ma (Krogh et al., 1984).

Metamorphic and Structural History

There have been at least three major orogenic events that have affected the Sudbury Igneous Complex (see recent reviews by Riller et al., 2010; Mukwakwami et al., 2011). The Penokean orogeny occurred between 1870 and 1820 Ma, concurrent with the formation of the SIC, and produced greenschist facies metamorphism in the middle of the SIC along with penetrative deformation and greenschist to amphibolite facies metamorphism in the Huronian Supergroup. Evidence for Penokean deformation in the Sudbury area has been largely circumstantial and subsequent deformation events may be responsible for most of the deformation of the SIC (Mukwakwami et al., 2011), although a Penokean date has recently been obtained for a shear zone at the Garson Mine (Mukwakwami et al., submitted).

The Mazatzal-Labradorian orogeny occurred between 1.7 and 1.6 Ga, and caused north-over-south buckling (Mukwakwami et al., 2011) and south-over-north thrust faulting (Bailey et al., 2005; Mukwakwami et al., 2011) of the South Range of the SIC. These orogenic events are believed to have deformed the SIC to its present elliptical shape, but the preservation of original igneous contacts (e.g., undeformed Footwall Breccia, intact thermal aureoles) indicates that they had minimal effect in the North Range. The Grenville orogeny occurred between 1.2-1.0 Ga, but had little effect on the Sudbury Igneous Complex, being responsible only for reactivation of faults that cross-cut the SIC and uplift within the area of the SIC (Card et al., 1984).

In the North Range, where post-emplacement deformation and metamorphism have been minimal, the SIC is bordered by a wide contact metamorphic aureole consisting of (proximal to distal): 1) a zone of partial melting up to 20 m thick, 2) a zone of pyroxene hornfels facies up to 180 m thick, 3) a zone of hornblende hornfels facies up to 900 m thick, and 4) a zone of albite-epidote hornfels up to 1000 m thick (Dressler, 1984; Boast and Spray, 2006).

Ni-Cu-PGE Mineralization

The Ni-Cu-PGE mineralization in the Sudbury Igneous Complex occurs in a range of spatially different, but genetically interrelated environments (adapted from Farrow and Lightfoot, 2002; Farrow et al., 2005; Ames and Farrow, 2007 and references therein):

1) **contact ± footwall systems**

   a) **contact ore systems** occur at or near the base of the Main Mass of the SIC, may or may not be associated with footwall vein systems, and may include the following:

      i) disseminated pyrrhotite-pentlandite-(chalcopyrite) mineralization hosted by Sublayer norite, parts of which are unfractionated relative to average Sudbury ores (~5% Ni_{100}, ~5% Cu_{100}) but which may be internally fractionated into small-scale chalcopyrite-rich and chalcopyrite-poor domains, and parts of which are depleted overall in Ni-Os-Ir-Ru relative to average Sudbury ores

      ii) inclusion-bearing semi-massive pyrrhotite-pentlandite-(chalcopyrite) mineralization localized in embayments along the basal contact of the SIC and in veins within adjacent Footwall breccias, which may be weakly (e.g., Trillabelle) to strongly (e.g., Creighton) fractionated into chalcopyrite-rich and chalcopyrite-poor domains.

   b) **footwall vein systems** occur in footwall rocks, may be connected to (e.g., McCreedy West, Strathcona, Nickel Rim South, Morrison) or apparently disconnected from (e.g., McCreedy East 153) contact ores, are typically hosted by zones of Sudbury breccia, and may include some or all of the following:

      i) thicker (up to 5 m) chalcopyrite-(pentlandite)-(pyrrhotite)-rich sharp-walled veins with narrow (1-2 cm) actinolite-epidote alteration selvedges

      ii) thin (<5 cm, typically <2 cm) bornite-millerite-(chalcopyrite)-(pentlandite)-rich sharp-walled veins and stockworks

      iii) Au-Pt-Pd-Bi-Te-Sb-rich sulfide stockworks and disseminations occurring adjacent to epidote, amphibole, chlorite, carbonate, quartz, and magnetite alteration halos. Platinum-group elements occur as discrete platinum group minerals (e.g. froodite, michenerite, merenskyite)

2) **offset ore systems** occur in quartz diorite dikes or QD-bearing breccia belts and may include some or all of the following:

   a) **dike ore systems** are hosted by radial (e.g., Copper Cliff, Worthington, and Whistle) or concentric (e.g., Hess and Manchester offsets) and occur as elongate pods of coarse disseminated (blebby) to semi-massive mineralization that may be weakly to moderately fractionated

   b) **breccia belt ore systems** are hosted by concentric quartz diorite and Sudbury Breccia belts' (e.g., Frood-Stobie) and occur as elongate pods coarse disseminated (blebby) to semi-massive mineralization that may be weakly to moderately fractionated

Geology of the Levack Embayment

The Levack Embayment is a 2 km-wide (deep) and 7 km-long semi-circular embayment containing Sublayer norite and footwall breccias along the basal contact of the SIC in the northwest part of the Sudbury Structure (Fig. 1).

The footwall rocks in the Levack embayment are part of the 2647±2 Ma Archean Levack Gneiss Complex and consist of: i) migmatitic, quartz diorite to granodiorite gneisses with abundant mafic layers and xenoliths, ii) migmatitic paragneisses, iii) foliated tonalitic and granodioritic intrusions, possibly of anatectic origin, and iv) mafic, ultramafic, and anorthositic intrusions (Card et al., 1984). In this study, the host rocks for the Morrison deposit have been subdivided into felsic gneiss, mafic gneiss, and metagabbro to facilitate integration of mapping and drill core logging done by KGHM International company geologists into this study. The felsic gneisses are likely equivalent to the tonalitic gneisses, quartz diorite gneisses, granodiorite gneisses, and tonolitic and granodioritic intrusions of Card et al. (1984) and Legault et al. (2003). The mafic gneisses are likely equivalent to the migmatitic paragneisses of Card et al. (1984) and the dioritic gneisses and amphibolites of Legault et al. (2003). Metagabbro is a black, fine-grained rock of unknown origin that consists predominantly of plagioclase with minor altered mafic minerals. It may correspond to one of the mafic intrusions described by Card et al. (1984).

The footwall rocks below the Levack Embayment contain numerous semi-conformable zones of Sudbury Breccia, which may also include felsic, often granophyric-textured

cross-cutting dikes and pods that have been ambiguously termed “footwall granophyres”. They are interpreted to be partial melts generated from the heat of the SIC (e.g., Molnár et al., 2001; Péntek et al., 2009) or residual silicate melts from the crystallizing SIC (Hanley et al., 2011).

LEVACK-MORRISON SYSTEM

The Levack-Morrison system is located in the west-central part of the Levack Embayment (Fig. 1) and includes the Levack Main, Intermediate, Main Depths, No. 1, No. 2, No. 3, and No. 7 contact deposits, and the Morrison footwall deposit (Fig. 2). The Levack Main deposit was discovered in 1887 (first deposit discovered on the North Range) and the Levack contact deposits were mined between 1915-1929 and 1935-1997. The Morrison deposit was discovered in 2005 and is located ~150 metres below the Levack No. 7 deposit (Fig. 2). It has a strike length of greater than 75 m and extends for over 750 m parallel to the hanging wall side of a NE-SW striking, steeply-dipping (i.e., discordant) zone of Sudbury Breccia (Farrow et al., 2009).

The Morrison deposit was originally divided into two deposits, an upper Rob’s deposit and a lower Levack Footwall deposit (LFD). These two deposits were eventually shown to be continuous and in 2010 were renamed the Morrison deposit, in honour of former Inco exploration geologist and current KGHM International Executive Gord Morrison, and subdivided into three zones (from top to bottom: MD1 to MD3). The indicated resource as of December 2010 is 670000 tonnes at 2.74% Ni, 13.24% Cu, and 9.28 g/ton Pt+Pd+Au (QuadraFNX Mining Ltd., 2011).

Previous work by Farrow et al. (2009) demonstrated that the uppermost part of the deposit (MD1: formerly Rob’s deposit) consists of pods, veins, veinlets, and disseminations of pyrrhotite with lesser pentlandite, chalcopyrite, and pyrite. The lower parts of the deposit (MD2-3: former LFD) consists of veins and disseminations of chalcopyrite with lesser cubanite, pentlandite, bornite, and millerite. The veins become wider and more continuous with depth and the vein geometries have been interpreted to be influenced by the distribution of clasts within the host Sudbury breccia (Farrow et al., 2009).

This study has divided the Morrison deposit into three domains based on mineralogical, textural, and geochemical differences (Fig. 2): 1) a 400 m thick Cu-poor *upper domain*, equivalent to MD1 (former Rob's zone), 2) a 450 m thick Cu-intermediate and PM-depleted *middle domain*, equivalent to MD2, and 3) a 700 m thick Cu-rich *lower domain*, equivalent to MD3.

RESEARCH METHODS

Sample Collection from Underground Workings

Forty-one samples from 14 mine levels were collected. A significant effort was made to ensure that an accurate representation of ore types was collected. Wherever possible, samples were taken directly from active mine faces. These samples were preferable because they were not oxidized and had not accumulated dust from previous blasting and mining, so the field relationships were clearer. For veins narrower than approximately 50 cm, a continuous sample across the vein was taken where possible and a chip sample was taken when a continuous sample was not possible. For larger veins, the veins were subdivided into 2 to 4 segments and chip samples were taken for each segment. Where a fresh face could not be sampled, chip samples were taken from the stope back through the 4" x 4" protective screening or from the stope wall.

The focus on active mine faces ensured the best exposure and the freshest samples, but mine production schedules precluded detailed mapping. Each locality was photographed from multiple angles and at multiple scales, and detailed descriptions were made of the vein morphology and wall rocks where each sample was collected.

Sample Preparation

Each sample analyzed for geochemistry was thoroughly cleaned using water and a nylon brush, and sawed using a diamond-impregnated brass blade to remove any contamination and oxidation. The saw marks from all sawn surfaces were ground off using a diamond-bonded steel grinding lap to ensure there would be no contamination from the saw blade. Each sample was dried in air at low temperature, crushed with a jaw crusher containing case-hardened low-Cr steel plates, split using a stainless steel riffle splitter, pulverized in

agate ball mills, and analyzed at the Ontario Geoscience Laboratories (Geo Labs) in the Willet Green Miller Centre on the Laurentian University campus in Sudbury, Ontario.

Petrography

Each sample to be analyzed was examined macroscopically using a binocular microscope and microscopically using a compound petrographic microscope with plane-polarized and doubly-polarized reflected light and, when appropriate, plane-polarized and doubly-polarized transmitted light, to derive mineralogical and textural information relevant to their petrogenesis.

Structural Analysis

The strike, length, and width of 925 planar vein segments were measured on KGHM International maps of 9 levels (Upper domain: 2950L cuts 1 and 2, 3030L cut 1, 3050L cut 1, 3180L cut 1; Middle domain: 3330L cut 3, 3390L cut 1, 3630L cut 2; Lower domain: 3750L cut 3) using AutoCAD® 2010 software. Of these, 492 were in the upper domain, 295 were in the middle domain, and 138 were in the lower domain.

Because of the extent of mining activities during the time this analysis was completed, the information from only one level of the lower domain was available, so those results should be considered only preliminary. Another problem with this method of analysis is that because not every vein has a vertical dip, the width measured from the level plans does not necessarily represent the true vein width. The large number of vein segments measured, combined with the large variation in the widths of the veins, means that any variability created by not correcting for true width is minimal compared to the natural variation at the deposit. This method still has merit in examining the general trends in the deposit and providing a general idea about the orientation of the veins that contain the majority of mineralization.

Whole-Rock Geochemical Analysis

All analyses were done at Geoscience Laboratories in Sudbury, Ontario, Canada. Copper, Ni, Zn, and Fe were analyzed by inductively-coupled plasma atomic emission spectrometry after dissolution in an open vessel multi-acid digest. Cobalt and Zn were analyzed by flame atomic absorption spectroscopy (F-AAS). Arsenic, Bi, Pb, Te, Se, Sn,

and Co for one sample (that was under the lower limit of detection for F-AAS), were analyzed by inductively-coupled plasma mass spectrometry (ICP-MS) after dissolution in aqua regia. Lead for one sample was analyzed by wavelength-dispersive X-ray fluorescence spectrometry of a pressed powder pellet, as it was well above the maximum concentration limit for ICP-MS analysis. Gold, Pd, Pt, Rh, Ru, and Ir were preconcentrated by NiS fire assay, dissolved in acid, co-precipitated with Te, and analyzed by ICP-MS. Sulfur was analyzed by infrared absorption spectroscopy using a Leco® TGA-501 thermogravimetric analyzer. Lower limits of detection are given in Table EA1.

The samples analyzed for this study and the 58,518 samples in the KGHM International assay database were divided into three types using the method of Stout (2009): I: pyrrhotite-pentlandite-chalcopyrite, IIa: pentlandite-millerite-chalcopyrite, and IIb: millerite-bornite-chalcopyrite. In addition, each type was subdivided into high-S (>10 wt% S in whole-rock analysis) and low-S (<10 wt% S in whole-rock analysis) groups, which correspond to first-order veins and second-order veins, respectively.

100% Sulfide Normalization

Because of the variable amounts of wall rock and gangue minerals in the samples, all geochemical analyses were normalized to 100% sulfide by dividing each sample into pyrrhotite-pentlandite-chalcopyrite (Type I), chalcopyrite-pentlandite-millerite (Type IIa), or bornite-chalcopyrite-millerite (Type IIb) assemblages based on the Ni, Cu, and S contents, and the abundances of those phases were determined based on stoichiometric (chalcopyrite, bornite, millerite) or analyzed (pentlandite) mineral compositions. The method is summarized in Tables A1 and A2 and described in the Appendix to this paper.

Mineral Analysis

Pentlandite and pyrrhotite in representative samples was analyzed in situ by wavelength-dispersive or energy-dispersive X-ray emission spectrometry using a Cameca SX-100 electron probe microanalyser in the Ontario Geoscience Laboratories. For pentlandite, Ni and Fe were analyzed with a large LiF (LLiF) crystal and beam current of 30 nA, S was analysed with a PET crystal and a beam current of 30nA, and Co and Cu were analyzed with a LLiF crystal and a beam current of 200 nA. For pyrrhotite, S was analyzed with a

PET crystal and a beam current of 30nA, Fe was analyzed with a LiF crystal and a beam current of 30 nA, Co was analyzed with a LiF crystal and a beam current of 200 nA, and Ni was analyzed with a LLiF cystal with a beam current of 200 nA. A count time of 20 seconds and an accelerating voltage of 20 keV was used for all analyses. Raw data were corrected using the Cameca PAP correction routine by David Crabtree of the Geoscience Laboratories.

Four samples were examined for platinum group minerals using a Zeiss EVO-50 scanning electron microscope equipped with a thin window energy-dispersive X-ray spectrometer. No standards were used and only qualitative EDS results are therefore discussed.

RESULTS

Styles of Mineralization

The styles of mineralization in the Morrison deposit vary considerably, but can be broken down into three end-member types: I) steeply- to vertically-dipping first-order sulfide veins, II) irregular and discontinuous second-order sulfide and/or silicate veins, and III) associated disseminated mineralization within the country rocks. These generally correspond to the three types of mineralization recognized by Stout (2009) in the McCreedy East 153 deposit. First- and second-order veins can be further subdivided into a) inclusion-free veins with planar margins that occur typically within Sudbury breccia matrix or along clast-matrix boundaries, and b) irregular and inclusion-bearing veins within felsic domains such as leucosomes of mafic gneiss clasts and felsic granophyric-textured dykes. Disseminated mineralization also generally occurs in felsic domains (felsic gneisses, leucosomes, granophyric-textured dykes) close to first- and second-order veins.

The styles of mineralization are similar in the upper and middle domains, whereas the styles in the Lower domain are quite different. The types of mineralization are summarized in Table 1 and described below.

Upper Domain

Veins in the upper and middle domains are typically narrower and more irregular than in the lower domain. The majority of the veins are inclusion-bearing and have sharp but

irregular margins. The widths and the orientations of the veins change over a distance of meters, especially within second-order veins. Inclusion-free, planar-margined veins are rare in the Upper Domain. Where observed, they occur within areas containing a high proportion of Sudbury breccia matrix (Fig. 3A). Irregular and inclusion-rich veins are most abundant in areas with a high proportion of mafic gneiss clasts and the veins are generally confined to the leucosomes of these mafic gneiss clasts (Fig. 3B). In some places the entire leucosome has been replaced with sulfide, but in other places disseminations or patches of sulfides occur within the original leucosome. Where mineralization associated with granophyric textured dykes occurs in Sudbury breccia matrix-rich areas it is quite irregular. Where mineralization associated with granophyric textured dykes occurs in clast-rich areas, it is present along clast-matrix contacts and rarely within the actual clasts (Fig. 3C). Where the mineralization does occur within a clast, it is typically along a weakness such as a pre-existing contact in the clast. In some sulfide veins associated with leucosomes and granophyric textured dykes, the mineralogy grades from pyrrhotite-rich, through chalcopyrite-rich and locally into non-mineralized leucosome or dyke, all over distances of roughly 10 cm to 100 cm (Fig. 3D).

Middle Domain

Veins in the middle domain are slightly wider than in the upper domain and the increase in width occurs gradually with increasing depth. The only other observed difference between the upper and middle domains is that the middle domain contains small areas of abundant chlorite, actinolite, epidote, and carbonate, and localized magnetite associated with millerite-bearing second order veins and disseminations (see Mineralogy and Textures).

Lower Domain

In contrast to the veins from the upper and middle domains, the veins in the lower domain are dominantly wide, inclusion-free, and planar margined. The veins are quite regular, often disect felsic gneiss clasts, and also occur along clast-matrix boundaries. The margins of the first-order veins commonly contain splays of sulfide that protrude into the wall rock and locally contain splays of wall rock that are oriented sub-parallel to the vein margins (Fig. 3E). Second-order veins vary from containing predominantly sulfide

minerals to predominantly epidote, amphibole, and chlorite with minor sulfides, carbonate, and magnetite. The lower domain is the only area where sharp-walled amphibole and epidote veins with only minor sulfide minerals were observed in this study. In the rare areas with mafic gneiss clasts, second-order sulfide veins and disseminations of sulfides occur within leucosomes and granophyric textured felsic dykes/patches. These dykes are much smaller than in the upper and middle domains and are often confined to mafic gneiss leucosomes (Fig. 3F).

Metal Distribution

Published resource estimates and historically mined resources from Farrow et al. (2009) and QuadraFNX Mining Ltd. (2011) for the deposits of the Levack mine were analysed to examine the distribution of Cu and Ni within the Levack-Morrison system. The results of this analysis are presented in Table 2.

Structural Geology

Overview

The Morrison deposit consists of two structural domains with different geometries: an upper structural domain that plunges steeply to the northeast, markedly oblique to the overlying SIC basal contact, and a lower structural domain that plunges shallowly to the southwest, subparallel to the overlying SIC basal contact. The inflection occurs at the boundary between the middle domain and the lower domain. Although the structural domains appear to have well-defined orientations, first-order veins have somewhat variable strikes and steep to vertical dips, and second-order veins are extremely variable in both strike and dip.

If the area of the vein segments is not considered, the distribution of vein strikes is more-or-less random in the upper domain, shows a preference for NW-SE strikes (parallel to SIC basal contact) in the middle domain, and shows a preference for NNE-SSW strikes in the lower domain. If the veins are weighted by area (measured length multiplied by measured width), two dominant strikes of roughly 025^{o} and 060^{o} and one minor strike of 360^{o} are evident (Fig. 4). The upper domain contains veins in all three orientations, but the middle and lower domains are dominated by veins in the 025^{o} and 060^{o} orientations. Taken together, this means that the 025^{o} orientation is predominant, the upper domain

contains the widest range of vein orientations, the middle domain contains the most consistently-oriented veins (NE-SW, subparallel to the SIC basal contact), and the lower domain contains differently oriented large (020 ^{o} and 060^{o}) and small (330^{o}) veins.

Sudbury Breccia Morphology

The size, shape, and distribution of clasts within the Sudbury Breccia are extremely variable. Sudbury Breccia in close proximity and direct contact with sulfide mineralization varies from being matrix-rich with minor and typically rounded clasts to being clast-rich with in-situ brecciated clasts with the matrix occurring as veins between the clasts. In clast-rich areas, veins of Sudbury breccia matrix sometimes occur as multiple linked segments. Where these segments link, there are localized splays of the clasts in the veins of matrix material (Fig. 3C). There appears to be a higher proportion of mafic gneiss clasts in the upper and middle domains and a higher proportion of felsic gneiss clasts in the lower domain.

Mineralogy and Textures

Pyrrhotite and pentlandite occur as different morphologies throughout the deposit. Pentlandite types are summarized in Table 2 and pyrrhotite types are summarized in Table 3. The mineralogy and textures of the upper, middle, and lower domains are summarized in Table 4 and discussed below.

Textural Changes in Pyrrhotite-Pentlandite-Chalcopyrite-(Cubanite) Veins

In addition to the information in Table 4, the major features of Type I pyrrhotite-pentlandite-chalcopyrite-(cubanite) veins are as follows:

1) The abundance of chalcopyrite increases with depth. In the upper and middle domains, this increase corresponds to an increase in the domains of chalcopyrite and Po(II). In the Lower Domain, Po(II) domains are no longer present and chalcopyrite becomes the dominant mineral and typically occurs with cubanite laths.

2) Pyrrhotite in the upper domain contains pentlandite and chalcopyrite exsolution products and therefore is texturally consistent with having formed early. In contrast, the pyrrhotite in the lower domain is texturally one of the last minerals to form. The

timing of the pyrrhotite in the middle domain is less clear, but it appears that there is early Po(Ia) and Po(Ib) and later Po(V).

3) Po(Ia) crystals in the upper and middle domains are sometimes twinned and typically contain preferentially oriented Pn(Ia) flames and chalcopyrite lenses (Fig. 5A). Pn(Ia) flames decrease with depth and the preferentially oriented chalcopyrite lenses do not appear to change in abundance with depth. Pn(Ib) eyes also decrease in abundance with depth. These textures are consistent with those reported by Gregory (2005).

4) Pn(II) eyes are inclusion free at the top of the upper domain and become more inclusion rich with depth. These inclusions contain varying proportions of pyrrhotite and chalcopyrite. They are texturally similar to the pyrrhotite inclusions within poikilitic pentlandite in disseminated mineralization at the Gertrude orebody of the Creighton mine (Dare et al., 2010)

5) Pn(III) eyes in the lower domain are most abundant along vein margins and decrease in abundance, but increase in size in vein interiors.

6) Sphalerite is present as a primary magmatic mineral and is evenly distributed throughout the first-order veins in the lower domain. It occurs only in trace amounts, but is evenly distributed in the upper domain.

Textural Changes in Millerite ± Bornite-Bearing Veins

In addition to the information in Table 4, the major features of the millerite ± bornite-bearing veins are as follows:

1) The texture of millerite is slightly different in second-order millerite-chalcopyrite-pentlandite veins in the middle domain compared to millerite-chalcopyrite-(bornite) veins in the lower domain. Millerite in the middle and lower domains is euhedral, commonly twinned, and contains chalcopyrite or bornite along fractures, cleavage planes, or twinning planes. Millerite in the middle domain does not contain chalcopyrite or bornite along fractures, cleavage planes, or twinning planes.

2) Pn(II) in the middle domain is inclusion free, in contrast with PnII in the pyrrhotite-pentlandite-chalcopyrite-(cubanite) veins in the middle domain.

3) Second-order bornite-rich veins are less common in the study area than chalcopyrite-rich veins. These veins also grade along strike into millerite-rich veins with minor bornite and abundant silicate alteration minerals.

4) Pyrite was identified in only one sample in the middle domain, where it is fractured and corroded with some remaining euhedral grain boundaries, indications that it formed relatively early.

5) Epidote in the middle and lower domains is an early phase that is often highly fractured, with the fractures infiltrated by varying amounts of chalcopyrite, pentlandite, chlorite, actinolite, and carbonate (Fig. 5F). Chlorite occurs as irregular chlorite rosettes. Actinolite occurs as small acicular crystals and postdates the epidote. Carbonate occurs as subhedral crystals that are often strongly twinned.

Platinum Group Minerals (PGM) and Accessory Minerals

The only observed PGMs in first-order upper domain veins were Pt- and Te-rich moncheite $(Pt,Pd)(Te,Bi)_2$ that occurred along pyrrhotite grain boundaries. No first-order veins from the middle domain were analyzed.

PGM and accessory minerals identified in the first-order veins of the lower domain include paolovite Pd_2Sn and moncheite, both of which occur within chalcopyrite and PoIII, hessite Ag_2Te, altaite PbTe, and Se-bearing galena. Moncheite in the lower domain is more Pd- and Bi-rich compared to moncheite in the upper domain. Hessite, altaite, and Se-bearing galena generally occur as evenly distributed, discrete, and isolated grains within chalcopyrite and pyrrhotite, but one compound grain of hessite, altaitie, and moncheite was found.

The PGM identified in a second-order vein in the middle domain containing chalcopyrite-millerite-pentlandite irregular vein surrounded by amphibole, epidote, chlorite and calcite alteration were sperrylite $PtAs_2$ and merenskyite $Pd(Te,Bi)_2$. These PGM were hosted both in the sulfide and adjacent to the sulfides. For the PGM surrounding the sulfides, it is unclear whether they were actually in the surrounding silicates or within/adjacent to sulfides that are not in the plane of the thin-sections.

Mineralogy and Textures of Inclusions and Adjacent Wallrock

Inclusion-bearing sulfide veins contain inclusions of all host lithologies. The majority of the inclusions occur in chalcopyrite-rich portions of the veins or are rimmed by chalcopyrite (Fig 6B). In general, the inclusions consist mainly of varying amounts of plagioclase, quartz, biotite, chlorite, magnetite, and minor actinolite.

In the more plagioclase-rich inclusions, there tends to be a higher abundance of anhedral chlorite acicular actinolite and magnetite at the contact between the sulfide and the inclusion. In more quartz-rich inclusions, sulfides sometimes occur along grain boundaries and fractures within quartz. There are generally less hydrous silicates at the margins of these inclusions.

Rarely, inclusions grade from areas of granophyric intergrowths of quartz and alkali feldspar through areas of euhedral plagioclase surrounded by optically continuous patches of quartz (referred to as "flood quartz" by Morrison et al., 1994) into areas of euhedral quartz and plagioclase. Where sulfide veins are associated with granophryic textured dykes, the inclusions are mainly granophryic intergrowths of quartz and alkali feldspar. The feldspar is sometimes altered to fine grained chlorite. These inclusions have irregular concave and convex margins and are generally both surrounded by chalcopyrite and absent from any large domains that contain PoIa (Fig. 6B).

Both the adjacent wallrock and the vein inclusions contain textures that differ from the host rock that is more distal to the veins. The grain boundaries of euhedral quartz are often occupied by a thin film of plagioclase and the triple junctions are sometimes occupied by chalcopyrite (Fig. 7D). The plagioclase films are typically only 10-30 microns thick, but are sometimes thick enough to exhibit polysynthetic twinning (Fig 7A and 7B). Zones of poikiolitic quartz and occasionally zones of poikiolitic plagioclase occur surrounding polygonal plagioclase. Poikilitic magnetite rarely occurs surrounding polygonal plagioclase. Large polysynthetic laths of plagioclase are present and surrounded by optically continuous quartz patches. All these textures occur in close proximity to each other and sometimes occur adjacent to granophryic textured quartz and feldspar (Fig. 7C).

Whole Rock Geochemistry

Spatial Trends

The ores in the Morrison deposit vary in composition both laterally and with increasing depth. The focus of this study was on the changes that occur in first-order veins with depth, so those changes are better constrained than the lateral changes within the deposit or changes that occur in second-order veins with depth.

The trends in Cu, Ni, Pt, Pd, and Ag in the samples analyzed in this study correlate very well with those in the KGHM International database, which means that the values in the database can be used with confidence to define broader spatial variations. However, the detection limits for Au, Zn, and Co in the KGHM International database are too high to provide precise data for all areas of the Morrison deposit and for weakly mineralized samples. Ir, Te, Bi, Sn, and As were only analyzed in the samples collected for this study, so the variations in those elements are only based on a limited number of samples.

The grades (metal abundances in the whole-rock sample) and tenors (metal abundances in 100% sulfides, as described in the Appendix and designated as Me_{100}) of the samples analyzed in this study are given in Tables EA1 and EA2. The distribution of the different mineralization types is shown in Fig 9. Variations of Co_{100}, Ni_{100}, Cu_{100}, Zn_{100}, Pd_{100}, Ag_{100}, Pt_{100}, and Au_{100} with depth are shown in Fig. 10 and variations of As_{100}, Se_{100}, Rh_{100}, Sn_{100}, Te_{100}, Ir_{100}, Pb_{100}, and Bi_{100} with depth are shown in Fig. 11. The spatial trends are shown in Tables 5 and 6.

Sn_{100}, Te_{100}, Bi_{100}, As_{100}, Pb_{100}, Se_{100}, Ir_{100}, and Rh_{100} were only analyzed in hand samples so their variation can only be described from the bottom of the upper domain to the top of the lower domain. Sn_{100}, Te_{100}, Bi_{100}, As_{100}, Se_{100}, and Pb_{100} all decrease in the middle domain and then increase at the top of the lower domain. Their behaviour is similar to Pt_{100} and Pd_{100}. Both Pb_{100} and Bi_{100} are quite variable so the trends are not as pronounced as those of Sn_{100} and Te_{100}. Ir_{100} and Rh both decrease from the bottom of the lower domain to the top of the upper domain. It is unclear whether Ir_{100} and Rh_{100} increase or decrease in the lower domain.

Variations with S and Cu_{100}

Variations of Co, Ni, Zn, Pd, Ag, Pt, and Au with S are shown in Fig. EA1 (Electronic Appendix). All elements correlate strongly with S, indicating that they are hosted in sulfides or phases that exsolved from sulfides.

Cu tenor (Cu_{100}) is a good indicator of sulfide fractionation. Variations of Co_{100}, Ni_{100}, Zn_{100}, Pd_{100}, Ag_{100}, Pt_{100}, and Au_{100} with Cu_{100} are shown in Fig. 12 and variations of As_{100}, Se_{100}, Rh_{100}, Sn_{100}, Te_{100}, Ir_{100}, Pb_{100}, and Bi_{100} with Cu_{100} are shown in Fig. 13

When interpreting the geochemical variations in grab and assay samples, the following complications must be considered:

1) The channel samples of larger (Type I) veins normally did not include wall rocks, which contain numerous fine veinlets and disseminations and which were difficult to sample consistently, whereas grab samples of smaller (Type II) veins included parts of the wall rocks. This explains, at least in part, why Type II samples from the middle domain, which sampled weakly-mineralized wallrock and epidote-amphibole-rich areas, are more enriched in Au-Pt-Pd-Bi-Te-Se-Ag than Type I veins from the same area.

2) The same applies to routine assay sampling, where adjacent weakly-mineralized wall rocks (more likely to contain higher amounts of Au-Pt-Pd-Ag) were typically sampled separately from massive sulfide veins (more likely to contain lower amounts of those elements). This explains why low-S samples are uniformly more enriched in Au-Pt-Pd-Ag than high-S samples.

3) Another complication noted by Stout (2009) is that minor components progressively exsolve from higher-T phases as they cool (e.g., chalcopyrite and pentlandite from MSS, pyrrhotite and pentlandite from ISS, PGM from sulfides), so ores inevitably become increasingly more heterogeneous, and hand samples and drill core samples inevitably sample only subdomains of original melt and cumulate components. This is particularly true of drill core samples through zoned veins, which may sample the entire width of a vein, including core and marginal phases in their proper proportions, but which may also intersect disproportionate amounts of discontinuous marginal or core phases depending on the scale of the heterogeneities and the orientations of the vein and drill hole. Many of the very high Ni_{100} and very low Cu_{100} assays therefore

represent not only unmixing of high-T pentlandite-chalcopyrite and bornite-millerite (Naldrett et al., 1999; Beswick, 2002), but also sampling of heterogeneous bornite-millerite veins.

4) Plots involving large numbers of samples cannot adequately represent masses. It is obvious that the Levack-Morrison database is bimodal, but because so many samples plot on top of each other it is not obvious that 47% of the samples plot within the low-Cu cluster (<10% Cu_{100}, <10% Ni_{100}), 41% of the samples plot within the high-Cu cluster (10-35% Cu_{100}, <10% Ni_{100}), and 12% of the samples plot between the Ccp-Pn and Bn-Ml tie lines. Histograms better represent the mass balances, but are one-dimensional.

Mineral Chemistry

Pyrrhotite and pentlandite were analyzed in four representative samples from the bottom of the upper domain (3050L-1, 3050L-2), the middle domain (3510L), and the top of the lower domain (3810L). All analyzed samples are from first-order veins. In sample 3050L-1 the PnIa was too small to analyze so all the pentlandite analyses are from Type Ib, and -II pentlandite. No pentlandite was analyzed in millerite-bearing samples. The analyses for pyrrhotite and pentlandite are given in Table 7 and the key points are summarized below.

The compositions of pyrrhotite and pentlandite are relatively constant within samples, but are very different between the different samples analyzed. Ni contents of pyrrhotite decrease and Fe contents increase with depth. There is no change in the S content between the 3050-1L, 3050-2L, and 3510L level samples, but contents decrease between the 3510L and 3810L samples (Fig 13). The majority of Co analyses were below the 0.026 wt% detection limit. The compositional changes in the pentlandite are less straightforward than the changes in pyrrhotite. Ni contents decrease and Fe contents increase with depth in the deposit and there is a strong linear correlation between the Ni and Fe content. Cobalt content is the lowest in the 3050-1L and 3050-2L samples, highest in the 3510L sample and intermediate in the 3810L sample (Fig. 14 and 15).

DISCUSSION

As noted above, four principal models have been proposed for the Cu-PPGE-Au-rich nature of Sudbury footwall ores: 1) fractional crystallization of MSS ± ISS, 2) dynamic remelting of contact ores, 3) hydrothermal mobilization from contact ores, and 4) thermal diffusion.

Diffusion models have been discussed by Naldrett and Kullerud (1967), Keays and Crocket (1970), and Naldrett et al. (1982). They have not been evaluated experimentally in S-rich systems, but in systems containing 75% Fe, 10% Ni, 1% Cu, and 15% S (Brenan et al., 2010) S and Cu diffuse toward the hotter end of the system, Fe and highly siderophile elements diffuse toward the cooler end of the system in the order Pd-Au > Rh > Ru-Pt > Ir-Re-Os, and Ni shows no preference. Analogous results have been obtained in the Fe-Ni-P-S system (Jones and Walker, 1991) and in S, Fe, Ni, and Cu liquid metal systems (Lida and Guthrie, 1988). Although this order corresponds broadly to the fractionation observed in the Morrison and other deposits of this type, natural systems have higher Fe and Ni at higher temperatures and higher Pt at lower temperatures. So, although more experiments on relevant sulfide compositions are needed to better evaluate the role of diffusion, it does not appear that diffusion is the primary control on Fe, Cu, or Pt contents.

Hydrothermal models have been discussed by Farrow and Watkinson (1992, 1996, 1997), Farrow (1994), Watkinson (1994), Farrow et al. (1994), Marshall (1999), and Molnar et al. (1997, 2001). They are based on the presence of hydrous silicates (actinolite, epidote, chlorite) along veins margins and a preferential association of PGM with hydrous silicates. Although there is evidence for hydrothermal fluids *modifying* the ores in the Morrison deposit (see below), there are many problems with hydrothermal fluids *generating* any of the ores in the Morrison deposit:

1) Low-S samples (dangling veinlets and stockworks) in the upper and middle domains are systematically enriched in Pd-Pt-Au-Ag, unenriched in Co, and depleted in Ni relative to high-S samples (backbone veins). It might be argued that this is a hydrothermal signature, but these elements are not systematically different in low-S and high-S samples in the lower zone. These trends are more consistent with

magmatic fractionation within domains than with hydrothermal mobilization within or between domains.

2) The association of PGM with hydrous alteration minerals along the margins of the veins does not mean that they were deposited by hydrothermal fluids. PGMs may crystallize from low-T residual Au,Pt, Pd, Bi Sb-rich melts (e.g., Makovicky, 2002; Hanley, 2005, 2007; Helmy et al., 2005, 2007, 2010; Tomkins, 2010; see review by Holwell and McDonald, 2010) and/or exsolve from sulfides during cooling (Peregoedova and Ohnenstetter, 2002), so they are expected to occur along the margins of sulfides and silicates in any case.

3) The alteration selvedges along the veins are uniformly thin with no correlation to vein thickness, and are present at the contacts between massive sulfides and wall rocks in most magmatic Ni-Ci-PGE deposits, even volcanic deposits like Kambalda (Western Australia) and Raglan (Nunavut) where hydrothermal process played an insignificant role in ore genesis. They represent magmatic and/or metamorphic reaction between sulfides and wall rocks, and may have had a role in modifying the compositions of Bn-Ml-rich veins (see below), but do not appear to have been generated by a convective hydrothermal system.

4) If the heat and metal sources were the SIC, any fluids in the footwall (conate and/or generated by dehydration of footwall rocks) should remain ponded near the base of the SIC, not convect deeper into the footwall. These fluids facilitated partial melting and the formation of granophyric segregations and epidote-chlorite-actinolite-carbonate veins, but these zones are all cross-cut by Type I and Type II sulfide veins.

5) Although the wall rocks are altered to varying degrees, the alteration is not nearly as pervasive as in porphyry Cu, VMS, and lode Au deposits where metals have clearly been deposited from hydrothermal fluids, suggesting overall very low fluid:rock ratios and therefore little capacity to carry metals. For example, the solubility of Cu in a porphyry Cu fluid is of the order of 1000 ppm, so even assuming 100% depositional efficiency, deposition of 300-400 Ktons of Cu (amount of Cu in Strathcona Deep, McCreedy East 153, and Nickel Rim South footwall deposits) would require 300-400 Mtons of fluid and deposition of 67 Ktons of Cu (amount of Cu in Morrison) would

require 67 Mtons of fluid. Hanley et al. (2011) showed that the Cu contents of the highest temperature fluids in the footwall systems, which would have had the greatest capacity to dissolve and precipitate metals, were <100 ppm, which would require more than an order of magnitude more fluid.

6) The order of solubility of metals in hydrothermal fluids varies with the ligand(s) present (e.g., Cl^- vs. HS^-), fS_2 and fO_2, temperature and pH (e.g., Wood, 2002; Hanley, 2005) and few detailed studies have been done in magmatic Fe-Ni-Cu-(PGE) systems, but appears to be Pd > Au > Fe > Zn > Cu > Ni-Co >>> Ir (e.g., Lesher and Keays, 1984, 2002), which does not correspond to the observed zonation. Although footwall ores contain minor pyrite, the amounts are insignificant compared to those in porphyry Cu-Au, VMS Cu-Zn-Au, or lode Au systems where the metals have been deposited from high-T hydrothermal fluids.

7) Although Fe-Cu-Au-Pt-Pd are soluble in hydrothermal fluids, Ni-Co-Rh-Ru-Ir appear to be much less soluble (e.g., Lesher and Keays, 1984; Wood, 2002; Hanley, 2005). Rh-Ru-Ir are depleted in the deeper and distal parts of the system, but they are not as depleted as PGE mineralization known to have been deposited from or modified by hydrothermal fluids (e.g., Lesher and Keays, 1984; 2002; Hinchey and Hattori, 2005; Su and Lesher, 2012).

8) The reduction potentials for Au, Pt, and Pd are quite different, so their solubilities are normally quite different (see reviews by Wood, 2002; Hanley, 2005), but Pd and Pt are only locally decoupled at Morrison: both are enriched in the lower domain, depleted in the middle domain, and enriched in low-S samples compared to high-S samples – all consistent with fractional crystallization but coincidental if they were transported by hydrothermal fluids.

9) A better case can be made for Type III stockworks and disseminations, which involve much smaller amounts of metals, are associated with larger amounts of wall-rock alteration (Farrow et al., 2005), and occur in 'blind' disseminations that are more likely to have formed from very low viscosity supercritical hydrothermal fluids than sulfide melts. However, the coherent behaviour of Au-Pt-Pd-Bi-Te-Sb in these

systems is more consistent with them being mobilized by late-stage semimetal-rich melts than by hydrothermal fluids.

Taken together, these points do not support a major role for hydrothermal processes in the formation of Sudbury Type I Ccp-rich veins and stockworks and Type II Bn-Ml veins and stockworks.

Fractional crystallization of MSS ± ISS: Fractional crystallization models have been discussed by Hawley (1965), Keays and Crocket (1970), Li et al. (1992), Ebel and Naldrett (1996), and Naldrett et al. (1999). They are based on experimental (e.g. Li et al., 1996; Barnes et al., 1997) and empirical (e.g. Li et al., 1992) studies showing that Fe-Co-Ir-Os-Ru-Rh partition into MSS and that Cu-Pt-Pd-Au-As-Sb-Bi-Te-Se partition into residual sulfide melt. Ni appears to be less compatible in MSS at higher temperatures and S contents, but more compatible in MSS at lower temperatures and S contents (Li et al., 1996). Although most of the observed fractionation trends in the Morrison deposit (and other deposits) are broadly consistent with fractional or equilibrium crystallization of MSS and ISS (see below), there are several problems with this process producing all of the variations:

1) There is a thermal minimum (divide) in the Fe-Cu-S system (Fig. 18) that prevents sulfide melts originating on the Fe-rich, Cu-poor side of the system (like those at Sudbury) from crystallizing significant amounts of BorniteSS (Tsujimura and Kitakaze, 2004).

2) Geochemical trends (described above) and fractional crystallization models (described below) indicate that ~85% fractional crystallization of MSS is required to produce a liquid with >25 wt% Cu. If any liquid is trapped within the MSS cumulates, then the percentage of required fractional crystallization increases significantly.

3) Fractional crystallization also requires that the sulfide melt be able to form massive chalcopyrite veins in large parts of the system, but ISS does not appear to crystallize until the melts reach ~32 wt% Cu.

Dynamic Remelting: Dynamic remelting has been discussed by Lesher et al. (2008, 2009). It involves injection of sulfide melts into the footwall, high-degree (but incomplete) remelting during thermomechanical erosion of the footwall rocks, and incorporation of

residual MSS into Sublayer (which is depleted in Cu-PPGE-Au relative to the Sudbury average and locally up to 500m thick). This produces Cu-PPGE-Au-enriched sulfide melts and solves the mass balance problem (which is more of an issue in other systems than the Morrison system) by increasing the Cu-PPGE-Au contents of the sulfide melt before it enters the deep footwall. However, remelting (along the contact) followed by fractional crystallization of MSS±ISS (during emplacement of footwall systems) cannot drive the composition across the thermal divide and account for the crystallization of significant amounts of bornite and millerite.

Wallrock Interaction: The solution to the latter problem is that formation of bornite and millerite occurred as a consequence of high-T reaction of fractionated sulfide melts with the wall rocks. Transfer of Fe from the sulfide melt to the wall rocks would form Fe-rich reaction selvedges consisting of minerals such as epidote, actinolite, chlorite and magnetite and drive the sulfide melt composition across the thermal minimum into the part of the system where bornite and millerite could crystallize alone or together (Fig. 19). Only thinner veins would lose significant enough amounts of Fe, explaining why thicker veins contain bornite and/or millerite only along their margins and why thinner veins are more likely to be composed entirely of bornite and/or millerite.

Before discussing these points in more detail, it is important to examine some of the other constraints.

Mechanism of Vein Emplacement

Structural data provide an independent method of determining the feasibility of fractional crystallization of a sulfide melt.

The close confinement of footwall deposits to an enclosing zone of Sudbury Breccia indicates that the aphanitic isotropic nature of the breccia facilitated fracturing prior to or during sulfide emplacement. The importance of Sudbury Breccia as a host is underscored by the subperpendicular orientation of the upper and middle domains of the Morrison deposit (if rotated back to its original horizontal orientation: Golightly, 1994; Grieve, 1994) and its enclosing Sudbury Breccia unit, and the subparallel orientations of the lower domain of the Morrison deposit and the McCreedy East 153, McCreedy West, and Nickel Rim South footwall deposits and their enclosing Sudbury Breccia units.

The restriction of Type I (Ccp-rich) and II (Bn-Ml-rich) footwall deposits to within 400 m of the basal contact of the SIC suggests that their emplacement was roughly limited by the location of the 800^{o}C isotherm (e.g., thermal minimum in the Fe-Cu-S system is near 800^{o}C: Tsujimura and Kitakaze, 2004). The presence of Type III ("low-S" Au-Pt-Pd-Bi-Te-Sb-rich) footwall deposits up to 600m from the basal contact suggests that their emplacement may be limited by the location of the 500^{o}C isotherm (e.g., thermal minimum in the Pd-Bi-Te system is 490^{o}C: Hoffman and MacLean, 1976). However, given that the pyroxene hornfels zone (~650-800^{o}C, depending on pressure and composition) is ~200 m wide and the hornblende hornfels zone (~500-650^{o}C depending on pressure and composition) is ~900m wide (Dressler, 1984; Boast and Spray (2006), this leaves much scope for discovery of deeper Type III deposits.

The veins in the Morrison deposit appear to have formed by dilation rather than by replacement. The low intergranular permeability of the Levack Gneiss Complex and Sudbury Breccia, the relatively high viscosity of sulfide melt (lower than a silicate melt, but higher than aqueous fluid), and the inability of sulfide melts to wet pore spaces filled with silicate melt (Rose and Brenan, 2001; Mungall and Su, 2005) indicate that the melt infiltrated by fracture flow rather than porous flow. Unloading caused by thermomechanical erosion of footwall rocks along the contact (see discussion by Prevec and Cawthorn, 2002) and tectonic readjustment of the crater floor may have facilitated infiltration of sulfides into underlying rocks, but the presence of veins filled with sulfide but never quartz diorite melt suggests that flow was driven by density differences rather than by differential stress. The presence of several thicker (backbone) veins and many thinner (dangling) veins suggests that infiltration involved opening of favourably oriented pre-existing structures before new fractures were created in intact rock (see discussion by Cox et al., 2001).

Whether or not sulfide melt fractionates during emplacement depends on the rate of emplacement: if emplacement is slow, there is more opportunity for sulfide melt to cool and fractionate, but if emplacement is fast, there is less opportunity for sulfide melt to cool and fractionateThe systematic geochemical fractionation downward and outward in the system is interpreted to (Figs. 11-12) suggest that emplacement was relatively slow,

and thereby indicative of a passive density-driven rather than active tectonically-driven process.

The lack of a major change in the orientation of the sulfide veins between the upper-middle and lower domains despite the change in overall orientation, from almost vertical to subhorizontal, and the orientations of the veins themselves are inconsistent with the sulfide melt generating fractures and fluid flowing by invasion percolation (see Cox et al., 2001 and reference therein). A sulfide melt at the basal SIC contact would exert a vertical force on the footwall rocks (i.e., maximum compressive stress (σ_1) would be vertical) and any resulting fractures would be either vertical extensional fractures (opening horizontally) or shear fractures with a dip of roughly 60 degrees, depending on the magnitude of the least compressive stress (σ_3) (see Cox and Ruming, 2004 and references therein). Any conjugate pairs of shear fractures would have horizontal intersection lines. Both the vertical orientation of the Morrison deposit sulfide veins and the vertical vein intersection lines suggests that the process creating the necessary dilation for vein emplacement was different from the process that caused the sulfide to fill the dilated space. This geometry is also consistent with a gravitational and thermal control on the movement of sulfide melt. The melt would have initially moved downward due to its greater density relative to its surrounding host rocks. Once the liquid reached a depth where the rocks were too cold to allow further downward movement (~800 ^{o}C isotherm) it would have begun to move roughly horizontally, parallel to whatever isotherm allowed the liquid to remain molten (Lesher et al., 2008, 2009). The upper and middle domains represent the portion of the Morrison deposit where movement of sulfide melt was subvertical (predominantly density-controlled), whereas the lower domain represents the portion where movement was horizontal (primarily thermally-controlled).

It must be noted though that as the sulfide melt moved downward, it would have exerted a force on the wallrock that is proportional to the density difference between the melt and the surrounding wallrock multiplied by the height of the sulfide melt 'column'. If this force is greater than the tensile strength of the wallrock or any healed fractures then tensile fractures would have opened facilitating the flow of sulfide melt into these fractures. This force would increase with depth, which may also explain why the

orientation of the deposit changes from vertical to horizontal in the lower domain (see Solberg et al., 1977 and references therein).

The wall rock splays within some sulfide veins are consistent with the sulfides being emplaced into a series of en echelon fractures that linked together to create the splay. This style of veining is not consistent with a pressurized sulfide melt generating its own fractures, but is consistent with sulfide melt infiltrating pre-existing fractures that were created by high differential stresses (see Cox et al., 2001 and references therein). The decrease in the proportion of Sudbury breccia matrix that occurs at the top of the lower domain along with a decrease in vein size in the middle domain followed by an increase in the lower domain suggests that the permeability of the lower domain was higher than the upper and middle domains.

Pentek et al. (2011) and Hanley (2011) suggested that the close association of footwall veins with felsic granophyric segregations indicates a role for the segregations in structurally and texturally preparing the footwall for vein emplacement. The host rocks in the Upper and Middle Domains of the Morrison deposit are mafic gneiss leucosome > granophyre ~ felsic gneiss > unmodified Sudbury matrix, and in the Lower Domain felsic gneiss > unmodified Sudbury Breccia matrix > mafic gneiss leucosome >> granophyre. This suggests that sulfide veins and granophyric segregations both occur in areas where the footwall rocks were hotter. Greater degrees of contact metamorphism have been observed below embayments in the Cape Smith Belt (Lesher, 2007) and in the Abitibi Greenstone Belt (Houlé et al., 2012), so although not yet mapped, it seems likely that Sudbury embayments are also surrounded by zones of greater contact metamorphism and therefore greater propensity to host footwall vein mineralization.

Mode of Crystallization

Parental Sulfide Melt Composition

The composition of the parental sulfide melt for the Morrison deposit is difficult to estimate. The Sudbury average is ~5% Ni_{100} and ~5% Cu_{100} (e.g., Farrow and Lightfoot, 2002; Naldrett, 2004), but the compositions of Sudbury ores would have varied locally with magma:sulfide mass ratio (R factor: Campbell and Naldrett, 1979) and with the

degree of any dynamic remelting that may have occurred as the SIC continued to erode the footwall rocks and generate Sublayer (Lesher et al., 2008, 2009).

The bulk composition of the Levack-Morrison system, as presently constrained, is of the order of 6.1% Ni_{10} and 4.1% Cu_{10} (Table 2). The bulk composition of the Upper Domain is 5.8% Ni_{10} and 4.2% Cu_{10}, not significantly different. As noted in the Introduction, both have Ni/Cu ratios that are too high to represent parental sulfide melts and most likely contain significant amounts of accumulated MSS.

Our approach has been to use the composition of the bulk Levack-Morrison system and Upper Domain as a target for the first MSS cumulates and to use those Ni and Cu contents to constrain the abundances of the other elements that are required to model the variations in the rest of the Morrison deposit by fractional crystallization of MSS and ISS. This will not prove that fractional crystallization of MSS and ISS are responsible for the variations, but it will allow us to determine if these process are reasonable and if other processes are required.

Crystallization Models

In order to evaluate the fractionation of the ores in the Morrison deposit we have modeled the crystallization of MSS and ISS using a modified version of a finite-difference model developed by J.P. Golightly and C.M. Lesher (unpubl.), in which the compositions of MSS (up until the melt composition reaches 32% Cu) or ISS (beyond that point) in equilibrium with the sulfide melt, calculated using experimentally-determined or estimated MSS/melt and ISS/melt partition coefficients (Table 8), are removed in finite increments. The residual liquid composition is calculated and the process is repeated until the majority of the liquid has crystallized.

MSS/melt partition coefficients vary with temperature and composition (see reviews by Makovicky, 2002; Barnes and Lightfoot, 2005). ISS/melt partition coefficients are less well characterized and have been estimated from the data of Kosyakov and Sinyakova (2010) and modified to fit the trends in the data.

Modeled and observed values are compared in Figures 16 and 17, and the key points are summarized below, focussing first on Type I (thicker veins) mineralization:

Contact Ores: Higher Co-Ni and low Cu-Pt-Pd-Au-Zn are consistent with them representing mixtures of MSS and trapped sulfide melt.

Upper Domain: High Co-Ni and low Pt-Pd-Au-Zn contents are equivalent to the most fractionated modeled MSS values, also suggesting that the upper domain formed from a more fractionated sulfide melt.

Middle Domain: Zn contents are as predicted from enrichment by removal of Zn-poor MSS (not accumulation of ISS). Low Pt-Pd-Au contents of the Middle Domain are not consistent with modelled Fe-MSS, ISS, or sulfide melt values. Using lower $D_{ISS/Melt}$ values for these elements would explain the decrease in these elements, but would not explain the changes in the Pt/Au, Pd/Au, and Pt/Pd ratios.

Lower Domain: The lower Zn and higher Au-Pd-Pt contents of the Lower Domain are consistent with fractional crystallization (not accumulation) of ISS. Ni appears to be initially incompatible in ISS, which is consistent with experimental data (Kosyakov and Sinyakova, 2010).

Low-S Mineralization: Type II veinlets and stockworks mineralization exhibit similar fractionation patterns with depth and simply reflect more extensive fractionation relatively to Type I veins.

Bornite ± Millerite-Rich Veins: The high Cu and Ni contents of these veins, many of which are mono- or bi-mineralic, cannot be explained by ISS fractionation. Although the Ni and Cu contents of these veins vary, the Ir-Rh (compatible in MSS, and immobile in hydrothermal fluids) and Pt-Pd-Au (incompatible in both MSS and ISS, variably mobile in hydrothermal fluids) are similar to chalcopyrite-rich Type I mineralization in the middle and lower domains, suggesting that they are related to Type I mineralization rather than having formed by a hydrothermal fluid. The most reasonable process is through loss of Fe to the wall rocks. Although the precise reaction is not known and must vary with country rock mineralogy and composition, it appears to have involved the breakdown of plagioclase, quartz, and biotite in the wall rocks to form Ca-Fe silicates (actinolite, epidote, chlorite), Fe oxide (magnetite), and Fe-Cu sulfides (bornite).

Hanley and Bray (2009) showed that actinolite-rich veins at Barnet are bordered by bleached zones that are depleted in Fe (17–75% by mass) and Mg (13–86%), and

enriched in Si (4–10%), Na (8–45%), Cl (20–280%), Br (18–176%), and I (38–129%), and Ni (32–247%), but such zones are rare at Morrison. Greater contributions of Fe from wall rocks instead of sulfide melts may explain the greater abundance of chalcopyrite and lower abundance of bornite-millerite at Barnet.

Because bornite contains less sulfur than ISS, the formation of bornite-rich veins by Fe-loss requires a 'sink' for the excess sulfur. The excess sulfur was likely transported by a S-rich vapour (also containing Fe, Cu) (Peregoedova et al., 2006), forming the disseminated pyrite and chalcopyrite that occur in alteration selvages surrounding these veins.

It is unclear whether the reaction between sulfide melt and wall rock occurred when the sulfide was molten or solid, but because the reaction would have occurred more rapidly at higher temperatures and because a melt is more mobile than a solid it is likely that the reaction occurred near the solidus temperature rather than entirely in the subsolidus temperature range.

Although Fe-loss is required to form veins containing predominantly bornite and/or millerite, some of the *minor* bornite and millerite that occurs within chalcopyrite-rich second order veins may have formed by a primary magmatic process. Crystallization of Ni-rich MSS (Ni-MSS) and/or bornite solid solution (BnSS) from the residual metal formed from ISS fractional crystallization may have occurred as ISS, Ni-MSS, and BnSS are the minerals that likely crystallize at the eutectic point of the Cu-Ni-Fe-S system (Li et al., 1992; Ebel and Naldrett, 1996, 1997; Barnes et al., 1997; Peregoedova and Ohnenstetter, 2002 Helmey et al., 2007; Helmy et al., 2010; Sinyakova and Kosyakov, 2009; Kosyakov and Sinyakova, 2010).

Sulfide Accumulation

Mungall (2007) suggested that the footwall ores are MSS-ISS cumulates, but there are several problems with that suggestion:

1) ISS does not crystallize until the sulfide melt reaches ~32% Cu (Dutrizac, 1976; Naldrett et al., 1997), by which point the liquid represents only ~10% of the mass of a

system originally containing 5% Ni_{100} and 5% Cu_{100} (average Sudbury ore) assuming a $D_{ISS/Liquid}$ of 0.2 for Cu.

2) ISS crystallizes from melts of similar composition (Sinyakova and Kosyakov, 2007, 2009; Kosyakov and Sinayakova, 2010), indicating that it need not be a cumulus phase.

3) Zn appears to partition moderately strongly into ISS (Caye et al.,1988), so ISS cumulates should be characterized by high Zn contents. Although Cu-rich ores are enriched in Zn relative to Cu-poor ores (Fig. 16), the amount is consistent with enrichment via fractionation of Zn-poor MSS, not with accumulation of Zn-rich ISS. Only the Lower domain has Zn contents high enough to contain significant amounts of cumulus ISS.

4) Based on the above fractional crystallization model, Pt, Pd, and Au in Type I mineralization in the Lower domain are best explained as a mixture of ISS cumulates and sulfide melt. The $D_{ISS/Liquid}$ for Pt appears to be the same as for MSS, but and the $D_{ISS/Liquid}$ for Pd is slightly higher explaining the increase in the Pd/Pt ratio that occurs in the lower domain.

5) Also based on the above fractional crystallization model, $D_{MSS/Liquid}$ and $D_{ISS/Liquid}$ for Au are similar and lower than both Pt and Pd. As a result of the lower D, the difference between Au in ISS and sulfide liquid is large and the Au/Pt and Au/Pt ratios in the lower domain can only be explained by a mixture of cumulus ISS and sulfide liquid (Fig 17). The lower domain mineralization appears to have formed from a liquid that underwent both fractional and equilibrium crystallization rather than as cumulates and trapped liquid.

Metal Mass Balance

The present spatial distribution of mineralization (Fig. 2) suggests that the Levack No. 7 contact and Morrison footwall deposits are part of the same system and may also be related to the Levack Main contact deposit, but it is not clear how the Morrison deposit is related to the Main Depth, Intermediate, No. 1, No. 2, and No. 3 contact deposits. Total resource data (production + measured + indicated + inferred) for known parts of the Levack-Morrison system are given in Table 2.

Although this compilation allocates all historical production to the Main contact deposit and does not include mineralization below the 1% Ni cut-off grade (i.e., large masses of low-grade Sublayer-hosted mineralization and low-grade footwall mineralization), we may draw several conclusions:

1) Cu/Ni ratio of the total system is 0.70± 0.49 (Table 2), therefore some of the contact ores included in the system are not part of the Morrison system (if they have undiscovered or eroded footwall systems of their own) and/or more footwall mineralization exists that has not been characterised to the level required for a published resource or remains to be found in the Morrison system (if the Morrison deposit contains all of the residual melts from all of the contact deposits).

2) Footwall ores presently account for only 1.6% of the mass of the total system, easily derived via a fractional crystallization process starting with an average Sudbury ore composition of ~5% Ni_{100} and ~5% Cu_{100} (Farrow and Lightfoot, 2002; Naldrett, 2004).

4.9 times the known amount of footwall ore (representing 7.3% of the total mass of the system) with similar Ni and Cu contents is required to balance the deficit and produce a total resource with 5% Ni_{100} and 5% Cu_{100} (Table 2). In that model footwall ore accounts for 8.8% of the mass of the total system, less easily derived via a partial fractional crystallization process.

Direction of Crystallization

Most models for the fractional crystallization of Sudbury footwall ores melt assume that the sulfide melt crystallized from the top down and inside out, but we must also consider the possibility that the sulfide melt crystallized from the bottom up and outside in.

Downward/outward crystallization requires that the sulfide melt is emplaced slowly, loses heat during emplacement, and crystallizes progressively lower temperature phases downward and outward. Upward/inward crystallization requires that the sulfide melt is emplaced rapidly, loses little heat during emplacement, and crystallizes progressively inward and upward.

The greater abundance of pyrrhotite-pentlandite (MSS) in the upper/central parts and chalcopyrite-cubanite (ISS) in the lower/peripheral parts of the Morrison deposit and most other footwall deposits supports the downward/outward crystallization model in general and suggests that crystallization of the upper and middle domains occured by this process. The lower domain appears to have crystallized more rapidly than the upper and middle domains and possibly crystallized from the outside-in.

The Type I high-sulfur (first order) veins in the lower domain are a mixture of cumulate ISS and crystallized sulfide liquid. This suggests that the sulfide liquid may have been emplaced rapidly into the lower domain and been trapped by the ~800 ^{o}C isotherm. The sulfide liquid was forced to cool from the outside in, by fractional crystallization where sulfide liquid could escape from the crystallized solids (thicker veins) and by equilibrium crystallization where the trapped liquid could not escape (thinner veins). Eventually the inward crystallization front would prevent any liquid from escaping and even the thick first-order veins crystallized by equilibrium crystallization.

The similar Pt, Pd, and Au in Type I and Type IIa and IIb mineralization suggests that the later formed by Fe-loss of a liquid that did not undergo significant fractional crystallization of ISS. This also is consistent with rapid and inward crystallization

Summary of Crystallization

The majority of the textural, mineralogical, and chemical changes within the first-order veins that host most of the mineralization in the Morrison deposit can be explained by a combination of:

1) Fractional crystallization of Fe-rich monosulfide solid solution (MSS) and fractional and equilibrium crystallization of Ni-bearing intermediate solid solution (ISS) with crystallization occurring primarily from the top-down in the upper and middle domain and from the outside-in in the lower domain.

2) Dynamic remelting of early formed shallow footwall mineralization creating a Cu-rich melt and crystallization of this melt by fractional and equilibrium crystallization.

The Cu-PPGE-Au-poor bulk composition of the Po-(Pn)-(Ccp) mineralization in the Levack contact-type deposit are consistent with accumulation of Cu-PPGE-Au-poor

MSS, and the Cu-(Ni)-PPGE-Au rich bulk compositions of the Ccp-Pn-Bn-Ml-(Po) mineralization in the Morrison deposit are consistent with having formed from a residual sulfide melt.

The first-order veins observed in this study are consistent with having formed from the accumulation of Fe-MSS and ISS that crystallized from the residual liquid formed from the fractional crystallization of contact-type deposits.

The pyrrhotite-rich upper domain formed from the accumulation of primarily Fe-MSS with potentially the minor accumulation of ISS. The middle domain formed from the accumulation of Fe-MSS and ISS. The chalcopyrite-rich lower domain formed from both the accumulation of ISS to form ISS cumulates and equilibrium crystallization of the sulfide melt in the lower domain to form non-cumulus ISS.

Textural and Mineralogical Evidence of Crystallization of a Sulfide melt

Although textural and mineralogical evidence alone cannot prove or disprove whether mineralization at the Morrison Deposit formed from crystallization of a sulfide melt, the majority of the textures and mineral compositions in the first-order veins and the textures of immediate wallrock are consistent with this mode of formation. Evidence for the crystallization and sub-solidus breakdown of MSS is as follows:

1) The textures and mineralogy in the pyrrhotite-rich upper domain are consistent with the breakdown of MSS and crystallized trapped liquid into pyrrhotite, pentlandite, and chalcopyrite. The PoIa and PnIa flames are consistent with having formed from the cooling of large euhedral MSS crystals. The PoIa and PnIb are consistent with the cooling of smaller anhedral MSS crystals.

   The chalcopyrite- and PoII- rich portions of sulfide veins may have formed from the solidification of crystallized trapped liquid. The PnII eyes that occur at the margin of the pyrrhotite-rich domains may have formed from a peritectic reaction between the MSS crystals and the trapped liquid (Hawley et al., 1943).

2) The mineral chemistry of pyrrhotite and pentlandite in the Morrison Deposit upper domain has similarities to the McCreedy East lower main orebody (Gregory, 2005).

Pyrrhotite has similar Fe, Ni, and S contents and pentlandite has similar proportions of Fe and Ni but pentlandite from the upper domain has less Co.

Unlike the abundance of research of the breakdown products of MSS, there is limited work on textures and mineralogy of the minerals that form from the breakdown of ISS (Cabri, 1973; Kosyakov and Sinyakova, 2010), or Hz-ISS (Peregoedova and Ohnenstetter, 2002). Despite this, there is enough data available to provide support for the crystallization of ISS at the Morrison deposit. Evidence for the crystallization and sub-solidus breakdown of Hz-ISS forming the Type I veins in the lower domain is as follows:

1) Because the first ISS that is expected to form during sulfide fractionation is more Fe-rich than both chalcopyrite and cubanite (Cabri, 1973), it is logical that Fe-rich phases such as pyrrhotite would exsolve from ISS.

2) Chalcopyrite with preferentially oriented cubanite laths is consistent with the breakdown of ISS (or Hz-ISS) into predominantly chalcopyrite. In the Cu-Fe-S system, the minerals that form during subsolidus cooling are dependent on the original ISS composition (Cabri, 1973). Fractional crystallization experiments (Sinyakova and Kosyakov, 2009) have shown that ISS can break down into predominantly chalcopyrite with preferentially exsolution laths of isocubanite (cubic polymorph of cubanite). The cubanite laths in the Type I veins contain fine veinlets of PoV that may have formed by subsequent cooling of iscubanite to cubanite+pyrrhotite. This texture has never been shown experimentally but the time over which the sulfide veins would have cooled would have been significantly longer than experimental cooling times. The PoIII that occurs as veinlets in the chalcopyrite is also consistent with forming from late-stage exsolution. This pyrrhotite has very low Ni, lower S and higher Fe than the pyrrhotite in the upper and middle domain, which is also consistent with it forming by a different mechanism and exsolution from MSS.

3) The PnIII with preferentially oriented mackinawite and chalcopyrite laths is consistent with exsolution from Hz-ISS. Upon the cooling of Hz-ISS, Ni will exsolve into an Fe-rich pentlandite $(Fe_xNi_{1-x})_{9\pm y}S_8$ (Kosyakov and Sinyakova, 2010). The Morrison deposit PnIII has Fe/Ni >1 which is consistent with the experimental exsolved

pentlandite. The crystallographically-controlled mackinawite within the pentlandite and the PoIV occurring along fractures in the pentlandite are texturally consistent with forming from exsolution. This suggests that the pentlandite that initially formed from ISS was even more Fe-rich. The PnIV laths are also texturally consistent with having exsolved along chalcopyrite grain boundaries. Hazelwoodite solid solution is able to accommodate some Cu (Peregoedova and Ohnenstetter, 2002), so the preferentially oriented chalcopyrite laths in the PnIII also likely formed by exsolving from a Cu-bearing pentlandite. Other researchers have suggested that these textures formed by replacement of pentlandite by chalcopyrite and cubanite (Li et al., 1992), but this does not explain why pentlandite in veins in the middle and upper domains (that contain chalcopyrite+cubanite and chalcopyrite respectively) do not have the same crystallographically controlled "replacement".

4) The sphalerite that occurs in the veins is consistent with having exsolved from Hz-ISS. Natural ISS (isocubanite) from the East Pacific Rise contains up to 1 wt% Zn. Additionally, experimental ISS has been shown to contain significant Zn (Caye et al., 1988). The structures of ISS and chalcopyrite are very similar to sphalerite. Cu and Fe are in tetrahedral coordination in ISS and chalcopyrite, and Zn is in tetrahedral coordination in sphalerite (Szymanski, 1974). The middle domain contains minerals and textures that occur both in the pyrrhotite-rich upper domain and the chalcopyrite-rich lower domain and are consistent with forming from the subsolidus breakdown of MSS and ISS mixtures.

5) The Type Ia and Ib pyrrhotite suggests that MSS was still a crystallizing phase but the presence of cubanite, PnIV, and PoIV suggest that ISS was also a crystallizing phase (cumulate or liquid) as the textures of these minerals is not consistent with any of the natural or experimental breakdown products of MSS.

In addition to the mineralogy and textures of the sulfide veins themselves, further support for the veins forming from a sulfide melt is the changes in the texture of quartz and plagioclase feldspar that occur within the immediate wallrock to the veins:

1) The films of feldspar, plagioclase laths, and granophyric textured zone are consistent with a formation from localized insipient melting (Rosenberg and Riller, 2000). The

textures were only observed in extreme proximity to sulfide veins (i.e. within centimetres) and suggest that the immediate wall-rock of the sulfide veins experienced temperatures sufficient to cause localized incipient melting.

2) In areas where plagioclase feldspar occurs as a film along quartz grain boundaries, sulfide minerals often only occur at the triple junctions of the quartz gains and not along the entire grain edge. This distribution of sulfide likely occurs because the silicate melt that initially surrounded the quartz crystals was removed at the triple junctions before the grain edges. Sulfide melt is wetted by silicate melt, so it can only infiltrate areas where silicate melt is absent (e.g., Mungall and Su, 2005).

3) The infiltration of sulfide melt into areas that are more susceptible to melting explains why both first- and second-order veins occur within the leucosomes of mafic gneiss clasts and within granophyric textured dykes. This mechanism is consistent with the idea that sulfide veins have "replaced" the leucocratic dykes known as "footwall granophyres" but differs in the mechanism. Hanley at al., (2005; 2010) propose a chemical replacement whereas this mechanism is a physical replacement.

Requirement of Additional Processes

Fractional and equilibrium crystallization of a sulfide melt can explain the majority of the variation at the Morrison deposit but cannot explain some of the geochemical variation and the presence of hydrous alteration minerals associated with sulfide mineralization. An additional process or processes are required to explain these phenomena:

1) The decrease of Pt, Pd, Bi, Te, and Sn in Type I high-S mineralization in the middle domain followed by a rapid increase in these elements at the top of the lower domain cannot be explained by fractional crystallization.

   Although an order of magnitude decrease in the $D_{ISS/Liquid}$ relative to the $D_{MSS/Liquid}$ for Pt, and Pd could explain the decreases in the individual elements it cannot explain the changes in the Pt/Pd, Pt/Au, and Pd/Au ratios that occur in the Morrison Deposit (Fig. 17).

2) The same magnitude decrease in Pt, Pd, and Au that occurs in the middle domain also occurs in some of the Bn- and/or Ml- bearing mineralization in the lower domain.

The mineralogy of these depleted lower domain veins is consistent with being more fractionated ISS (Ccp >> Ml) and Bn- and Ml- bearing (Bn >> Ccp = Ml; Ml >> Ccp). If these veins formed by fractional or equilibrium crystallization of a sulfide melt (even with a very low $D_{ISS/liquid}$ for Pt and Pd), then these veins should not be depleted but rather enriched.

These depleted veins are likely the source for Pt, Pd, and Au that are enriched in type 2a and 2b mineralization associated with hydrous alteration minerals.

Model for Morrison Deposit Formation

A preferred model for the formation of the Morrison deposit is shown in Figure 20 and presented below:

1) A sulfide melt was transported from the SIC into a zone of Sudbury Breccia at some point during the crystallization of contact-type mineralization. As this liquid began to cool, MSS began to crystallize.

   Due to the higher density of the sulfide melt in equilibrium with the crystallizing MSS, and the ability of sulfide melt to wet solid silicate phases, the liquid migrated further into the footwall in areas where it was physically possible to do so (e.g. pre-existing fractures, leucosomes in mafic gneiss clasts, granophyric textured dykes) (Ebel and Naldrett, 1996; Rose and Brenan, 2001; Hanley et al., 2011).

   Where the permeability was greater, the sulfide melt was present in larger volumes and crystallization of the sulfide melt occurred by fractional crystallization rather than equilibrium crystallization, creating MSS orthocumulates, and mesocumulates that make up the majority of the mineralization in the pyrrhotite-rich upper domain.

   Where the sulfide melt was only present in small quantities, fractional crystallization was limited and the sulfides crystallized primarily by equilibirium crystallization and created adcumulates, and crystalline sulfides of liquid composition that form portions of the second-order veins.

2) When the sulfide melt reached the top of the lower domain, the increase in permeability allowed the liquid to move very quickly through the lower domain. This higher rate of flow allowed the sulfide melt to crystallize from the outside inward.

The most peripheral veins cooled too fast to fractionate and represent liquid compositions. Some of the liquid was able to fractionate and formed first-order veins consisting of ISS orthocumulates and mesocumulates. Other portions of the liquid were unable to fractionate and crystallized by equilibrium crystallization and formed first-order veins consisting of adcumulates or mineralization that represents liquid compositions.

3) The bornite- and millerite-rich mineralization formed by Fe-loss from the sulfide melt by interaction with the wallrock and deep groundwater.

   Where the veins were thin, the Fe-loss was enough to modify the liquid composition to where Bn and Ml could form. Where the veins were thick, the Fe-loss (that would have mainly occurred at the vein margins) would have been buffered by the remaining sulfide melt preventing the composition of the liquid from changing significantly.

4) The same wallrock and groundwater interaction partitioned precious metals and other elements from the sulfide and into a fluid/vapour phase. This interaction created the depleted sulfides in the middle and lower domains and to the PGE-rich mineralization spatially associated with epidote-amphibole-(chlorite)-(carbonate) alteration.

Implications for Exploration

The major exploration implications of this research are as follows:

1) The majority of the mineralization in footwall deposits appear to have formed through high-temperature magmatic processes and will likely be restricted to footwall zones close to the SIC basal contact.

2) Type IIa and IIb veins that consist predominantly of bornite and millerite cannot form through fractional crystallization of a sulfide liquid and require fluid/wallrock interaction to form.

   a) Although the bornite and millerite dominant sulfide veins may themselves be low in TPM, the areas surrounding them are prospective for PPGE-Bi-Te-rich “low S” mineralization.

3) Zones where Type I sulfide veins are depleted in PPGE relative to Ni-Cu-Co-IPGE may indicate the presence of adjacent PPGE-Bi-Te-rich “low S” mineralization.

When performing geochemical studies, be it for mineral deposit delineation or deposit exploration, it is important to sample the sulfide veins and surrounding alteration zones separately. Doing so will allow the determination of whether PPGE have been transferred to the adjacent wallrock, suggesting that the exploration target will include a "low S" PPGE zone, or whether the PPGE are restricted to the sulfide veins themselves. In addition, analysis for sulfur will allow calculation of Me_{100} values that will aid in determining whether PPGE zones may be present.

CONCLUSIONS

The Fe-Cu-Ni-Pd-Pd-Au mineralization in the Morrison deposit is similar to other footwall mineralization associated with the SIC. The veins appear to have been emplaced preferentially into zones of Sudbury Breccia that were within 400m of the basal contact of the SIC, because that lithology is finer-grained and more susceptible to fracturing and because that zone was within the thermal aureoles of the cooling SIC limiting the penetration of sulfide melts. The mineralogical, textural, and geochemical zoning in the chalcopyrite-pentlandite-pyrrhotite-rich parts of the Morrison deposit are best explained by partial fractional and/or equilibrium crystallization of MSS and ISS. Bornite ± millerite-rich mineralization formed by reaction of residual sulfide melts with wall rocks, consuming Fe to form actinolite-magnetite-epidote-chlorite reaction zones and driving the melt across the thermal divide in that part of the Fe-Cu-Ni-S system to crystallize bornite ± millerite. Au-Pt-Pd appear to have been more mobile than the other metals, although it is not clear yet whether the Morrison deposit contains associated zones of "low-S" Au-Pd-Pt-Bi-Te-rich mineralization as in some other footwall systems on the North Range.

ACKNOWLEDGEMENTS

This paper represents part of EN's MSc thesis at Laurentian University. Financial support was provided by an NSERC-Discovery grant to CML and NSERC-IPS and SEG Canada Foundation scholarships to EN. We are very grateful to KGHM International for providing access to the deposit, drill cores, data, and maps. We are also grateful to Drs. Bruno Lafrance, Catharine Farrow, Pedro Jugo, and Jacob Hanley for their helpful and informative reviews.

REFERENCES

Ames, D.E., and Farrow, C.E.G., 2007, Metallogeny of the Sudbury mining camp, Ontario, *in* Goodfellow W.D., ed., Mineral deposits of Canada: A synthesis of major deposit-types, district metallogeny, the evolution of geological provinces, and exploration methods: Geological Association of Canada, Mineral Deposits Division, Special Publication No. 5, p. 329–350.

Bailey, J., Lafrance, B., McDonald, A.M., Fedorowich, J.S., Kamo, S., and Archibald, D.A., 2005, Mazatzal-Labradorian-age (1.7-1.6 Ga) ductile deformation of the South Range Sudbury impact structure at the Thayer Lindsley mine, Ontario: Canadian Journal of Earth Science, v. 41, p. 1491–1505.

Barnes, S-J. and Lightfood, P.C., 2005, Formation of magmatic nickel-sulfide ore deposits and processes affecting their copper and platinum-group element contents: ECON. GEOL. 100TH ANNIV. VOL., 179–213.

Barnes S-J., Makovicky, E., Makovicky, M., Rose-Hansen, J., and Karup-Moller, S., 1997, Partition coefficients for Ni, Cu, Pd, Pt, Rh, and Ir between monosulfide solid solution and sulfide melt and the formation of compositionally zoned Ni-Cu sulfide bodies by fractional crystallization of sulfide melt: Canadian Journal of Earth Science, v.34, p. 366–374.

Beswick, A.E., 2002, An Analysis of Compositional Variations and Spatial Relationships within Fe-Ni-Cu Sulfide Deposits on the North Range of the Sudbury Igneous Complex: ECON. GEOL., v. 97, p. 1487–1508.

Boast, M., and Spray, J.G., 2006, Superimposition of a thrust-transfer fault system on a large impact structure: implications for Ni-Cu-PGE exploration at Sudbury: ECON GEOL, v. 101, p. 1583–1594.

Brenan, J.M., and Bennett, N., 2010, Soret Separation of highly siderophile elements in Fe-Ni-S melts: Implications for solid metal-liquid metal partitioning: Earth and Planetary Science Letters, v. 298, p.299–305.

Cabri, L.J., 1973, New data on phase relations in the Cu-Fe-S system: ECON GEOL. v. 68, p. 443–454.

Campbell, I.H., and Naldrett, A.J., 1979, The influence of silicate: sulfide ratios on the geochemistry of magmatic sulfides: ECON GEOL, v. 74, p. 1503–1505.

Card, K.D., Gupta, V.K., McGrath, P.H., and Grant, F.S., 1984, The Sudbury structure: Its geological and geophysical setting: Ontario Geological Survey Special Volume 1, p. 25–43.

Caye, R., Cervelle, B., Cesbron, F., Oudin, E., Picot, P., and Pillard, F., 1988, Isocubanite, a new definition of the cubic polymorph of cubanite $CuFe_2S_3$: Mineralogical Magazine, v. 52, p. 509–514.

Chyi, L.L., and Crocket, J.H., 1976, Partition of platinum, palladium, iridium, and gold among coexisting minerals from the deep ore zone, Strathcona Mine, Sudbury, Ontario: ECON. GEOL., v. 71, p. 1196–1205.

Cox, S.F., Knackstedt, M.A., Braun, J., 2001, Principles of structural control on permeability and fluid flow in hydrothermal systems: Reviews in Economic Geology, v. 14, p.1–24.

Cox, S.F., and Ruming, K., 2004, The St Ives mesothermal gold system, Western Australia – a case of the golden aftershocks?: Journal of Structural Geology, v. 26, p.1109–1125.

Dare, S.A.S., Barnes, S.J., Prichard, H.M., and Fisher, P.C., 2010, The Timing and Formation of Platinum-Group Minerals from the Creighton Ni-Cu-Platinum-Group Element Sulfide Deposit, Sudbury, Canada: Early Crystallization of PGE-Rich Sulfarsenides: ECON GEOL, v.105, p. 1071–1096.

Dietz, R.S., 1964, Sudbury structure as an astrobleme: Journal of Geology, v. 72, p. 412–343.

Dressler, B.O., 1984, The Effects of the Sudbury Event and the Intrusion of the Sudbury Igneous Complex on the Footwall Rocks of the Sudbury Structure: Ontario Geological Survey Special Volume 1, p. 97–136.

Dutrizac, J.E., 1976, Reactions in Cubanite and Chalcopyrite: Canadian Mineralogist, v. 14, p. 172–181.

Ebel, D.S., and Naldrett, A.J., 1996, Fractional Crystallization of Sulfide Ore Liquids at High Temperature: ECON GEOL, v. 91, p. 607–621.

Ebel, D.S., and Naldrett, A.J., 1997, Crystallization of of sulfide liquids and the interpretation of ore composition. Canadian Journal of Earth Science, v.34, p. 352–365.

Farrow, C.E.G., 1994, Geology, alteration, and the role of fluids in Cu-Ni-PGE mineralization of the footwall rocks to the Sudbury Igneous Complex, Levack and Morgan townships, Sudbury district, Ontario: Ph.D. Thesis, Carleton University, Ottawa, 373p.

Farrow, C.E.G., and Watkinson, D.H., 1992, Alteration and the Role of Fluids in Ni, Cu and Platinum-Group Element Deposition, Sudbury Igneous Complex Contact, Onaping-Levack area, Ontario: Mineralogy and Petrology, v. 46, p. 67–83.

Farrow, C.E.G., and Watkinson, D.H., 1996, Geochemical Evolution of the Epidote Zone, Fraser Mine, Sudbury, Ontario: Ni-Cu-PGE Remobilization by Saline Fluids: Exploration Mining Geology, V.5, p. 17–31.

Farrow, C.E.G., and Watkinson, D.H., 1997, Diversity of Precious-metal mineralization in Footwall Cu-Ni-PGE Deposits, Sudbury, Ontario: Implications for hydothermal models of formation: The Canadian Mineralogist, v. 35, p. 817–839.

Farrow, C.E.G., Watkinson, D.H., and Jones, P.C., 1994, Fluid inclusions in sulfides from North and South Range Cu-Ni-PGE deposits, Sudbury Structure, Ontario: ECON. GEOL., v. 89, p. 647–655.

Farrow, C.E.G. and Lightfoot, P.C., 2002, Sudbury PGE revisited: towards an integrated model: Canadian Institute of Mining Metallurgy and Petroleum, Special Volume 54, p. 273–298.

Farrow, C.E.G., Everest, J.O., King, D.M., Jolette, C., 2005, Sudbury Cu (-Ni)-PGE systems: Refining the classification using McCreedy West mine and Podolsky project case studies: Mineralogical Association of Canada Short Course 35, p. 163–180.

Farrow, C.E.G., Everest, J.O., and Frayne, M., 2009, Technical Report on Mineral Properties in the Sudbury Basin, Ontario – An Update to December 31, 2008 for FNX Mining Company Inc. p. 1–163.

Gibbins, W.A., and McNutt, R.H., 1975, Rubidium-Strontium Mineral Ages and Polymetamorphism at Sudbury, Ontario: Canadian Journal of Earth Science, v.12, p. 1990-2003.

Golightly, P.J., 1994, The Sudbury Igneous Complex as an impact melt; evolution and ore genesis: Ontario Geological Survey Special Volume 5, p. 105–118.

Gregory, S.K., 2005, Geology, Mineralogy, and Geochemistry of Transitional Contact/Footwall Mineralization in the McCreedy East Ni-Cu-PGE Deposit, Sudbury Igneous Complex: Unpublished M.Sc. Thesis, Sudbury, Canada, Laurentian University, 148p.

Grant, R.W., and Bite, A., 1984, Sudbury Quartz Diorite Offset Dikes: Ontario Geological Survey Special Volume 1, p. 275–300.

Grieve, R.A.F., 1994, An impact model of the Sudbury Structure: Ontario Geological Survey Special Volume 5, p. 119-132.

Grieve, R.A.F., Ames, D.E., Morgan, J.V., and Artemieva, N., 2010, The evolution of the Onaping Formation at the Sudbury impact structure: Meteorics & Planetary Science, v. 45, p. 759–782.

Hanley, J.J., 2007, The role of arsenic-rich melts and mineral phases in the development of high-grade Pt-Pd mineralization within Komatiite-associated magmatic Ni-Cu sulfide horizons at Dundonald Beach south, Abitibi subprovince, Ontario, Canada: ECON. GEOL. v. 102, p. 305–317.

Hanley, J.J., and Bray, C.J., 2009, The trace metal content of amphibole as a proximity indicator for Cu-Ni-PGE mineralization in the footwall of the Sudbury Igenous Complex, Ontario, Canada: ECON. GEOL. v. 104, p. 113–125.

Hanley, J.J., Mungall, J. E., Pettke, T., Spooner, E.T.C., and Bray, C.J., 2005, Ore metal redistribution by hydrocarbon-brine and hydrocarbon-halide melt phases, North

Range footwall of the Sudbury Igneous Complex, Ontario, Canada: Mineralium Deposita, v. 40, p. 237–256.

Hanley, J., Ames, D., Barnes, J., Sharp, Z., and Guillog, M., 2011, Interaction of magmatic fluids and silicate melt residues with saline groundwater in the footwall of the Sudbury Igneous Complex, Ontario, Canada: New evidence from bulk rock geochemistry, fluid inclusions and stable isotopes: Chemical Geology, v. 281, p. 1–25.

Hawley, J.E., 1965, Upside-down zoning at Frood, Sudbury, Ontario: ECON. GEOL., v.60, p. 529–575.

Hawley, J.E., Colgrove, G.L., and Zurbrigg, H.F., 1943, The Fe-Ni-S system, and introduction with new data on the crystallization of pyrrhotite and pentlandite: ECON. GEOL. V. 38, p. s335–388.

Helmy, H.M., Ballhaus, C., and Berndt-Gerdes, J., 2005, The formation of Pt, Pd, and Ni tellurides during cooling of Fe-Ni-Cu sulfide: Results of experiments and implications for natural systems: Geochemistry, Mineralogy and Petrology, v. 43, p. 87–92.

Helmy, H.M., Ballhaus, C., Berndt, J., Bockrath, C., and Wohlgemuth-Ueberwasser, C., 2007, Formation of Pt, Pd and Ni tellurides: experiments in sulfide-telluride systems: Contributions to Mineralogy and Petrology., v. 153, p.577–591.

Helmy, H.M., Ballhaus, C., Wohlgemuth-Ueberwasser, C., Fonseca, R.O.C., and Laurenz, V., 2010, Partitioning of Se, As, Sb, Te and Bi between monosulfide solid solution and sulfide melt – Application to magmatic sulfide deposits: Geochemica and Cosmochemica Acta, v.74, p. 6174–6179.

Hinchey, J.G., and Hatori, K.H., 2005, Geology, petrology, and controls on PGE mineralization of the southern Roby and Twilight zones, Lac des Iles Mine, Canada: ECON GEOL., v.100, p. 43–61.

Hoffman, E.L., and MacLean, W.H., 1976, Phase relations of michenerite and merenskyite in the Pd-Bi-Te system: ECON. GEOL., v. 71, p. 1461–1468.

Holwell, D.A., and McDonald, I., 2010, A Review of the Behaviour of Platinum Group Elements within Natural Magmatic Sulfide Ore Systems: Platinum Metals Review: v. 54, p. 26–36.

Houlé, M.G., Lesher, C.M., and Davis, P.C., 2012, Thermomechanical erosion at the Alexo Mine, Abitibi greenstone belt, Ontario: implications or the genesis of komatiite-associated Ni-Cu-(PGE) mineralization: Mineralium Deposita, v. 47, p.105–128.

Jones, J.H., and Walker, D., 1991, Thermal Diffusion in Metal-Sulfide Liquids: Early Results: Proceedings of Lunar and Planetary Science, v. 21, p. 367–373.

Keays, R.R., and Crocket, J.H., 1970, A Study of Precious Metals in the Sudbury Nickel Irruptive Ores: ECON GEOL., v. 65, p. 438–450.

Keays, R.R., Nickel, E.H., Groves, D.I., and McGoldrick, P.J., 1982, Iridium and palladium as discriminants of volcanic-exhalative, hydrothermal, and magmatic nickel sulfide mineralization: ECON GEOL., v. 77, p.1535–1547.

Kosyakov, V.I., and Sinyakova, E.F., 2010, Primary, Secondary, and Admixture Zonation of Copper-Nickel Ores during Fractional Crystallization of Sulfide Melts: Doklady Earth Sciences, v. 432, p. 829–834.

Krogh, T.E., Davis, D.W., and Corfu, F., 1984, Precise U-Pb zircon and baddeleyite ages for the Sudbury area: Ontario Geological Survey Special Volume 1, p. 431–446.

Legault, D., Lafrance, B., Ames, D.E., 2003, Structural study of Sudbury breccia and sulphide veins, Levack embayment, North Range of the Sudbury structure, Ontario: Geological survey of Canada Current Research 2003-C1, 9p.

Lesher, C.M., 2007, Ni-Cu-(PGE) deposits in the Raglan area, Cape Smith belt, New Québec, *in* Goodfellow W.D., ed., Mineral Deposits of Canada: A Synthesis of Major Deposits-Types, District Metallogeny, the Evolution of Geological Provinces, and Exploration Methods: Geological Association of Canada, Mineral Deposits Division Special Publication 5, p. 351–386.

Lesher, C.M., and Keays, R.R., 1984, Metamorphically and hydrothermally mobilized Fe-Ni-Cu sulfides at Kambalda, Western Australia, *in* Buchanan, D.L., and Jones,

M.J., eds., Sulfide deposits in mafic and ultramafic rocks, Proceedings of International Geological Correlation Projects 161 and 91, Third Nickel Sulfide Field Conference, Perth, Western Australia: London, Inst. Mining Metallurgy, p. 62–69.

Lesher, C.M., and Keays, R.R., 2002, Komatiite-associated Ni-Cu-(PGE) deposits: Geology, mineralogy, geochemistry and genesis: Canadian Institute of Mining, Metallurgy and Petroleum Special Volume 54, p. 579–618.

Lesher, C.M., Golightly, J.P., Huminicki, M.A.E., and Gregory, S., 2008, Magmatic-hydrothermal fractionation of Fe-Ni-PGE mineralization in the Sudbury Igneous Complex: Goldschmidt 2008, Vancouver, Abstract no. 1568.

Lesher, C.M., Golightly, J.P., Gregory, S.K., Huminicki, M.A.E., and Pattison, E.F., 2009, Genesis of Ni-Cu-PGE mineralization associated with the 1.85 Ga Sudbury impact event: 2009 AGU-GAC-MAC Meeting, Toronto, Ontario.

Li, C., Naldrett, A.J., Coats, C.J.A., and Johannessen, P., 1992, Platinum, Palladium, Gold, and Copper-Rich Stringers at the Strathcona Mine, Sudbury: Their Enrichment by Fractionation of a Sulfide melt: ECON. GEOL., v.87, p. 1584–1598.

Li, C., Barnes. S.J., Makovicky, E., Rose-Hansen, J., and Makovicky, M., 1996, Partitioning of nickel, copper, iridium, rhenium, platinum, and palladium between monosulfide solid solution and sulfide melt: Effects of composition and temperature: Geochimica et Cosmochimica Acta, v. 60, p. 1231–1238.

Lida, T., and Guthrie, R.L.,1988, The Physical Properties of Liquid Metals: Oxford, Clarendon Press, 288 p.

Lightfoot, P.C., Keays, R.R., Morrison, G.G., Bite, A., and Ferrell, K.P., 1997, Geochemical relationships in the Sudbury igneous complex; origin of the main mass and offset dikes: ECON GEOL, v. 92, p. 289–307.

Makovicky, E., 2002, Ternary and quaternary phase systems with PGE: Canadian Institute of Mining Special Volume 54, p. 131–175.

Marshall, D., Watkinson, D., Farrow, C., Molnár, F., and Fouillac, A.M, 1999, Multiple fluid generations in the Sudbury igneous complex: fluid inclusion, Ar, O, H, Rb, Sr evidence: Chemical Geology, v. 154, p.1–19.

McDonough, W.F., and Sun, S.S., 1995, The Composition of the Earth: Chemical Geology, v. 120, p. 223–253.

Molnár, F., Watkinson, D.H., Jones, P.C., and Gatter, I., 1997, Fluid Inclusion Evidence for Hydrothermal Enrichment of Magmatic Ore at the Contact Zone of the Ni-Cu-Platinum-Group Element 4b Deposit, Lindsley Mine, Sudbury, Canada: ECON. GEOL., v. 92, p. 674–685.

Molnár F., Watkinson, D.H., and Jones, P.C., 2001, Multiple Hydrothermal Processes in Footwall Units of the North Range, Sudbury Igneous Complex, Canada, and Implications for the Genesis of Vein-type Cu-Ni-PGE Deposits: ECON GEOL, v. 96, p. 1645–1670.

Morrison, G.G., Jago, B.C., and White, T.L., 1994, Footwall Mineralization of the Sudbury Igneous Complex: Ontario Geological Survey Special Volume 5, p. 57–64.

Mukwakwami, J., Lafrance, B., and Lesher, C.M., 2011, Back-trusting and overturning of the southern margin of the 1.85 Ga Sudbury Igneous Complex at the Garson mine, Sudbury, Ontario: Precambrian Research, v. 196-197, p. 81–105.

Mukwakwami, J., Lafrance, B., Lesher, C.M., Tinkham, D.K., Rayner, N., and Ames, D.E., *submitted*, Fabrics and Textures of deformed and metamorphosed Ni-Cu-PGE sulfide ores at Garson Mine and their implications for sulfide mobilization processes: Canadian Journal of Earth Sciences.

Mungall, J.E., 2007, Crystallization of magmatic sulfides: An empirical model and application to Sudbury ores: Geochimica et Cosmochimica Acta, v.71, p. 2809–2819.

Mungall, J.E., and Su, S., 2005, Interfacial tension between magmatic sulfide and silicate liquids: Constraints on kinetics of sulfide liquation and sulfide migration throughout silicate rocks: Earth and Planetary Science Letters, v. 234, p. 135–149.

Naldrett, A.J., 1981, Nickel sulfide deposits: Classification, composition, and genesis: ECON. GEOL. 75TH ANNIV. VOL., p628–685.

Naldrett, A.J., 1999, World-class Ni-Cu-PGE deposits: key factors in their genesis: Mineralium Deposita, v. 34, p. 227–240.

Naldrett, A.J., 2004, Magmatic sulfide deposits: Geology, geochemistry, and exploration: Berlin, Springer, 727 p.

Naldrett, A.J., and Kullerud, G., 1967, A Study of the Strathcona Mine and Its Bearing on the Origin of the Nickel-Copper Ores of the Sudbury District, Ontario: Journal of Petrology, v.8, p. 453–531.

Naldrett, A.J., Innes, D.G., Jowa, J., and Gorton, M.P., 1982, Compositional Variations within and between Five Sudbury Ore Deposits: ECON GEOL., v. 77, p. 1519–1534.

Naldrett, A.J., Ebel, D.S., Asif, M., Morrison, G., and Moore, C.M., 1997, Fractional crystallization of sulfide melts as illustrated at Noril'sk and Sudbur: Eur. J. Mineral, v.9, p. 365–377.

Péntek, A., Molnár, F., Watkinson, D.H., and Jones, P.C, 2008, Footwall-type Cu-Ni-PGE Mineralization in the Broken Hammer Area, Winser Township, North Range, Sudbury Structure: ECON. GEOL., v. 103, p.1005–1028.

Péntek, A., Molnár, F., Watkinson, D.H., Jones, P.C., and Mogessie, A., 2011, Partial melting and melt segregation in footwall units within the contact aureole of the Sudbury Igneous Complex (North and East Ranges, Sudbury Structure), with implications for their relationship to footwall Cu-Ni-PGE mineralization: International Geology Review, v. 53, p. 291–325.

Peregoedova, A., and Ohnenstetter, M., 2002, Collectors of Pt, Pd and Rh in a S-poor Fe-Ni-Cu Sulfide System at 760C: Experimental Data and Application to Ore Deposits: The Canadian Mineralogist, v. 40, p. 527–561.

Peregoedova, A., Barnes, S.J., and Baker, D.R., 2006, An experimental study of mass transfer of platinum-group elements, gold, nickel and copper in sulfur-dominated vapour at magmatic temperatures: Chemical Geology, v. 235, p.59–75.

Prevec, S. A., and Cawthorn, R.G., 1992, Postimpact Crater Modification by Melt Sheet-Footwall Interaction and Constraints on Melt Sheet Evolution: Meteoritics & Planetary Science, v. 34, Supplement, p. A94-A95.

QuadraFNX Mining Ltd., 2011, Annual Information Form For The Year Ended December 31, 2010 (http://www.sedar.com).

Riller, U., Lieger, D., Gibson, R.L., Grieve, R.A.F., and Stöffler, D., 2010, Origin of large-volume pseudotachylite in terrestrial impact structures: Geology, v. 38, p. 619–622.

Rose, L.A., and Brenan, J.M., 2001, Wetting Properties of Fe-Ni-Co-Cu-O-S Melts against Olivine: Implications for Sulfide Melt Mobility: ECON GEOL, v. 96, p.145–157.

Rosenberg, C., and Riller, U., 2000, Partial-melt topology in statically and dynamically recrystallized granite: Geology, v. 28, p. 7–10.

Rousell, D.H., Fedorowich, J.S., and Dressler, B.O., 2003, Sudbury Breccia (Canada): a product of the 1850 Ma Sudbury Event and host to Cu-Ni-PGE deposits: Earth-Science Reviews, v. 60, p. 147–174.

Sinyakova, E.F., and Kosyakov, V.I., 2007, Experimental Modeling of zoning in copper-nickel sulfide ores: Doklady Earth Sciences, v. 417A, p. 1380–1385.

Sinyakova, E.F., and Kosyakov, V.I., 2009, Experimental Modeling of Zonality of Copper-Rich Sulfide Ores in Copper-Nickel Deposits: Doklady Earth Sciences, v. 427, p. 787–792.

Solberg, P., Lockner, D., and Byerlee, J., 1977, Shear and Tension Hydraulic Fractures in Low Permeability Rocks: Pure and Applied Geophysics, v. 115, p. 193–198.

Stout, A.E., 2009, Geology, Mineralogy, and Geochemistry of the McCreedy East 153 Cu-Ni-PGE Deposit, Sudbury, Ontario: Unpublished M.Sc. Thesis, Utrecht, The Netherlands, Utrecht University, 39p.

Su, S., and Lesher, C.M., 2012, Genesis of PGE mineralization in the Wengeqi mafic-ultramafic complex, Guyang County, Inner Mongolia, China: Mineralium Deposita, v.47, p.197–207.

Szymanski, J.T., 1974, The crystal structure of high-temperature $CuFe_2S_3$: Zeitschrift für Kristallographie: v. 140, p. 240–248.

Thompson, L.M., and Spray, J.G., 1994, Pseudotachylitic rock distribution and genesis within the Sudbury impact structure: Geological Society of America Special Paper 293, p. 275–287.

Tomkins, A,G., 2010, Wetting facilitates late-stage segregation of precious metal-enriched sulfosalt melt in magmatic sulfide systems: Geology, v. 38, p. 951-954.

Tsujimura, T., and Kitakaze, A., 2004, New phase relations in the Cu-Fe-S system at 800°C; constraints of fractional crystallization of a sulfide liquid: Neues Jahrbuch für Mineralogie - Monatshefte, v. 2004, p. 433-444.

Watkinson, D.H., 1994, Fluid-Rock interactions at contact of Lindsley 4b Ni-Cu-PGE orebody and enclosing granitic rocks, Sudbury, Canada: Transactions of the Institution of Mining and Metallurgy. Section B. Applied Earth Science. v. 103, p. 121–128.

Wood, S.A., 2002, The aqueous geochemistry of the platinum-group elements with applications to ore deposits: Canadian Institute of Mining and Metallurgy Special Volume 54, p. 211–249.

CHAPTER 3 - Appendix

100% Sulfide Normalization for Bn- and Ml-bearing Mineralization

Most normative sulfide calculations are designed for pyrrhotite-pentlandite-chalcopyrite assemblages (e.g., Naldrett, 1981). Because the ores in Sudbury footwall deposits also contain significant amounts of bornite and millerite, they will produce erroneous results. Following the method of Stout (2009), the mineralization is divided into pyrrhotite-pentlandite-chalcopyrite, chalcopyrite-pentlandite-millerite, and chalcopyrite-bornite-millerite assemblages based on the molar proportions of S, Ni, and Cu. After the appropriate assemblage is determined, the mole proportion of the minerals in that assemblage are determined by sequentially assigning Cu and Ni to the appropriate phases and assigning excess S to pyrrhotite or pyrite. A detailed description of the process is as follows:

Step 1: Conversion of Ni, Cu, and S from Weight Percent to Mole Percent

Moles of Ni, Cu, and S are determined by dividing the abundance of each element in weight percent by the molecular weight of the element, assuming that weight percent represents g/100g:

e.g., Ni (grams) / Ni molecular weight (grams/mol) = Ni (moles)

Step 2: Determining the Appropriate Assemblage

If the number of moles of S is insufficient to form millerite from available Ni and chalcopyrite from available Cu then bornite must be present because there is no mineral present with a higher metal/S ratio than millerite. If bornite is present the assemblage must be chalcopyrite-bornite-millerite.

If bornite is not present, but the moles of S are insufficient to form pentlandite from available Ni and chalcopyrite from available Cu, then millerite must be present and the assemblage must be chalcopyrite-pentlandite-millerite. Because pentlandite can have varying a Ni/Fe ratio, a composition of pentlandite must be chosen for the normalization. For this study a pentlandite composition of $Fe_{4.5}Ni_{4.5}S_8$ was used.

If the moles of S are sufficient to produce pentlandite and chalcopyrite from the available Ni and Cu then the assemblage will be pyrrhotite-pentlandite-chalcopyrite.

Step 3: Determining the abundances of the varying minerals

The equations for determining the proportions of the varying minerals are given in Table A1 and the methodology is summarized below.

The calculation for the pyrrhotite-pentlandite-chalcopyrite assemblage is straightforward. All of the Cu is used to form chalcopyrite, all of the Ni is used to form pentlandite, and all of the remaining S is used to form pyrrhotite. The composition of pyrrhotite used in this study was $Fe_{0.9}S$.

The calculation for the chalcopyrite-bornite-millerite assemblage is more complicated. All of the Ni is used to form millerite, but Cu is used to form both chalcopyrite and bornite. Because there are two unknowns (the abundance of chalcopyrite and the abundance of bornite) and two variables (Cu and S), a system of two linear equations can be solved to determine the abundance of chalcopyrite and bornite. These equations and a method of solving them are given in Table A2.

The calculation for the chalcopyrite-pentlandite-millerite assemblage is similar to that for the chalcopyrite-bornite-millerite assemblage. All of the Cu is used to from chalcopyrite and all of the Ni is used to form both pentlandite and millerite, with the proportions determined by solving two linear equations.

Step 4: Determining the Total Calculated Weight Percent of the Sulfide Minerals

The weight percent of each mineral is determined by multiplying the molar abundance of each mineral by the molecular weight of that mineral. This weight percent represents the calculated percent of each mineral in the original sample. Adding together the weight percentages of all the minerals present in each sample gives the total weight percent of sulfide minerals within that sample:

(Calculated moles of Ml)•(Molecular weight of millerite) = Weight percent of millerite

Step 5: Determining the 100% Sulfide Normalized Element Values

To determine the abundance of each element in 100% sulfides (designated by a subscript 100 in this study), the abundance of each element in the original analysis is divided by the calculated total weight percent sulfide calculated in Step 4 and multiplied by 100:

[Ni (wt %)]/[(Weight percent of millerite)•100] = Ni_{100} (wt %)

FIGURES

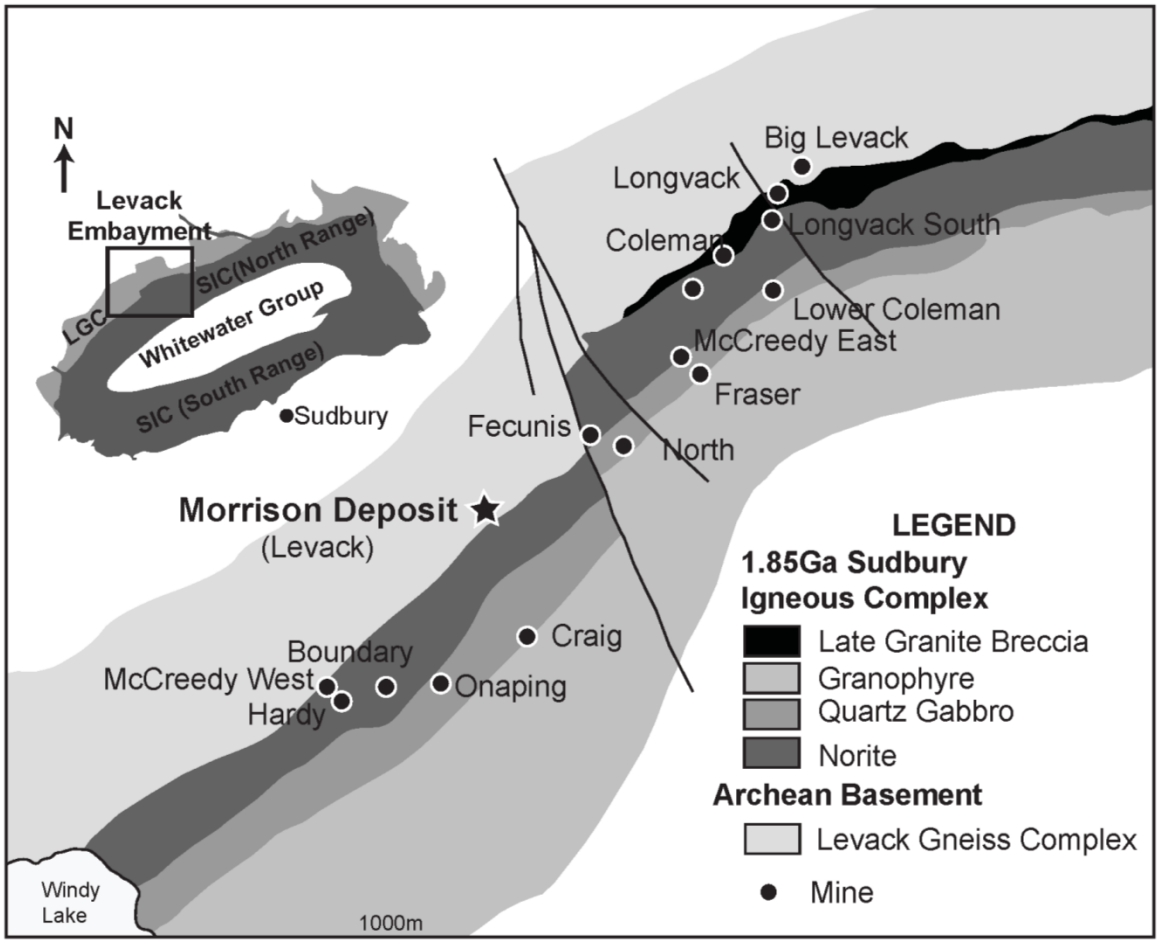

Fig 1. Overview of the Levack embayment (modified from Ames and Farrow, 2002; Gregory, 2005).

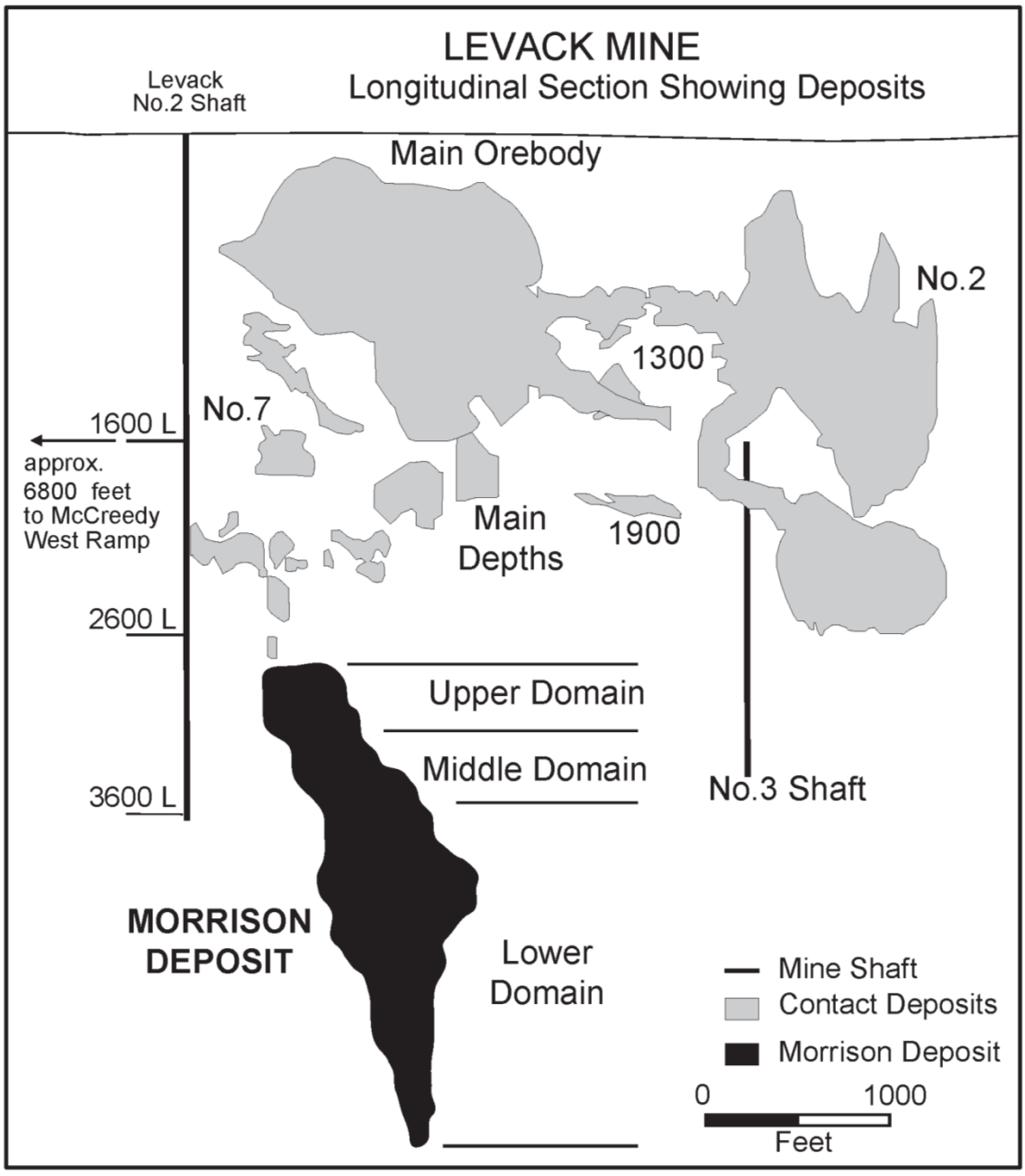

Fig 2. Schematic north-south cross-section of the Morrison deposit (modified from Farrow et al., 2007).

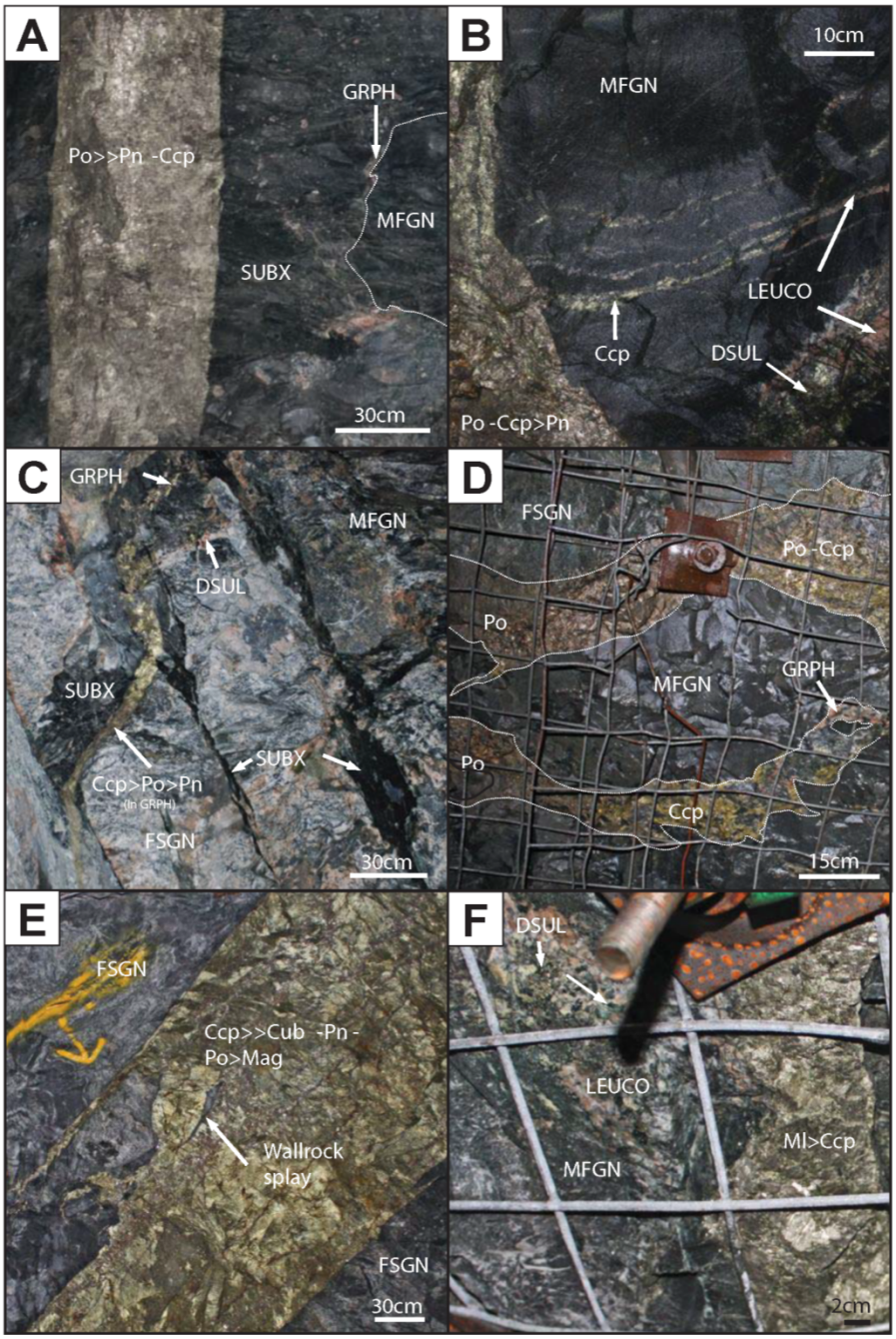

Fig 3. Style of mineralization at the Morrison Deposit. A) Sharp-walled and planar-margined vein in the upper domain in matrix-rich Sudbury breccia. B) Second-order vein in the middle domain following a leucosome in a mafic gneiss clast. C) Second-order vein in the middle domain within a granophyric-textured dyke (footwall granophyre). The vein occurs along a clast-matrix contact and grades into a non-mineralized granophyric-textured dyke towards the top of the photograph. Note also the vein of Sudbury breccia matrix separating two felsic gneiss clasts. D) First-order vein in the middle domain within a granophyric-textured dyke that occurs along the contact between a more felsic and more mafic portion of a Sudbury breccia clast. A small second-order splay grades from pyrrhotite-rich, through chalcopyrite-rich, and into non-mineralized granophryic-textured dyke. E) Sharp-walled and planar-margined chalcopyrite-rich vein in the bottom of the middle domain. Vein occurs within a felsic gneiss clast and contains a wall-rock splay within the vein and a splay of sulfide vein within the wallrock. F) Second-order millerite-bearing vein in the lower domain with patchy sulfides occurring within the leucosome of a mafic gneiss clast. Vein orders as described in the text.

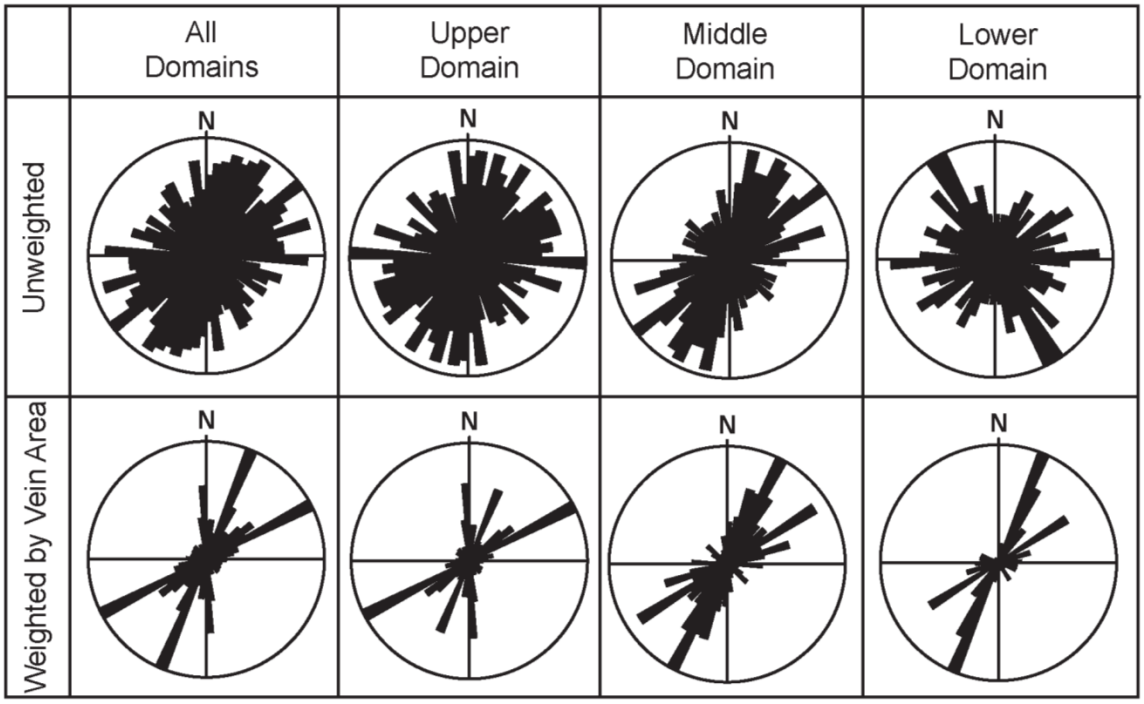

Fig 4. Rose diagrams of the orientations of Morrison deposit sulfide veins. North arrow represents true north.

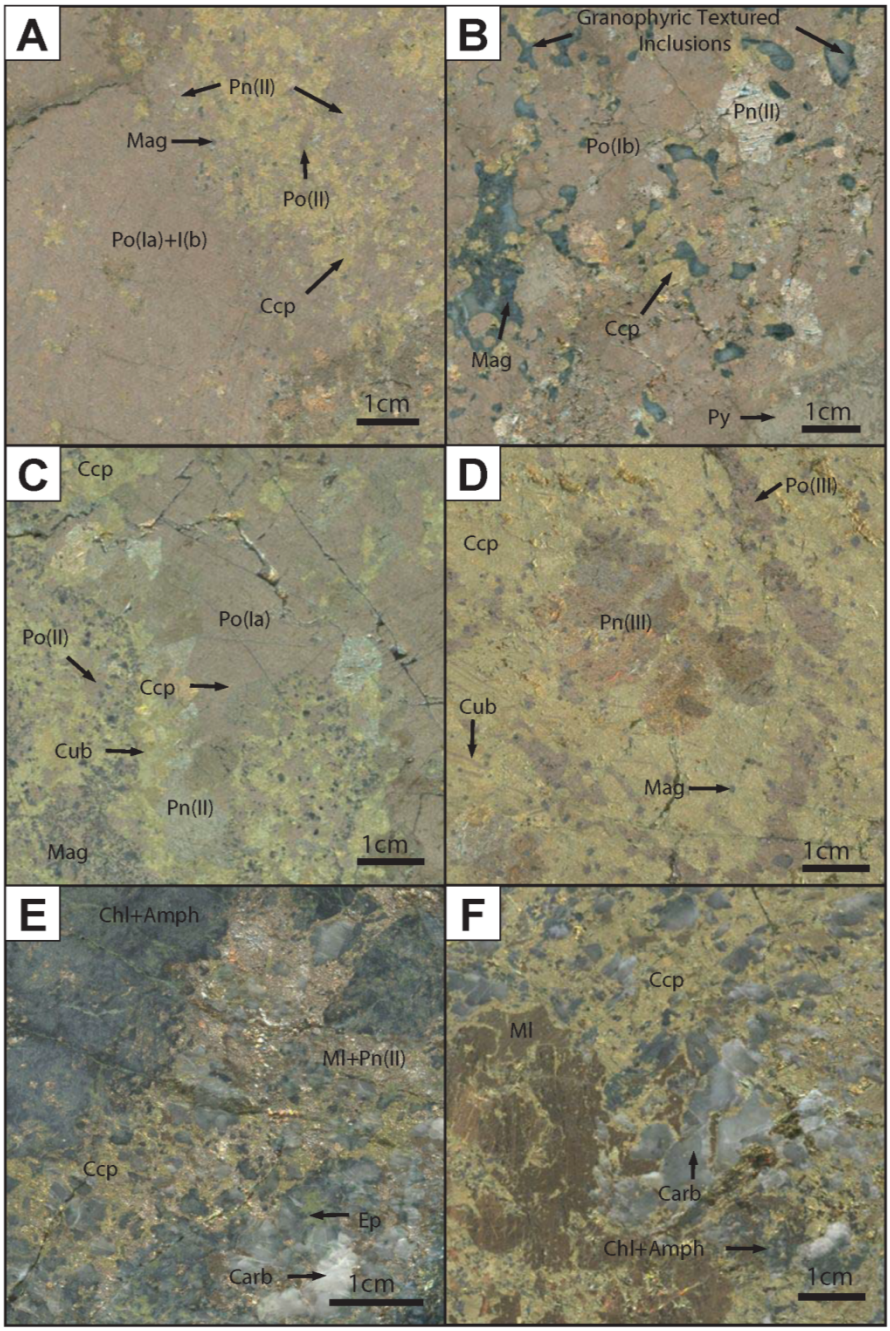

Fig 5. A) First-order pyrrhotite-rich vein in the upper domain showing Po(Ia) and Po(Ib) domains separated from a domain of chalcopyrite and Po(II) by Pn(II) eyes. B) Second-order pyrrhotite-rich vein in the top of the middle domain that is associated with a granophryic-textured dyke. The inclusions are granophyric textured, have irregular and concave and convex margins, and are surrounded by chalcopyrite. Magnetite is concentrated at the margins of some of these inclusions. C) Chalcopyrite-rich vein in the middle domain with a large domain of Po(Ia) with chalcopyrite laths separated by a domain of chalcopyrite, Po(II), cubanite, and magnetite. The two domains are separated by euhedral and subhedral Pn(II) eyes. Magnetite surrounds small sub-mm silicate inclusions. D) First-order chalcopyrite-rich vein in the top of the lower domain with a large Pn(III) eye, cubanite laths, and Po(III) veinlets. E) Second-order millerite-bearing vein from the top of the middle domain. Vein is spatially associated with a chlorite- and amphibole-rich domain, a carbonate-rich domain, and a small, and patchy epidote-rich domain. F) Second-order millerite-bearing vein from the lower domain with spatially associated carbonate with lesser chlorite and amphibole. Vein orders and mineral types as described in text.

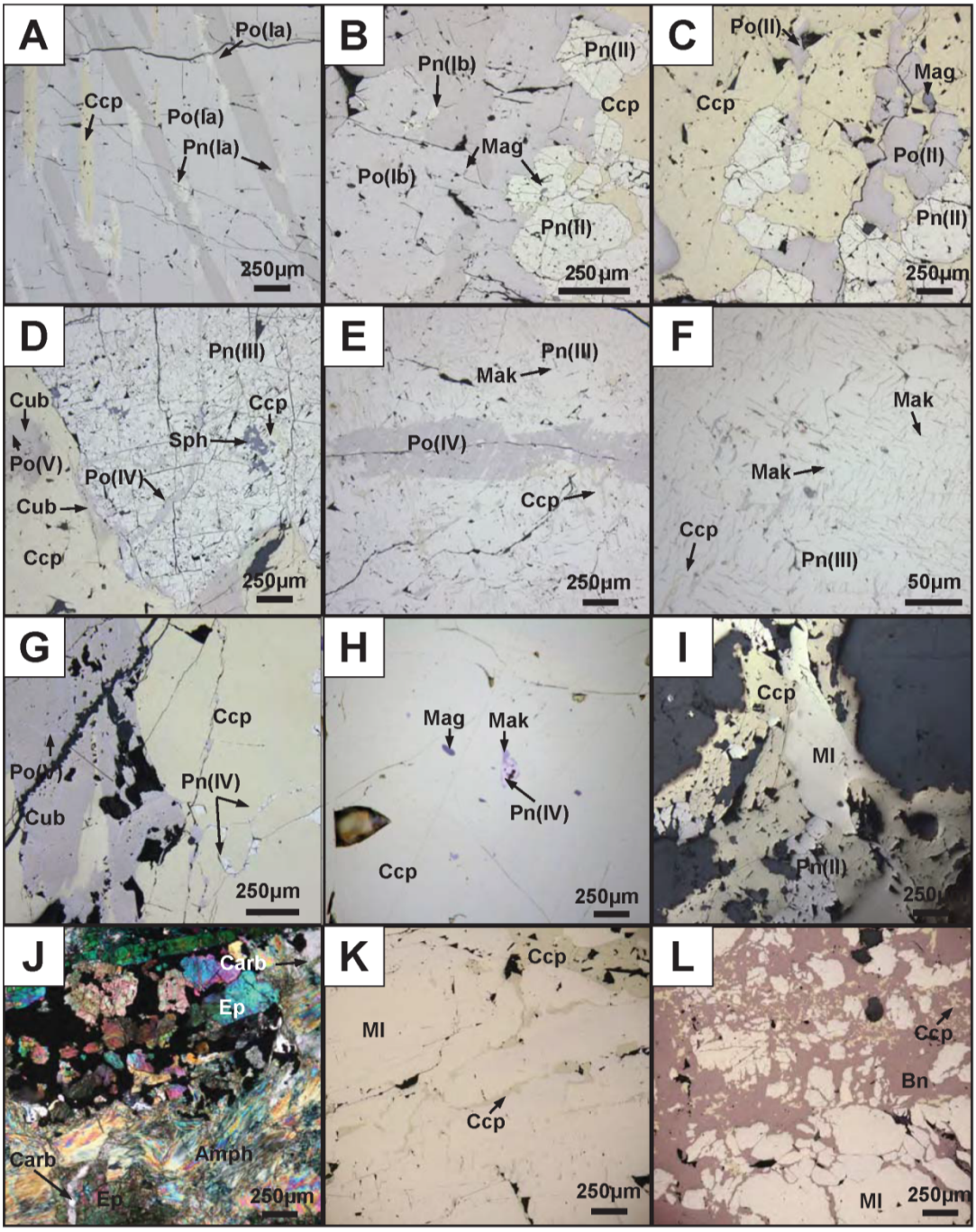

Fig 6. Textures of first- and second-order mineralization. A) Pyrrhotite-rich portion of a vein in the top of the middle domain containing twinned PoIa with chalcopyrite laths and PnIa flames that are parallel to the pyrrhotite basal parting and twinning plane. B) Pyrrhotite-rich portion of a vein in the upper domain containing PoIb with PnIb eyes and chains and PnII eyes (inclusion bearing). C) Chalcopyrite-rich portion of the same vein as (B) with PoII and PnII eyes. D) Chalcopyrite-rich vein in the top of the lower domain with PnIII eyes (mackinawite bearing), PoV in a cubanite patch, and sphalerite. E) Same vein as (D) with Po(IV) within Pn(II) (with mackinawite and chalcopyrite laths). F) Closeup of (E) showing mackinawite and chalcopyrite laths. G) Vein in the top of the middle domain with Po(V) in a cubanite patch and Pn(IV) chains within chalcopyrite. H) Same vein as (G) with Pn(IV) and makinawite. I) Second-order vein in the middle domain. J) Alteration associated with a second-order millerite-bearing vein in the middle domain. K) Second-order millerite-rich vein in the lower domain. L) Second-order millerite-, bornite, and chalcopyrite-bearing vein in the lower domain.

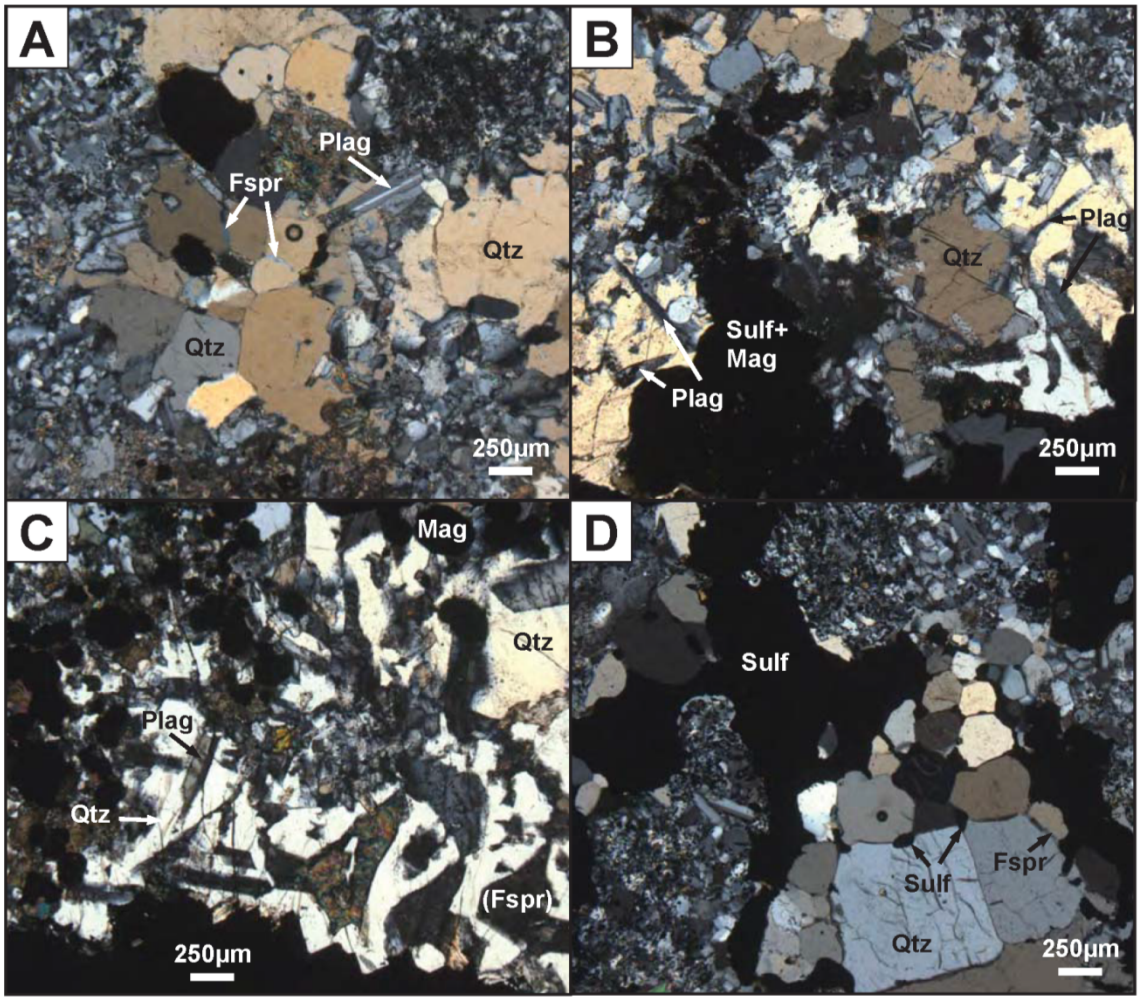

Fig 7. Thin section microphotographs showing possible partial melting textures. A) Felsic gneiss immediately adjacent to a pyrrhotite-rich vein in the upper domain. Gneiss contains thin films of feldspar and larger plagioclase laths surrounding quartz grains. B) Same area as (A) but with more abundant plagioclase and irregular quartz. C) Felsic gneiss surrounding a chalcopyrite-rich vein in the middle domain. Gneiss contains irregular quartz and plagioclase laths grading into granophyric-textured quartz and (partially altered feldspar). D) Area adjacent to (A) with sulfides (primarily chalcopyrite) occurring along quartz triple junctions and fractures. The sulfide is almost entirely absent from the quartz grain boundaries (which contain feldspar films).

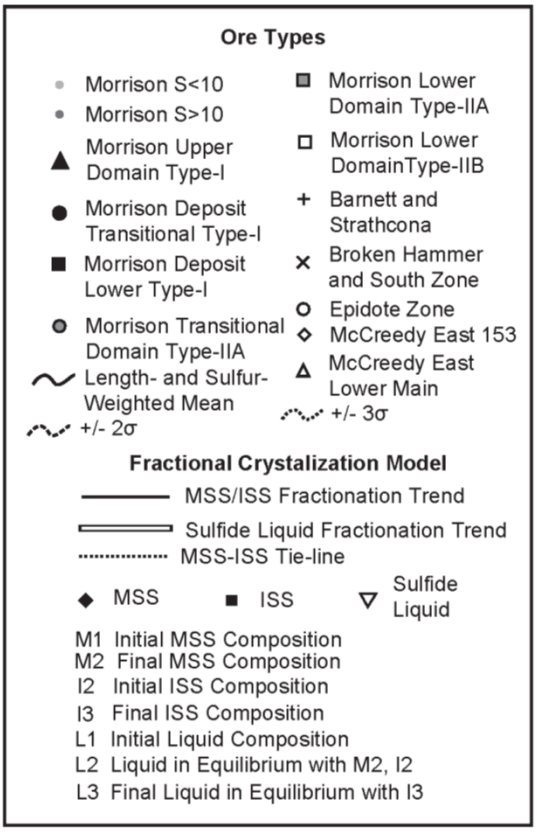

Fig 8. Legend for Figures 9, 10, 11, 12, 13, 16, and 17.

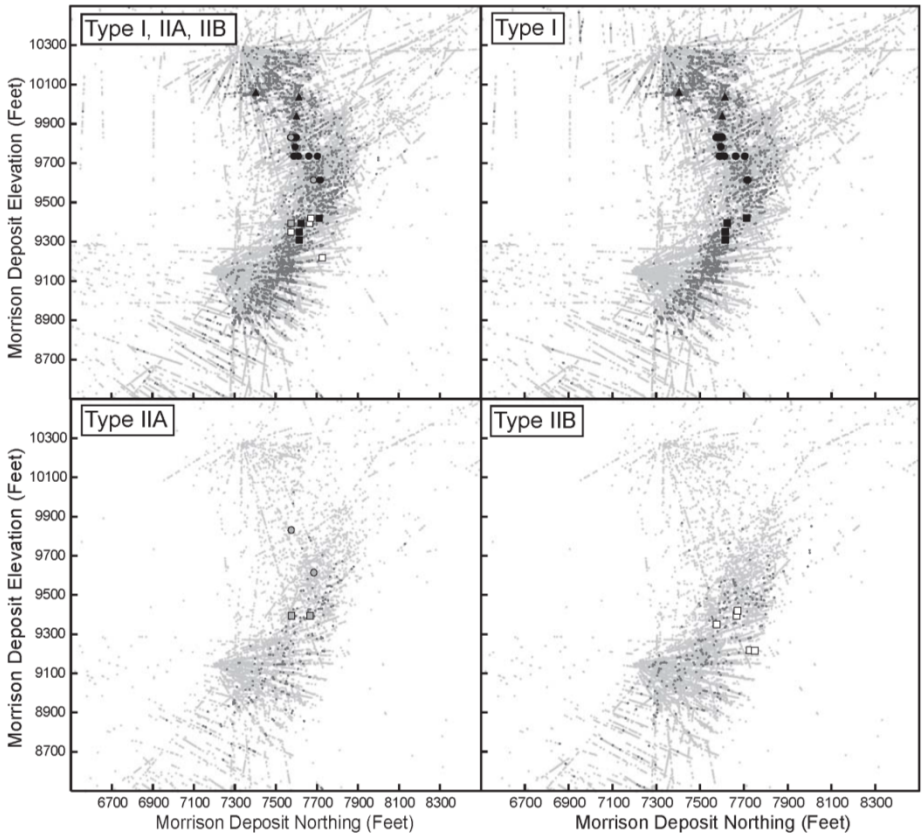

Fig 9. Vertical cross section (Levack mine grid, oriented with 'north' at 322.4^{o}) showing the distribution of Type I, IIa, and IIb mineralization.

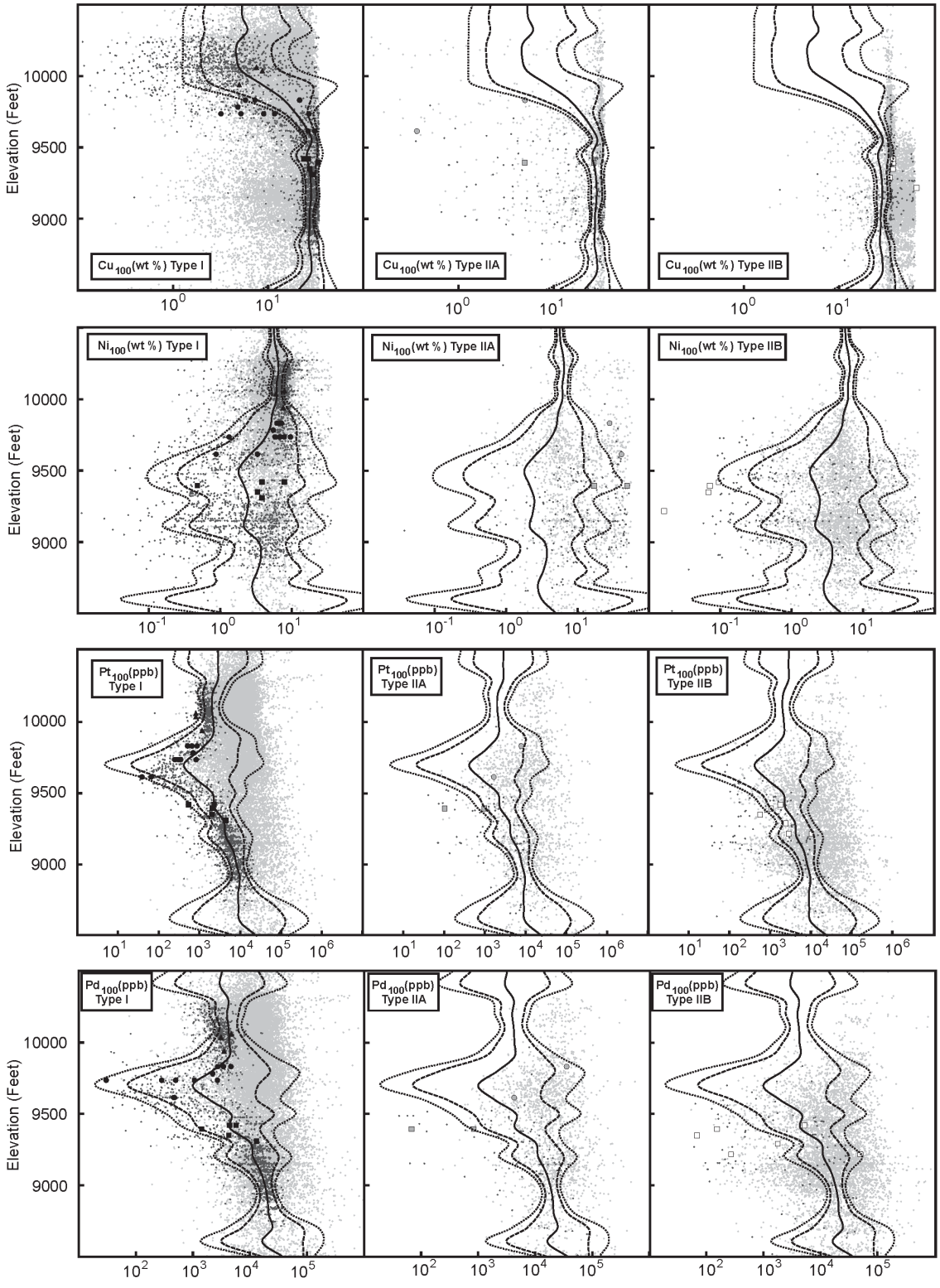
Elevation (Feet)
10000
9500
9000
Cu100(wt %) Type I
Cu100(wt %) Type IIA
Cu100(wt %) Type IIB
Ni100(wt %) Type I
Ni100(wt %) Type IIA
Ni100(wt %) Type IIB
Pt100(ppb) Type I
Pt100(ppb) Type IIA
Pt100(ppb) Type IIB
Pd100(ppb) Type I
Pd100(ppb) Type IIA
Pd100(ppb) Type IIB

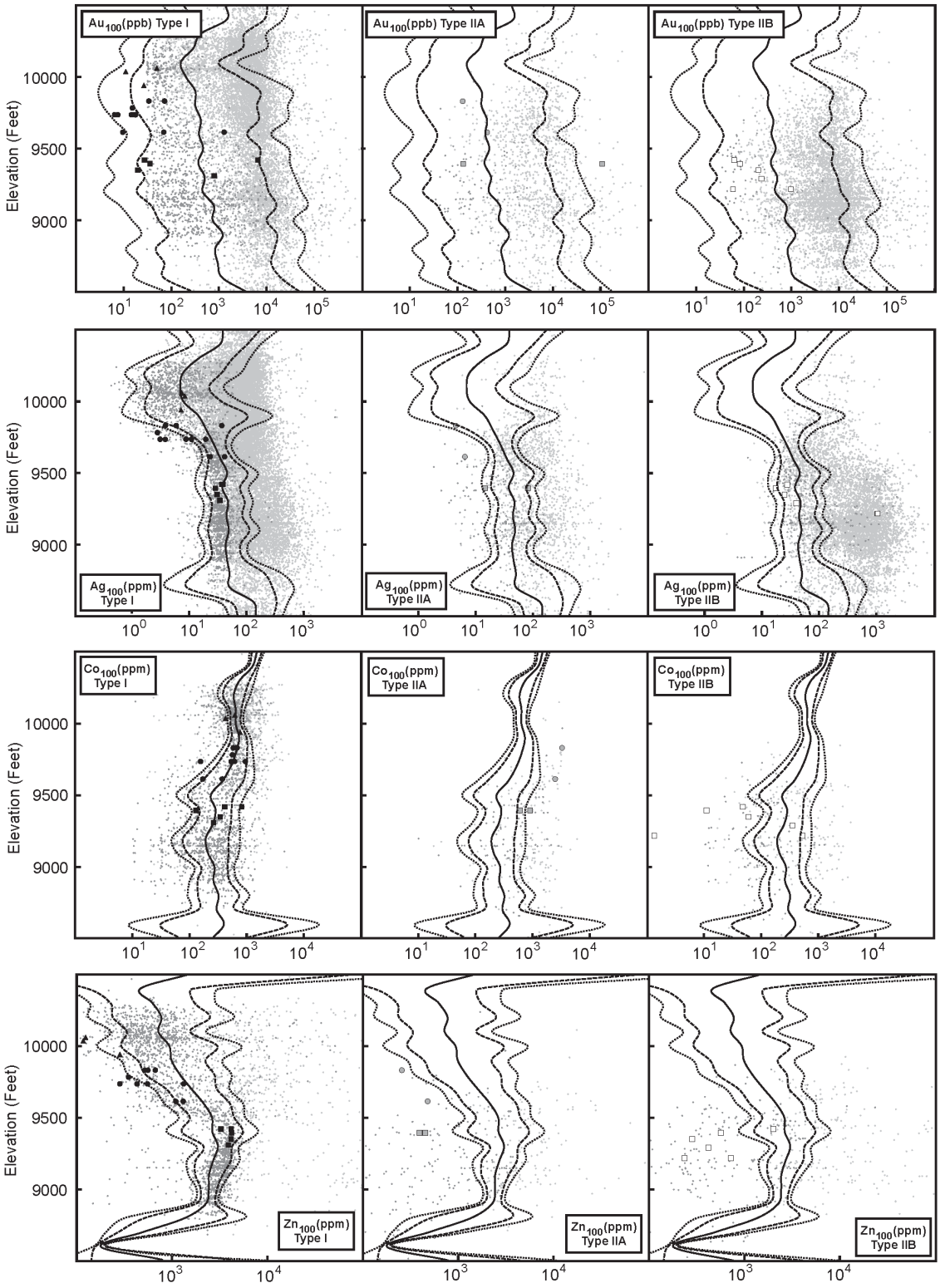

Fig 10. Element vs. depth (Levack mine grid) plots showing elemental distributions in the Morrison Deposit for Cu, Ni, Pt, Pd, Au, Ag, Co, Zn.

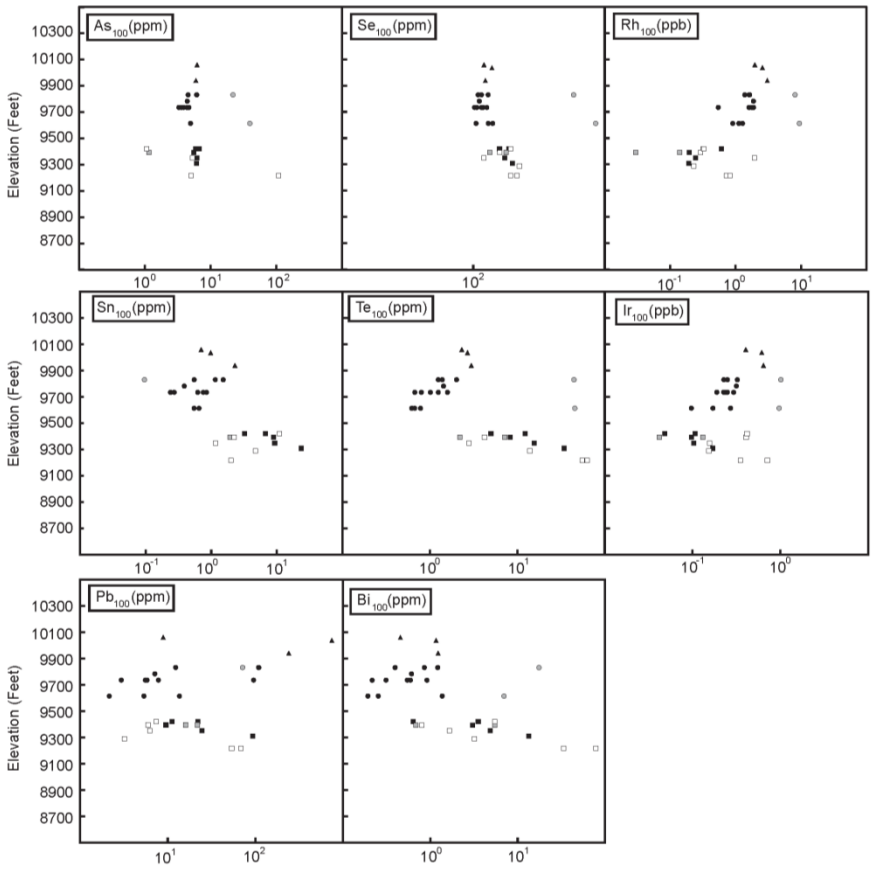

Fig 11. Element vs. depth (Levack mine grid) plots showing elemental distributions in the Morrison Deposit of As, Se, Rh, Sn, Te, Ir, Pb, Bi.

ALL
CT
UD
MD
LD
Ni100 (wt %)
Pt100 (ppb)
Pd100 (ppb)
Au100 (ppb)
Cu100 (wt %)

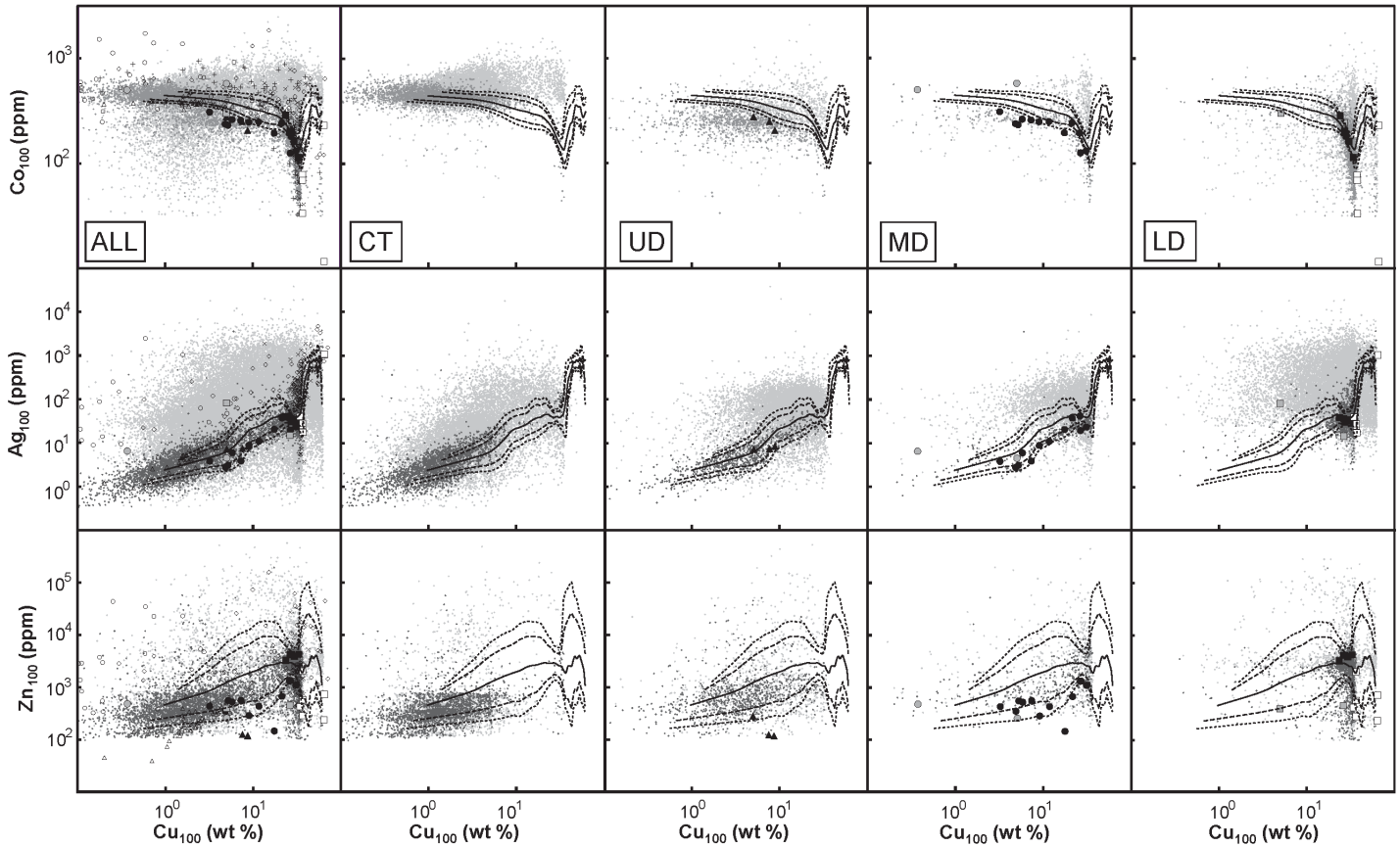

Fig 12. Element$_{100}$ vs. Cu$_{100}$ plots for whole-rock samples from the Morrison Deposit for Ni, Pt, Pd, Au, Ag, Co, and Zn.

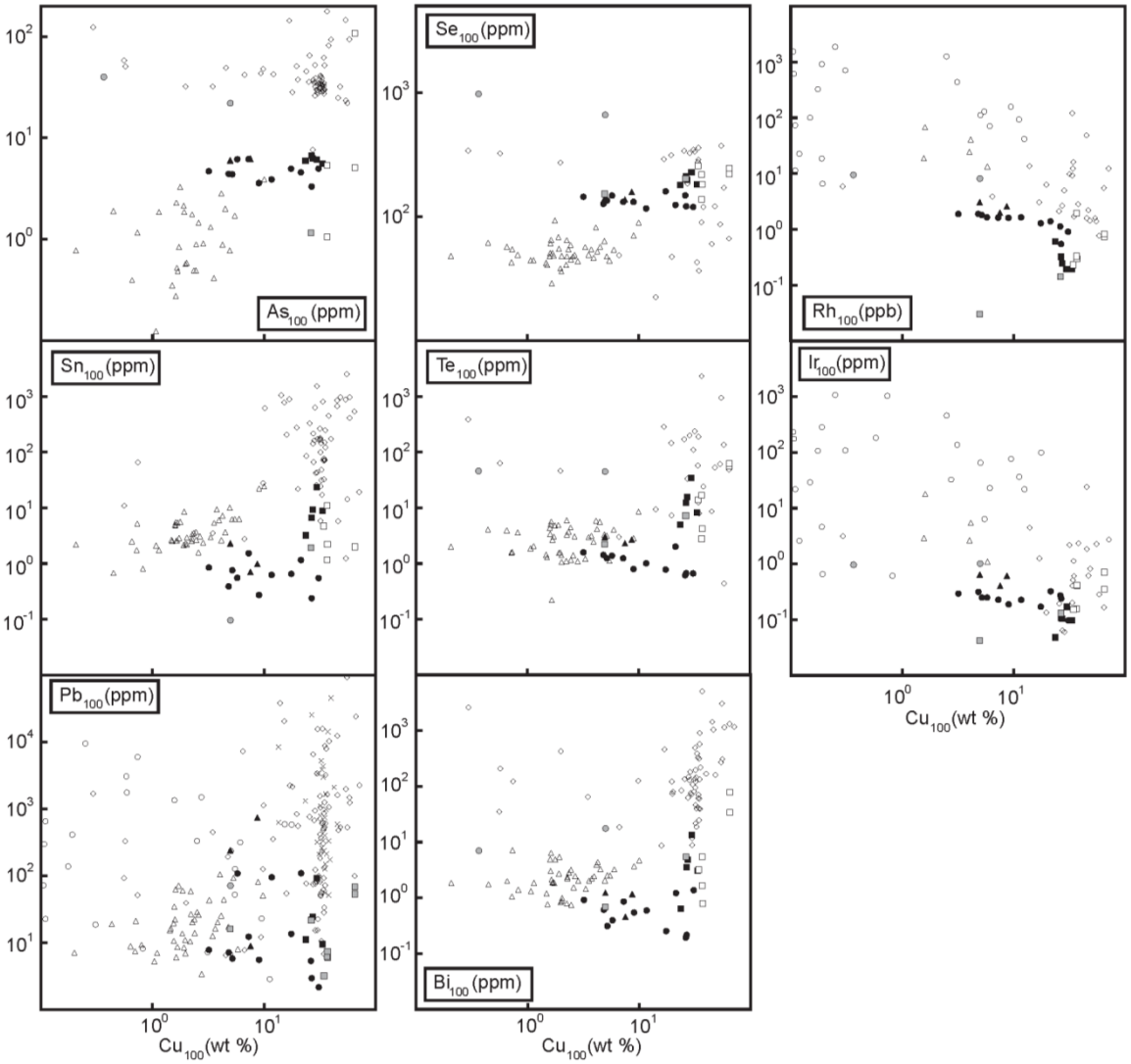

Fig 13. Element$_{100}$ vs. Cu$_{100}$ plots for whole-rock samples from the Morrison Deposit for As, Se, Rh, Sn, Te, Ir, Pb, Bi.

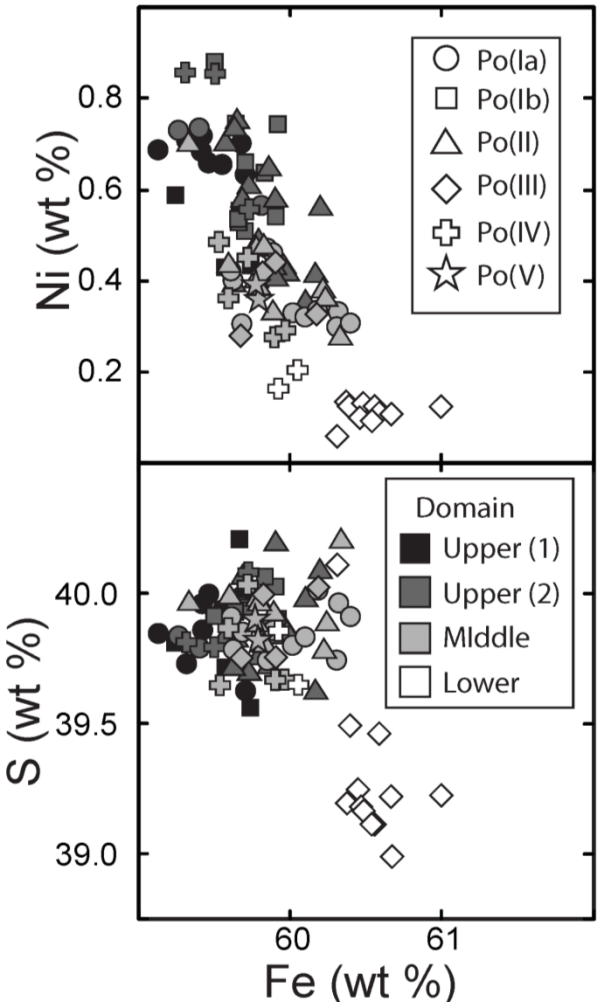

Fig 14. Fe, S, and Ni in pyrrhotite in the Morrison Deposit.

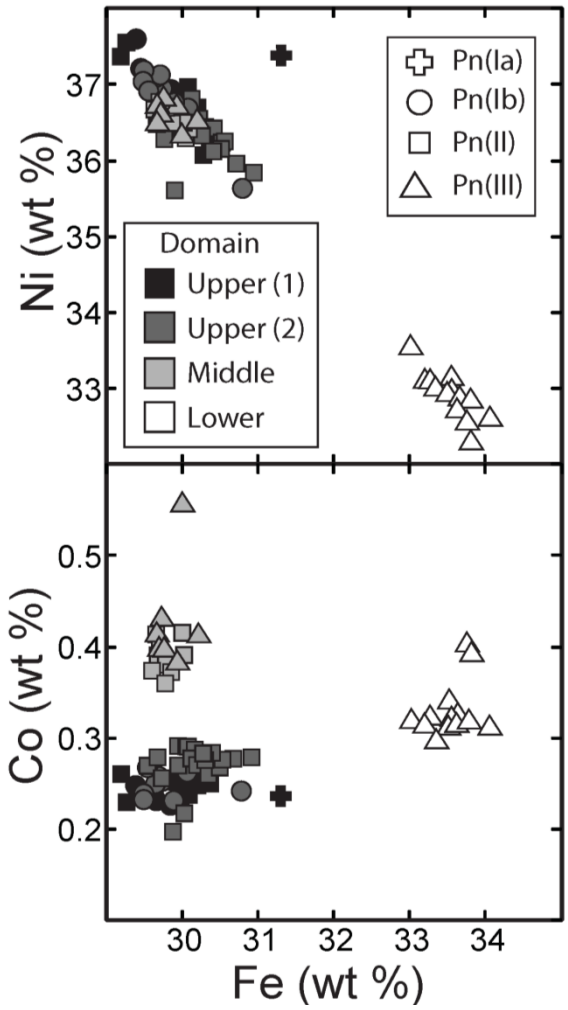

Fig 15. Ni, Fe, and Co in pentlandite in the Morrison Deposit.

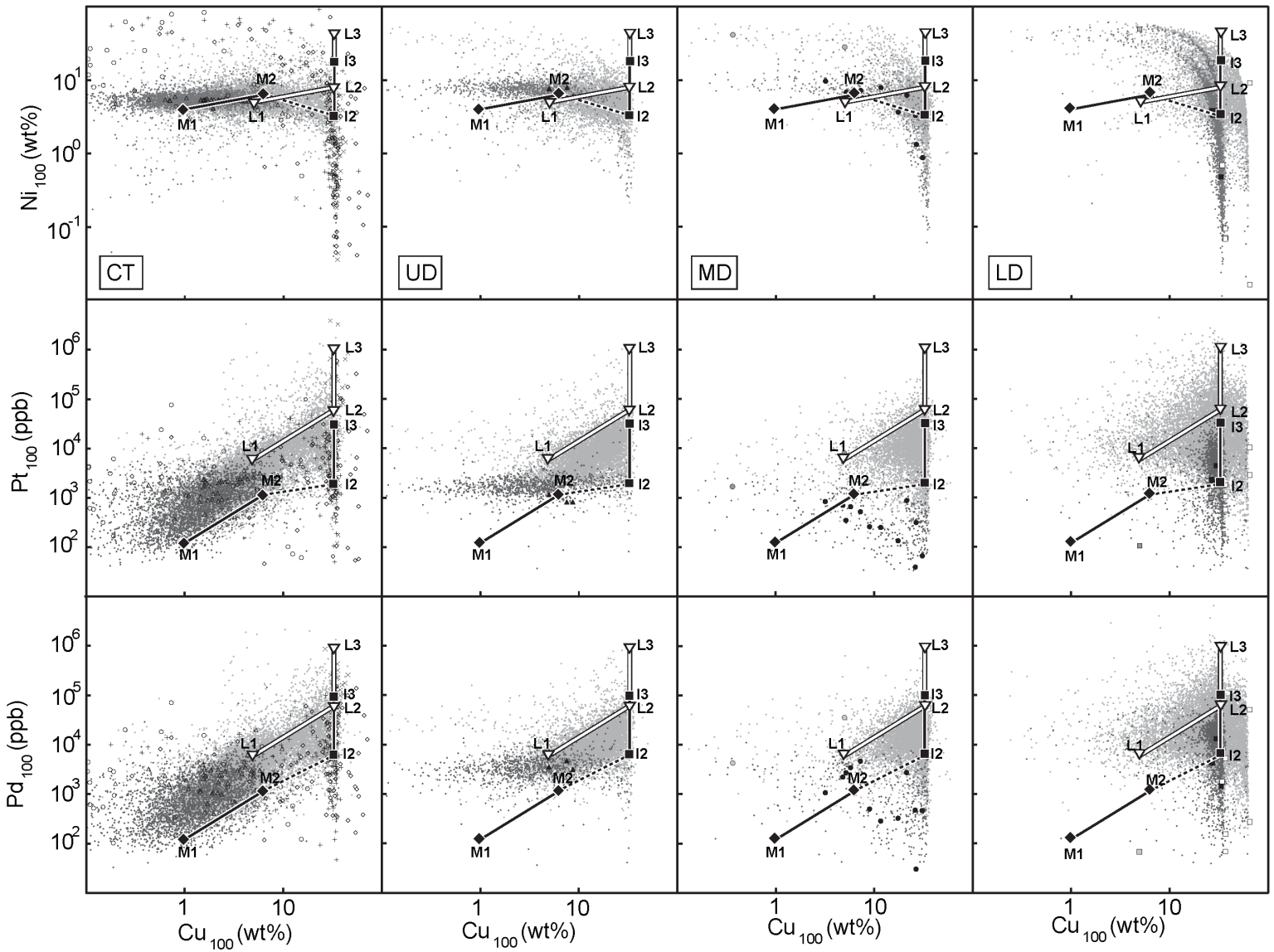
CT
UD
MD
LD
Ni100 (wt%)
Pt100 (ppb)
Pd100 (ppb)
Cu100 (wt%)
L3
I3
L2
I2
L1
M2
M1

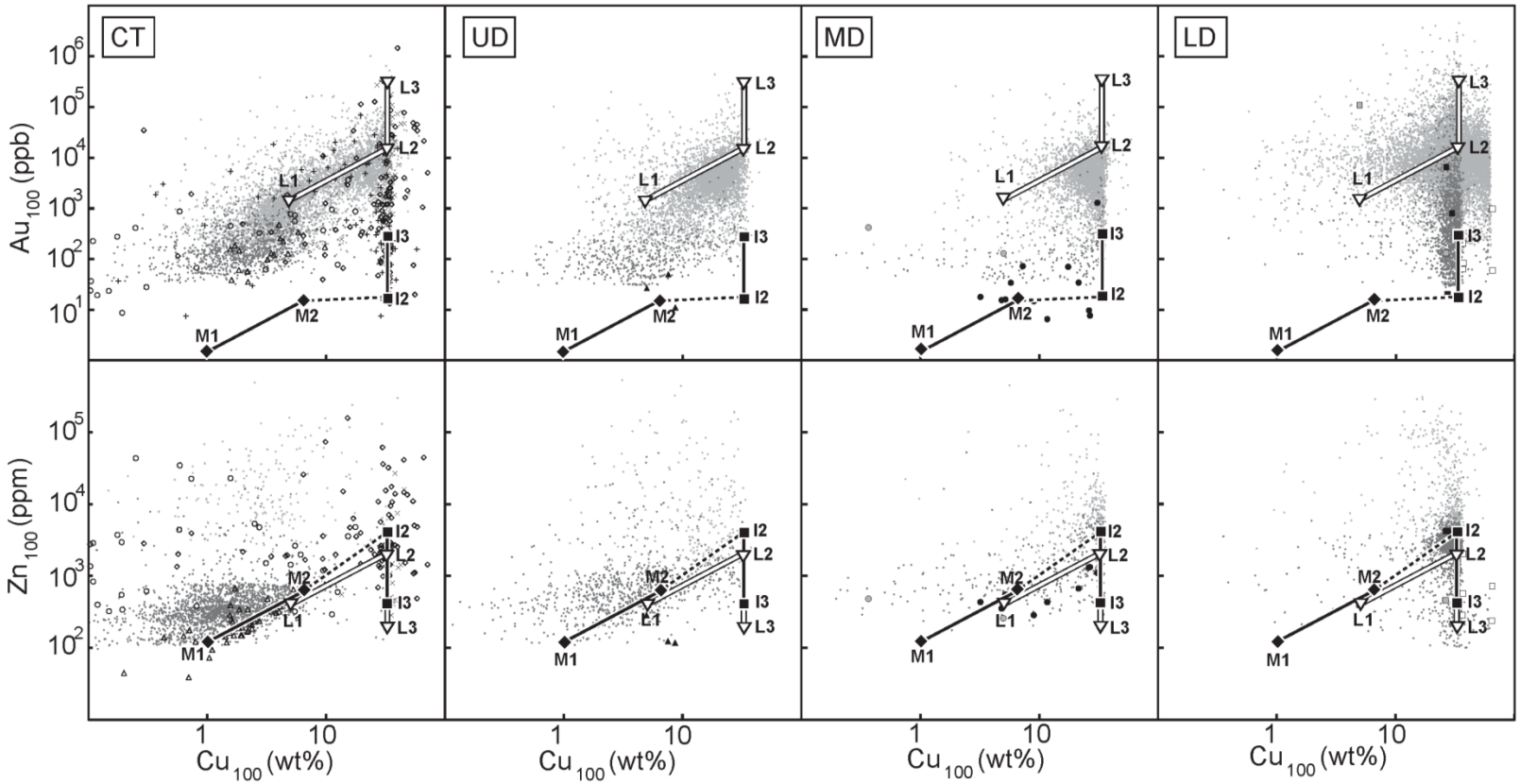

Fig 16. Modeled sulfide melt and solid fractionation trends superimposed on whole-rock geochemical data for the Morrison deposit. Data for Barnet showing (Farrow and Watkinson, 1997), Fraser Epidote zone (Farrow and Watkinson, 1996), McCreedy East Lower Main (Gregory, 2005), McCreedy East 153 (Stout, 2009), Strathcona (Li et al., 1992), and Broken Hammer and South zones (Péntek et al., 2008) are also shown. Finite-difference fractional crystallization models are based on methods established by J.P. Golightly and C.M. Lesher (unpubl.) and Mungall (2007); initial sulfide melt compositions and partition coefficients are given in Table 8.

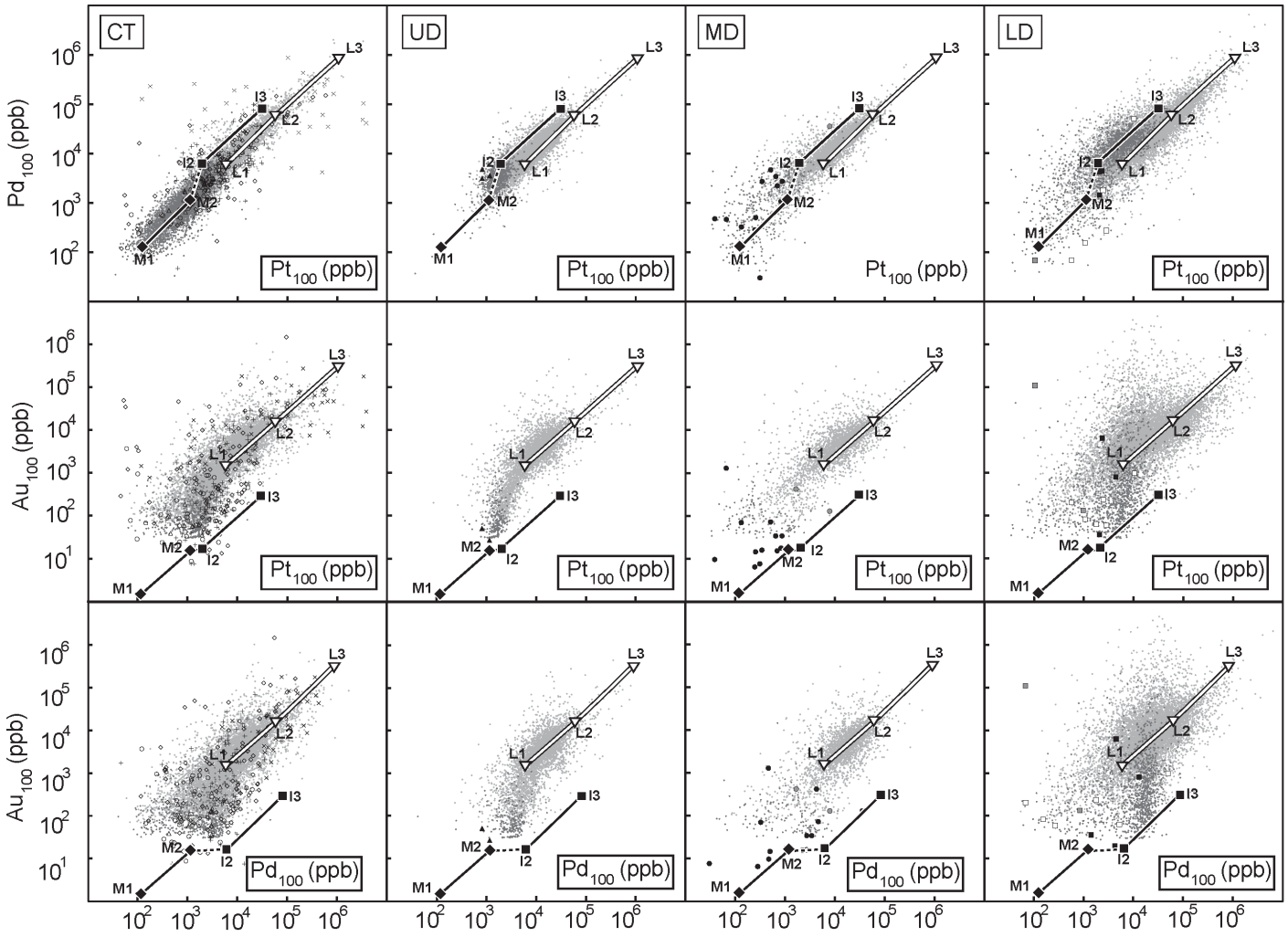

Fig 17. Pd/Pt, Au/Pt, and Au/Pd ratios for modeled sulfide melt and solid fractionation trends superimposed on whole-rock geochemical data for the Morrison Deposit. Data for Barnet showing (Farrow and Watkinson, 1997), Fraser Epidote zone (Farrow and Watkinson, 1996), McCreedy East Lower Main (Gregory, 2005), McCreedy East 153 (Stout, 2009), Strathcona (Li et al., 1992), and Broken Hammer and South zones (Péntek et al., 2008) are also shown.

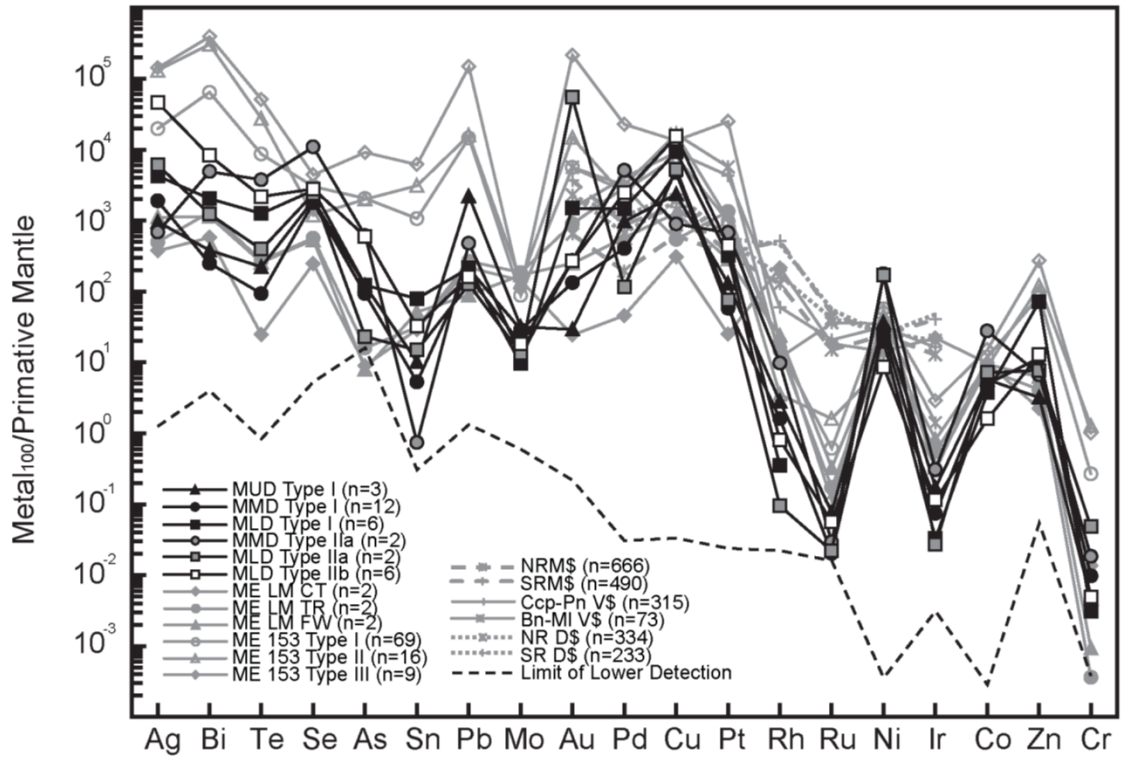

Fig 18. Extended element plot with values normalized to Primitive Mantle (McDonough and Sun, 1995) and plotted in order of incompatibility (Lesher and Keays, 2002). Data from McCreedy East Lower Main (ME LM) (Gregory, 2005), McCreedy East 153 (ME 153) (Stout, 2009), average North and South Range massive, vein, and disseminated sulfides (NR, SR, M$, V$, D$), average footwall Ccp-Pn veins, and average footwall Bn-Ml veins (Naldrett et al., 1999) are also plotted.

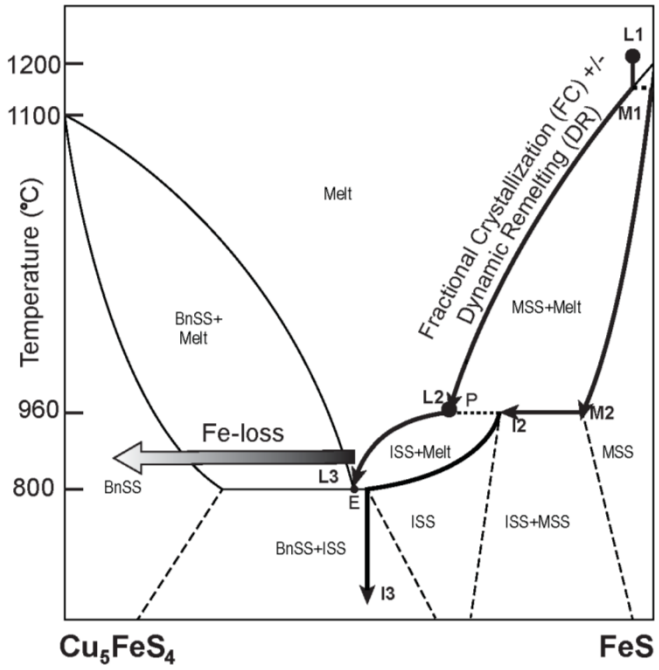

Fig 19. Schematic section through the bornite-pyrrhotite section of the Fe-Cu-S system showing fractional crystallization and Fe-S loss models for the formation of the various ore types in the Morrison deposit (based on data from Dutrizac, (1976) and Tsujimura and Kitakaze, (2004).

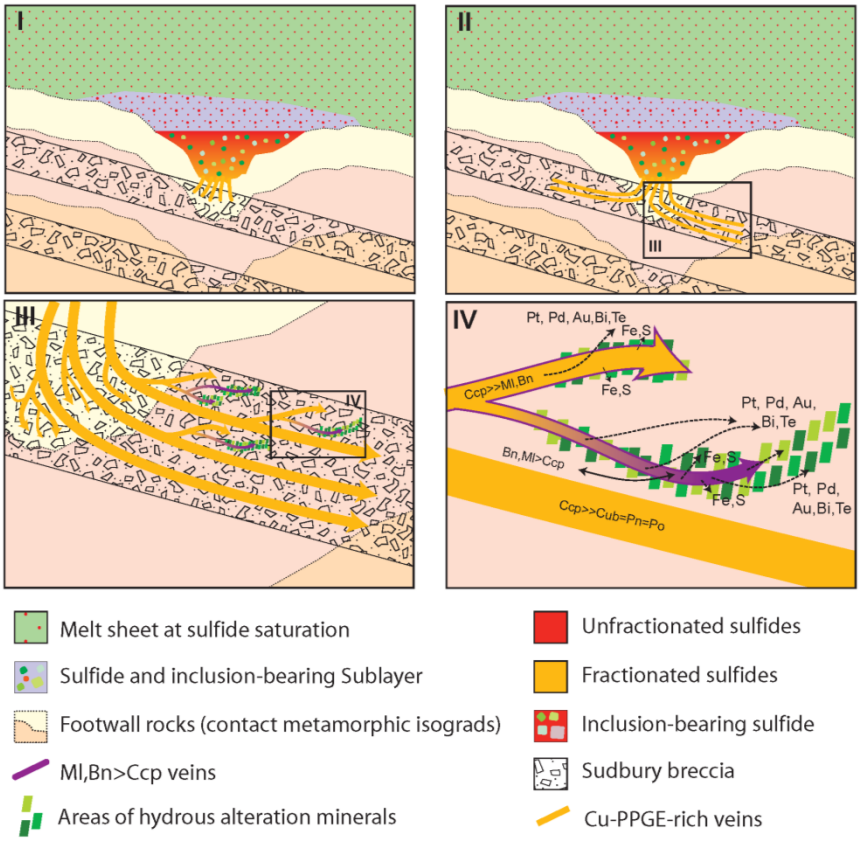

Fig 20. Schematic diagram for the formation of the Morrison Deposit (modified from Lesher et al., 2009).

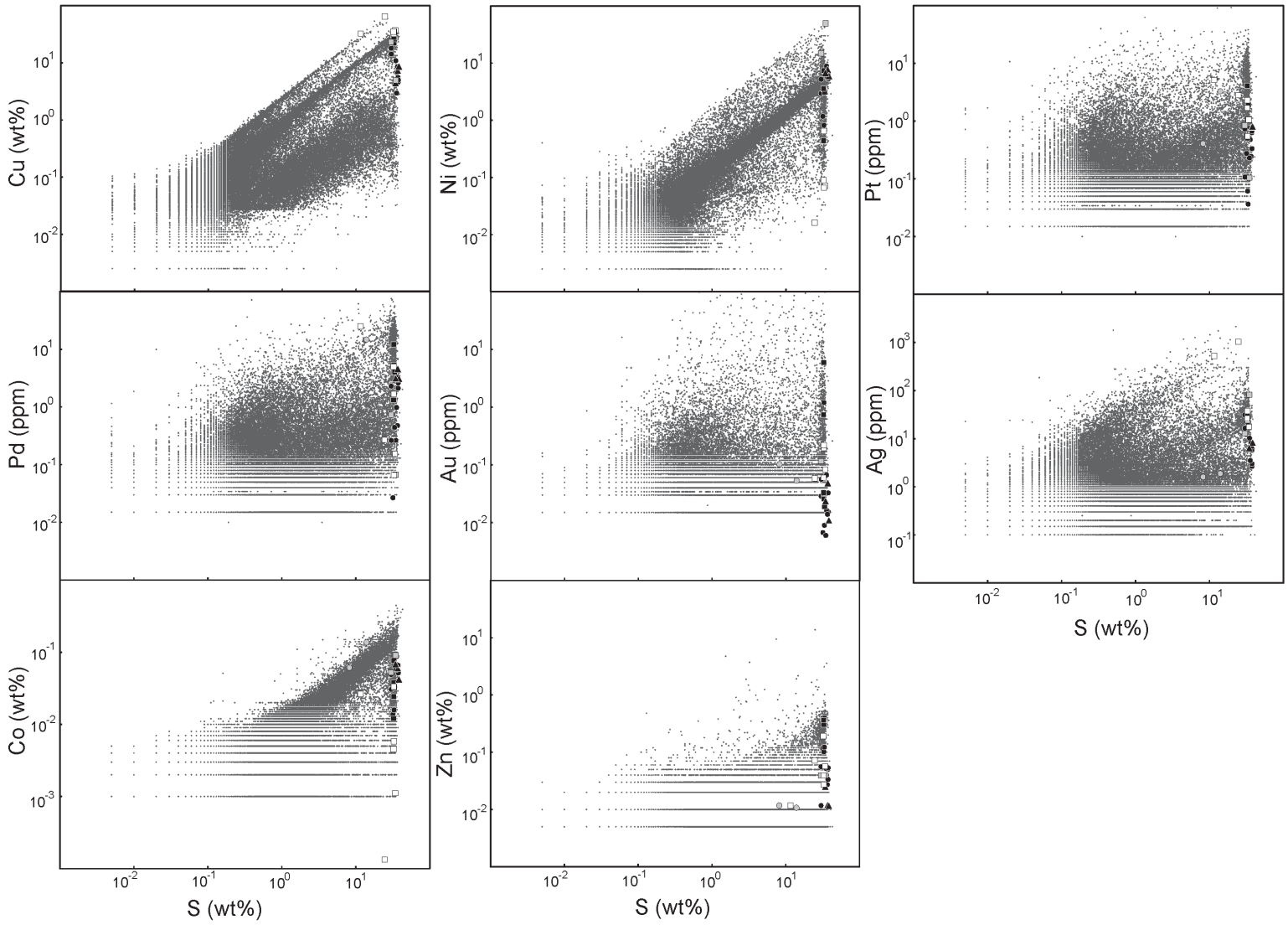

Fig A1. Element vs. Sulphur for whole-rock samples from the Morrison Deposit for Cu, Ni, Pt, Pd, Au, Ag, Co, and Zn.

TABLES

Table 1. Summary of variations in mineralization styles within the Morrison deposit.

	Vein Types			Country Rocks			
Domain	**Planar Sharp-Walled**	**Irregular Inclusion-Bearing**	**Vein Thickness**	**Mafic Gneiss Leucosome**	**Granophyre**	**Sudbury Breccia Matrix**	**Felsic Gneiss**
Upper							
First-Order Veins	+	+++	0.3-0.5 m	+++	++	+	++
Second-Order Veins	+	+++	<1-30 cm	+++	++	+	++
Disseminations	N/A	N/A	N/A	+++	++	+	++
Middle							
First-Order Veins	+	+++	0.3-1 m	+++	++	+	++
Second-Order Veins	+	+++	<1-30 cm	+++	++	+	++
Disseminations	N/A	N/A	N/A	+++	+	+	++
Lower							
First-Order Veins	+++	+	0.3-3 m	+	rare	++	+++
Second-Order Veins	+++	+	<1-30 cm	+	rare	++	+++
Disseminations	N/A	N/A	N/A	rare	++	rare	+++

+++ abundant, ++ common, + uncommon, N/A not applicable

Table 2: Mass balance calculations for the Levack-Morrison contact and footwall system.

Location	Type	Category	Short Tons	Cu %	Ni %	Cu/Ni	Cu_{10}/Cu_{30} %	Ni_{10}/Ni_{30} %
Main (incl. all historical contact)	Contact	Total Resource	62,302,700	1.30	2.00	0.65	3.94	6.06
No. 1	Contact	Total Resource	779,000	1.21	2.85	0.42	2.98	7.02
No. 2	Contact	Total Resource	1,023,000	1.00	2.20	0.46	3.14	6.86
No. 3	Contact	Total Resource	1,188,000	1.62	2.13	0.76	4.32	5.68
20 Pillar	Contact	Total Resource	186,000	0.56	2.17	0.26	2.05	7.95
34 Pillar	Contact	Total Resource	94,200	0.55	2.14	0.26	2.04	7.96
MW-LV Contact	Contact	Total Resource	78,200	0.15	0.89	0.17	1.44	8.56
No. 7	Contact	Total Resource	690,900	0.46	1.52	0.30	2.31	7.69
No. 7 Extension	Contact	Total Resource	263,000	0.35	1.42	0.25	1.99	8.01
1300	Contact	Total Resource	291,300	0.69	2.13	0.33	2.45	7.55
1900	Contact	Total Resource	176,500	1.92	2.28	0.84	4.57	5.43
MD2-3 (LFD)	Footwall	Total Resource	1,100,000	9.61	2.13	4.51	24.6	5.44
MD1 (Rob's)	Transitional	Total Resource	203,200	1.52	2.11	0.72	4.19	5.81
Total	Contact+ Transitional	Total Resource	67,072,800	1.28	2.01	0.64	3.90	6.10
Total	Footwall	Total Resource	1,100,000	9.61	2.13	4.51	24.6	5.44
Total	System	Total Resource	68,172,800	1.42	2.01	0.70	4.23	6.09
Total	Footwall	Calc. Missing	4,125,000	9.61	2.13	4.51	24.6	5.44
Total	System	Calc. Total	71,910,800	2.05	2.05	1.00	5.00	5.00

Tonnages and grades from Farrow et al. (2009) and QuadraFNX Mining Ltd. (2011). Ni_{10} and Cu_{10} = Ni and Cu grades normalized to 10% Ni+Cu (used for contact and MD1); Ni_{30} and Cu_{30} = Ni and Cu grades normalized to 30% Cu+Ni (used for MD2-3); Total resources is sum of measured, indicated, and inferred resource categories; Calc. Missing is the calculated missing footwall mineralization based on the above values; Calc. Total is the calculated total number of short tons in the Levack-Morrison system with a calculated average grade of 2.02% Cu and 2.02% Ni.

Table 3: Pyrrhotite and pentlandite types at the Morrison Deposit.

Type	Abundance By Domain			Description	Interpretation
	Upper	Middle	Lower		
Po Ia	++++	+++		10-50 mm euhedral crystals often containing, i) a well developed 0001 basal parting, ii) PnIa exsolved along the basal parting, and iii) chalcopyrite laths parallel to the basal parting	MSS
Po Ib	++++	+++		0.25-10 mm anhedral and sometimes round grains that contain PnIb exsolved along grain boundaries	MSS
Po II	++++	+++		0.25-10 mm irregular, anhedral grains that are intermixed with Ccp	MSS-ISS
Po III		+	++++	1-10 mm wide veinlets that occur within the Ccp-rich portions of some veins	Exsolution from ISS or Ccp
Po IV			++	0.2-0.3 mm wide flames that occur along fractures within Pn and along Pn grain boundaries; texturally very similar to pentlandite flames that exsolve from MSS	Exsolution from Pn
Po V		++	++	1-10 µm veinlets and rare patches within cubanite	Exsolution from ISS
Pn Ia	++++	+++		10-30 µm intragranular and intergranular flames	Intermediate to late-stage exsolution from MSS
Pn Ib	++++	+++		1-2 mm chains and eyes	Early to intermediate-stage exsolution from MSS
Pn II	++++	+++		5-10 mm eyes that often contain domains of Po and more rarely Ccp ± Po	Early exsolution from MSS
Pn III			++++	5-50 mm eyes that often contain, i) oriented, micron sized laths of Mak that radiate from multiple points within the Pn, and ii) Ccp needles along preferentially oriented planes within Pn	Exsolution from ISS. Mak laths and Ccp laths are crystallographically controlled
Pn IV		++	++	10-50 µm laths that contain chalcopyrite needles	Exsolution from ISS

++++ very abundant, +++ abundant, ++ common, + present, Tr trace, (blank) not observed

Table 4. Mineralogy and textures of mineralized sulfide/silicate veins at the Morrison deposit.

Domain/ Order	Po	Pn	Ccp	Cub	Sph	Mak	Mag	Bn	Ml	Py	Alteration Minerals	Description	Fig.
Upper													
First	++++	++	++		Tr		+			Late		Domains of Po Ia (sharp walled veins) and Po Ib (veins in leucosomes and granophyric dykes) surrounded by domains of sometimes preferentially oriented Po II, Ccp. Mag (1-2mm subhedral and rare euhedral) grains in all domains. Py, (along grain boundaries, secondary)	5A-B, 6B-C
Second	+++	++	++		Tr		+			Late			
Middle													
First	+++	++	+++	+	+	Tr	+			Late		Po Ia ± Ib with rare Pn Ia ± Ib surrounded by Ccp and Po II with Pn II (that rarely contains Po IV). Rare Pn IV (with Mak) increases toward the bottom. Po III and Cub (0.5 x 5mm laths and patches containing Po V) occurs towards the bottom of the middle domain. Mag (Subhedral to euhedral). Sph (anhedral and sometimes with chalcopyrite inclusions). Py, (along grain boundaries, secondary)	6A 6G-H
Second	+++	++	+++	+	+	Tr	+			Late			
Second		++	+++						+++	Tr	Ep, Amph, Carb, Chl	Ml, massive (sometimes with a well developed cleavage). Ccp occurs as massive zones. Pn occurs as eyes at Ml, Ccp boundary. Py, (along grain boundaries, secondary)	6I-J
Lower													
First	++	++	+++	++	+	+	+					Ccp, massive (with 0.5mm x 5mm Cub laths), Po III and lesser Po V. Pn III, (with Ccp needles, Mak laths, and sometimes Po IV) mainly along vein margins. Rare Pn IV. Mag (1-2mm subhedral and rare euhedral crystals), Sph (1-2mm anhedral and sometimes with chalcopyrite inclusions).	5D 6D-F
Second			++++				+		+		(Carb), (Amph)	Ccp, massive. Ml, 1-2mm anhedral crystals. Mag, 0.5-1 mm subhedral crystals.	
Second			++						+++		Chl, Carb, Amph, Ep	Domains of large Ml, (often twinned, with Ccp laths). Domains of Ccp, massive.	5F 6K
Second			+					++++	Tr			Bn, massive. Ccp, along fractures and as ~1 mm length laths.	
Second		++++	+									Pn III with Ccp occurring at vein margins.	
Second			+					+++	+++		Ep, Amph, Chl	Ml, large euhedral crystals (with well developed cleavage and often twinned). Bn, along Ml cleavage planes and fractures. Ccp, laths (within Bn) and irregular patches.	6L

++++ very abundant, +++ abundant, ++ common, + present, Tr trace. Bn = bornite Cu_5FeS_4, Ccp = chalcopyrite $CuFeS_2$, Cub = cubanite $CuFe_2S_3$, Mag = magnetite Fe_3O_4, Mak = mackinawite $(Fe,Ni)_{1+x}S$, Ml = millerite NiS, Pn = pentlandite $(Fe,Ni)_9S_8$, Po = pyrrhotite $Fe_{1-x}S$, Py = pyrite FeS_2, Sph = Sphalerite (Zn,Fe)S, Chl = chlorite, Carb = carbonate, Ep = epidote, Amph = amphibole

Table 5: Abundance of Low-S vs. High-S samples at the Morrison deposit

	Co	Ni	Cu	Zn	Pd	Pt	Au	Ag
UD	LS ~ HS	LS < HS	LS > HS	LS > HS	LS > HS	LS > HS	LS >> HS	LS >> HS
MD	LS ~ HS	LS ~ HS	LS ~ HS	LS ~ HS	LS >> HS	LS >> HS	LS >> HS	LS > HS
LD	LS ~ HS	LS ~ HS	LS ~ HS	LS ~ HS	LS ~ HS	LS > HS	LS >> HS	LS > HS

UD = upper domain, MD = middle domain, LD = lower domain; LS=low sulfur; HS=high sulfur

Table 6: Schematic representation of geochemical changes at the Morrison deposit

	Co		Ni		Cu		Zn		Pd		Pt		Au		Ag	
	HS	LS	HS	LS	HS	LS	HS	LS	HS	LS	HS	LS	HS	LS	HS	LS
UD								ID								
MD																
LD																

UD-MD = upper-middle domain, MD-LD = middle-lower domain; / = decrease, \ = increase, | = constant; ID = insufficient data; LS=low sulfur; HS=high sulfur

Table 7: Electron probe microanalyses of pyrrhotite and pentlandite in four first-order veins in the three domains of the Morrison deposit.

Domain	Level	Fe (wt%)	Ni (wt%)	Co (wt%)	S (wt%)
Pyrrhotite					
Upper (Lower Part)	3050L-1 (n = 12)	59.1-59.7 59.5, 59.5, 0.2	0.428-0.721 0.622, 0.658, 0.102	<0.026	39.6-40.2 39.9, 39.9, 0.2
Upper (Lower Part)	3050L-2 (n = 31)	59.4-60.2 59.8, 59.9, 0.2	0.352-0.879 0.598, 0.577, 0.148	<0.026	39.6-40.2 39.9, 39.9, 0.1
Middle	3510L (n = 32)	59.3-60.4 59.9, 59.9, 0.3	0.237-0.700 0.384, 0.371, 0.087	<0.026	39.6-40.2 39.8, 39.9, 0.1
Lower	3810L (n = 14)	59.9-61.0 60.5, 60.5, 0.3	0.059-0.203 0.120, 0.117, 0.033	<0.026	39.0-40.1 39.4, 39.2, 0.3
Pentlandite					
Upper (Lower Part)	3050L-1 (n = 15)	29.2-31.3 29.9, 30.0, 0.5	35.1-37.6 36.7, 36.8, 0.6	0.227-0.263 0.243, 0.241, 0.006	33.1-33.7 33.3, 33.2, 0.1
Upper (Lower Part)	3050L-2 (n = 32)	29.5-30.9 30.2, 30.2, 0.4	35.6-37.1 36.4, 36.3, 0.4	0.198-0.290 0.267, 0.270, 0.020	32.6-33.3 33.0, 33.0, 0.2
Middle	3510L (n = 17)	29.6-30.2 29.8, 29.8, 0.17	36.3-36.8 36.6, 36.6, 0.1	0.361-0.554 0.403, 0.393, 0.043	32.9-33.2 33.1, 33.0, 0.1
Lower	3810L (n = 14)	33.0-33.5 33.4, 33.4, 0.1	32.3-33.6 32.9, 32.9, 0.3	0.297-0.403 0.329, 0.319, 0.031	33.271-33.563 33.6, 33.4, 0.1

Notes: 3050-1L, 3050-2L, and 3810L are sharp-walled veins and 3510L is a vein within a granophyric textured dyke. The two samples from the upper domain are from different portions of the same vein. 3050L-1 is from a pyrrhotite-rich portion of the vein that contains PoIa and PoIb and PnIa, PnIb, and PnII. 3050L-2 is from a chalcopyrite-rich portion of the vein that contains PoIII and PnII. Range is on top line, mean, median, and standard deviation are on second line.

Table 8: Initial liquid composition, $D_{MSS/liquid}$ and $D_{ISS/liquid}$ for fractional crystallization numerical model.

Element	Initial Sufide Liquid	$D_{MSS/liquid}$	$D_{ISS/liquid}$
Cu	5 wt%	0.2	1
Pd	6000 ppb	0.02	0.1
Zn	400 ppm	0.3	2
Ni	5 wt%	0.8	0.4
Pt	6000 ppb	0.02	0.03
Au	1500 ppb	0.001	0.001

Table A1: Formulas for determining the normative abundances of minerals in whole-rock geochemical analyses and used to recalculate the analyses to 100% sulfides.

Assemblage	Po	Pn	Ccp	Ml	Bn
Po-Pn-Ccp	$[M_S-(N^S_{Pn}\bullet M_{Pn})]-(N^S_{Ccp}\bullet M_{Ccp})$	M_{Ni}/N^{Ni}_{Pn}	M_{Cu}/N^{Cu}_{Ccp}	0	0
Ccp-Pn-Ml	0	$[M_S-(N^S_{Ccp}\bullet M_{Ccp})-M_{Ni}]/(N^S_{Pn}-N^{Ni}_{Pn})$	M_{Cu}/N^{Cu}_{Ccp}	$M_{Ni}-(N^{Ni}_{Pn}\bullet M_{Pn})$	
Ccp-Bn-Ml	0	0	$[M_{Cu}-(N^{Cu}_{Bn}M_{Bn})]/N^{Cu}_{Ccp}$	$N^{Ni}_{Ml}\bullet M_{Ni}$	$[((N^S_{Ccp}/N^{Cu}_{Ccp})\bullet M_{Cu})-(M_S-(M_{Ni}\bullet(N^{Ni}_{Ml})))]/[M^S_{Bn}-((N^S_{Ccp}\bullet N^{Cu}_{Bn})/N^{Cu}_{Ccp})]$

Abbreviations: $\mathbf{M_{Cu}}$ = moles Cu, $\mathbf{M_{Ni}}$ = moles Ni, $\mathbf{M_S}$ = moles S, $\mathbf{M_{Bn}}$ = moles bornite, $\mathbf{M_{Ccp}}$ = moles chalcopyrite, $\mathbf{M_{Ml}}$ = moles Ml, $\mathbf{M_{Pn}}$ = moles pentlandite, $\mathbf{N^S_{Bn}}$ = formula units of S in bornite, $\mathbf{N^S_{Ccp}}$ = formula units of S in chalcopyrite, $\mathbf{N^s_{Ml}}$ formula units of S in millerite, $\mathbf{N^S_{Po}}$ = formula units of S in Po, $\mathbf{N^S_{Pn}}$ = formula units of S in pentlandite, $\mathbf{N^{Cu}_{Bn}}$ = formula units of Cu in bornite, $\mathbf{N^{Cu}_{Ccp}}$ = formula units of Cu in chalcopyrite, $\mathbf{N^N_{Ml}}$ formula units of N in millerite, $\mathbf{N^{Ni}_{Pn}}$ = formula units of N in pentlandite

Table A2: Equations for determining the moles of bornite through substitution method.

Number	Equation	Action
(1)	$M_{Cu} = (N^{Cu}_{Ccp} \bullet M_{Ccp}) + (N^{Cu}_{Bn} \bullet M_{Bn})$	
(2)	$M_S^* = (N^S_{Ccp} \bullet M_{Ccp}) + (N^S_{Bn} \bullet M_{Bn})$	
(3)	$M_{Ccp} = (M_{Cu}/N^{Cu}_{Ccp}) - ((N^{Cu}_{Bn}/N^{Cu}_{Ccp}) \bullet M_{Bn})$	Rearrange (1) to solve for M_{Ccp}
(4)	$M_S^* = (N^S_{Ccp} \bullet (M_{Cu}/N^{Cu}_{Ccp}) - ((N^{Cu}_{Bn}/N^{Cu}_{Ccp}) \bullet M_{Bn})) + (N^S_{Bn} \bullet M_{Bn})$	Substitute $[(M_{Cu}/N^{Cu}_{Ccp}) - ((N^{Cu}_{Bn}/N^{Cu}_{Ccp}) \bullet M_{Bn})]$ for $[M_{Ccp}]$ in (2)
(5)	$M_{Bn} = [((N^S_{Ccp}/N^{Cu}_{Ccp}) \bullet M_{Cu}) - M_S^*]/ [M^S_{Bn} - ((N^S_{Ccp} \bullet N^{Cu}_{Bn})/N^{Cu}_{Ccp})]$	Rearrange (3) to solve for M_{Bn}

Notes: Equations 1 and 2 are used to determine the abundances of bornite and chalcopyrite. Equations 3-5 are used to solve for the moles of bornite. Once the moles of bornite are determined from Equation 5, the value can be substituted for M_{Bn} in Equation 3 to determine the moles of chalcopyrite. Abbreviations: $\mathbf{M_{Cu}}$ = moles Cu, $\mathbf{M_{Ni}}$ = moles Ni, $\mathbf{M_S}$ = moles S, $\mathbf{M_{Bn}}$ = moles bornite, $\mathbf{M_{Ccp}}$ = moles chalcopyrite, $\mathbf{M_{Ml}}$ = moles Ml, $\mathbf{N^S_{Bn}}$ = formula units of S in bornite, $\mathbf{N^S_{Ccp}}$ = formula units of S in chalcopyrite, $\mathbf{N^s_{Ml}}$ formula units of S in millerite, $\mathbf{N^{Cu}_{Bn}}$ = formula units of Cu in bornite, $\mathbf{N^{Cu}_{Ccp}}$ = formula units of Cu in chalcopyrite, $\mathbf{N^{Ni}_{Ml}}$ formula units of Ni in millerite, $\mathbf{M_S^*} = M_S - (N^{Ni}_{Ml} \bullet M_{Ni})$